Geometry and Physics
of Charged Rotating Discs of Dust
in Einstein-Maxwell Theory

DISSERTATION

zur Erlangung des akademischen Grades
doctor rerum naturalium (Dr. rer. nat.)

vorgelegt dem Rat der
Physikalisch-Astronomischen Fakultät
der Friedrich-Schiller-Universität Jena

von M.Sc. David Rumler
geboren am 23.08.1993
in Starnberg, Deutschland

Abstract

Within general relativity geometrical and physical properties of the charged rotating disc of dust, which is an axisymmetric, stationary and reflection symmetric solution of the Einstein-Maxwell equations, are investigated. A rigid rotation around the axis of symmetry and a constant specific charge $\epsilon \in [0,1]$ are assumed in this model. The disc solution is given in terms of a post-Newtonian expansion up to the tenth order, where a "relativity parameter" $g \in [0,1]$ is used as the expansion parameter. It connects the regime of Newtonian physics, for $g \ll 1$, with the ultra-relativistic regime, for $g \to 1$, where black hole formation is expected.

Inspired by the Ehrenfest paradox, the proper spatial geometry of the charged rotating disc of dust is discussed. Firstly, the ratio of circumference to radius (as seen by co-rotating and non-rotating observers) is analysed with regard to the paradox, and secondly, the intrinsic spatial curvature of the disc, i.e. the Gaussian curvature, is determined and examined in detail (in particular under various limiting cases). An essential role plays the specific charge, since it effectively serves as a regulator of the rotation speed of the disc. By decreasing the specific charge from 1 to 0, the rotational speed of the corresponding disc configurations increases from zero to a maximum value. A key observation is that such a reduction of the specific charge causes a transition from positive to negative curvature.

As far as the physical properties are concerned, the surface mass density is addressed first. Similar to viscous fluids or elastic materials, the charged rotating disc of dust shows a reaction to an increase of the rotation speed. Furthermore, gravitational and electromagnetic multipole moments are calculated and discussed. It turns out that the individual mass, angular momentum, electric and magnetic moments are ordered in the sense that higher moments have a lower absolute value. For sufficiently relativistic disc configurations, an ergosphere of torus-like shape forms within the disc. It grows with g and eventually expands beyond the disc. Finally, equatorial circular orbits of neutral test particles in the exterior spacetime of the charged rotating disc of dust are analysed. In addition, for both neutral and charged test particles, general formulae in closed form for angular velocity, specific energy and specific angular momentum are derived, which hold for any (exterior) asymptotically flat, axisymmetric, stationary and reflection symmetric (electro-)vacuum spacetime.

Kurzfassung

Im Rahmen der allgemeinen Relativitätstheorie werden geometrische und physikalische Eigenschaften der geladenen rotierenden Staubscheibe untersucht, die eine achsensymmetrische, stationäre und reflexionssymmetrische Lösung der Einstein-Maxwell-Gleichungen darstellt. Es wird eine starre Rotation um die Symmetrieachse und eine konstante spezifische Ladung $\epsilon \in [0, 1]$ in diesem Model vorausgesetzt. Die Scheibenlösung ist durch eine Post-Newtonsche Entwicklung bis zur zehnten Ordnung gegeben, wobei als Entwicklungsparameter ein "Relativitätsparameter" $g \in [0, 1]$ verwendet wird. Er verbindet das Regime der Newtonschen Physik, für $g \ll 1$, mit dem ultrarelativistischen Regime, für $g \to 1$, in dem die Bildung Schwarzer Löcher erwartet wird.

Angeregt durch das Ehrenfest-Paradoxon wird die "wahre" räumliche Geometrie der geladenen rotierenden Staubscheibe diskutiert. Zum einen wird das Verhältnis von Umfang zu Radius (aus Sicht von mitrotierenden und nichtrotierenden Beobachtern) im Hinblick auf das Paradoxon analysiert und zum anderen wird die intrinsische räumliche Krümmung der Scheibe, sprich die Gaußsche Krümmung, bestimmt und eingehend untersucht (insbesondere unter verschiedenen Grenzfällen). Eine wesentliche Rolle spielt dabei die spezifische Ladung, da sie effektiv als Regulator der Rotationsgeschwindigkeit der Scheibe dient. Verringert man die spezifische Ladung von 1 auf 0, so steigt die Rotationsgeschwindigkeit der entsprechenden Scheibenkonfigurationen von Null auf einen Maximalwert. Eine wichtige Beobachtung ist, dass eine solche Verringerung der spezifischen Ladung einen Übergang von einer positiven zu einer negativen Krümmung bewirkt.

In Bezug auf die physikalischen Eigenschaften wird zunächst die Oberflächenmassendichte behandelt. Ähnlich wie bei viskosen Flüssigkeiten oder elastischen Materialien zeigt die geladene rotierende Staubscheibe eine Reaktion auf eine Erhöhung der Rotationsgeschwindigkeit. Weiterhin werden gravitative und elektromagnetische Multipolmomente berechnet und diskutiert. Es stellt sich heraus, dass die einzelnen Massen-, Drehimpuls-, elektrischen und magnetischen Momente geordnet sind in dem Sinne, dass höhere Momente einen niedrigeren Absolutbetrag haben. Für hinreichend relativistische Scheibenkonfigurationen bildet sich innerhalb der Scheibe eine Ergosphäre von torusartiger Form. Sie wächst mit g und dehnt sich letztendlich über die Scheibe hinweg aus. Abschließend werden äquatoriale Kreisbahnen von neutralen Testteilchen in der äußeren Raumzeit der geladenen rotierenden Staubscheibe analysiert. Dabei werden, sowohl für neutrale als auch geladene Testteilchen, allgemeine Formeln in geschlossener Form für die Winkelgeschwindigkeit, die spezifische Energie und den spezifischen Drehimpuls hergeleitet, die für jede (äußere) asymptotisch flache, achsensymmetrische, stationäre und reflexionssymmetrische (Elektro-)Vakuumraumzeit gelten.

Contents

Contents

1 Introduction

The general theory of relativity represents probably the most beautiful of all existing physical theories.

(Landau and Lifshitz, The Classical Theory of Fields)

Einstein's general theory of relativity, also known as general relativity, is not only aesthetically very appealing, but also one of the most successful theories in physics. Among other phenomena, it describes black holes, neutron stars, mergers of black holes and/or neutron stars, the generation and propagation of gravitational waves and the cosmological evolution of the universe. Over the years, countless experimental tests have confirmed the theoretical predictions of general relativity with incredible precision, see, e.g., [1–3].

In general relativity it is, however, rather challenging to find exact solutions to the Einstein equations that are not only of purely mathematical nature, but also satisfy concrete physical constraints. As a result there are only a few rigorous physical solutions. With regard to (charged) rotating matter sources the only physically relevant exact solutions are the rotating black hole solutions, i.e. Kerr [4] and Kerr-Newman [5], as well as the solution of the uncharged rotating disc of dust by Neugebauer and Meinel [6, 7].

Using methods from soliton theory, Neugebauer and Meinel were able to rigorously solve the boundary value problem of an infinitesimally thin, rigidly rotating disc made of dust. The derived disc solution is axisymmetric, stationary and reflection symmetric and it is given in terms of hyperelliptic theta functions. The individual dust particles within the disc travel on geodesics. In astrophysics, it may serve as a basic model for a rotating galaxy.

Similar to the Kerr-Newman solution that generalizes the Kerr solution by including an electric charge, the charged rotating disc of dust is a semi-analytic generalization of Neugebauer and Meinel's disc solution with a constant specific electric charge.[1] Due to the additional electromagnetic field, the motion of the charged dust particles is no

---

[1]Even though a (sustained) non-zero net charge is unlikely in an astrophysical setting, the additional charge parameter can nevertheless be of theoretical interest.

longer geodesic, but under the influence of the Lorentz force. In the Newtonian limit each dust particle is in an equilibrium of the gravitational, centrifugal and electric force. Changing the specific charge, therefore, directly affects the angular velocity of the disc. As a consequence, in the limiting case of vanishing specific charge the disc of dust has maximal rotation and in the case of maximal specific charge the disc is static. In a sense, the specific charge parameter thus serves as a regulator of the rotational speed of the disc by interpolating between maximal and zero rotation.

Specifically, the charged rotating disc of dust is an axisymmetric, stationary and reflection symmetric solution of the Einstein-Maxwell equations in terms of a post-Newtonian expansion up to tenth order, derived by Palenta and Breithaupt [8, 9]. As expansion parameter a "relativity parameter" is used that connects the regimes of Newtonian and ultra-relativistic physics. In the ultra-relativistic limit the formation of black holes is assumed.

The goal of this thesis is a detailed analysis of the (spatial) geometrical and physical properties of the charged rotating disc of dust. Particular emphasis is placed on their dependence on the specific charge (which also influences the angular momentum) and the relativity parameter. These include, among others, the disc's Gaussian curvature, its gravitational and electromagnetic multipole moments and the circular motion of test particles in the equatorial plane of the disc. Compared to the uncharged rotating disc of dust, the additional specific charge parameter offers even richer physics and allows the study of the impact of a change in angular velocity on the disc's spacetime. Results obtained in connection with the charged rotating disc of dust may also give general insights into the geometrical structure of the spacetime of charged, rotating bodies.

This thesis is structured as follows. In chapter 2, after a precise definition of the disc model, the boundary value problem for the charged rotating disc of dust is explicitly derived from the Einstein-Maxwell equations. It could be solved in terms of a post-Newtonian expansion that is described briefly in chapter 3. Ehrenfest's paradox, which concerns rigidly rotating discs within special relativity, was one of the motivations to study the proper spatial geometry of the charged rotating disc of dust. A review can be found in chapter 4. After this, the first of the two major chapters of this thesis follows. Chapter 5 covers the proper spatial geometry of the disc. First, questions related to Ehrenfest's paradox are addressed and then the Gaussian curvature of the disc is analysed. The second major chapter, chapter 6, focuses on the physical properties of the disc. Here, the proper surface mass density, multipole moments, the formation of an ergosphere and circular motion of test particles are investigated. In the end, chapter 7 concludes the thesis with a summary and an outlook.

The evaluation of the derived equations with the disc solution in terms of the post-Newtonian expansion was carried out with the help of the computer algebra systems Maple (primarily) and Mathematica (occasionally).

In this thesis a system of units with $G = 1$, $c = 1$ and $4\pi\epsilon_0 = 1$ is used, where G is Newton's gravitational constant, c the speed of light and ϵ_0 the electrical constant. Therefore length, time, mass, energy and electric charge all a have the same unit.

Latin indices denote a summation in the four spacetime dimensions, $i, j = 1, ..., 4$, and Greek indices a summation in the three spatial dimensions, $\alpha, \beta = 1, 2, 3$. Spatial coordinates are specified by $x^\alpha = (x^1, x^2, x^3)$ and the time coordinate by x^4.

Moreover, partial derivatives are abbreviated by a comma and covariant derivatives by a semicolon.

The compilation of this thesis is solely due to the author. However, chapter 5 is based on [10] published jointly with Kleinwächter and Meinel (as co-authors) and section 6.2 is based on [11] published together with Meinel (as co-author). Chapter 4 is furthermore orientated partly on [10] and chapters 2, 3 and 7 partly on [10] and [11]. In the publications, and also this thesis, Kleinwächter contributed numerical values (as well as two equations and a figure) computed from the solution of the uncharged rotating disc of dust for comparison with the charged rotating disc of dust. Meinel supported the preparation of the publications and this thesis in an advisory capacity as a supervisor. See also Ehrenwörtliche Erklärung.

2 Formulation of the disc problem within Einstein-Maxwell theory

In this chapter the rigidly rotating disc of constantly charged dust in the framework of Einstein-Maxwell theory is introduced. Exploiting axisymmetry and stationarity, underlying the disc problem, the electro-vacuum Einstein-Maxwell equations can be reduced to the Ernst equations. The disc problem can thus be formulated as a boundary value problem to those Ernst equations. At the end of the chapter, a brief introduction is given to a powerful analytic tool from soliton theory, the so-called inverse scattering method, which in principle can be applied here.

A detailed discussion of the problem of the uncharged rigidly rotating disc of dust, which was solved rigorously by Neugebauer and Meinel [6, 7], can be found in [12] (see also [13]).[1]

2.1 Model of the disc

We consider a thermodynamic equilibrium configuration of an infinitesimally thin disc of dust with constant specific electric charge $\epsilon = \frac{\rho_{\text{el}}}{\mu} \in [-1, 1]$ that is rigidly rotating around the axis of symmetry with constant angular velocity Ω [8, 9, 14]. Dust is a perfect fluid with vanishing pressure and ρ_{el} and μ denote the electric charge density and the baryonic mass density of the disc, respectively. Due to the constant angular velocity the disc cannot be arbitrarily large and needs to have a finite coordinate radius ρ_0. The disc is illustrated in fig. 2.1, with coordinates to be introduced shortly.

For an equilibrium configuration, spacetime is stationary, implying the existence of an associated Killing vector $\boldsymbol{\xi}$. We also demand axisymmetry, characterized by another Killing vector $\boldsymbol{\eta}$ that commutes with $\boldsymbol{\xi}$. Furthermore, the problem is reflection symmetric with respect to the equatorial plane of the disc.

Before thermodynamic equilibrium is reached, we allow for some arbitrarily small viscosity such that a rigid rotation can be established between the circular layers of the disc by friction. Without viscosity differential rotation is possible [16]. Excess heat generated by friction is radiated away until the state of equilibrium with constant Ω

---

[1]This chapter is partly orientated on [10], [11] and [12].

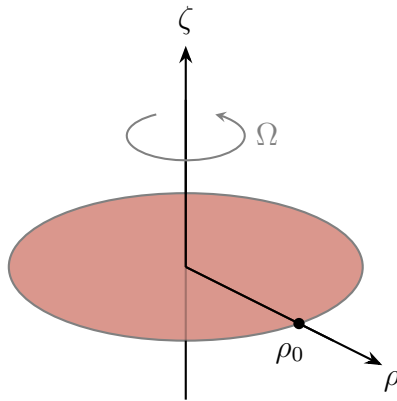## 2 Formulation of the disc problem within Einstein-Maxwell theory

Figure 2.1: Infinitesimally thin disc of charged dust rotating rigidly with angular velocity Ω around the axis of symmetry ζ (after [15]).

is reached. At equilibrium, the viscosity no longer has any influence and can be set to zero and the model of the perfect fluid (with vanishing pressure) can be assumed.

Furthermore, any deviation from the circular shape of the disc and therefore from axisymmetry would result in the generation of gravitational waves until an equilibrium configuration forms [17].

Using axisymmetry and stationarity the metric of a rotating perfect fluid body, and thus also of the charged rotating disc of dust, can be written in the form[2] [19, 20]:

$$\mathrm{d}s^2 = g_{ij}\mathrm{d}x^i\mathrm{d}x^j = f^{-1}\left[h\left(\mathrm{d}\rho^2 + \mathrm{d}\zeta^2\right) + W^2\mathrm{d}\varphi^2\right] - f\left(\mathrm{d}t + a\,\mathrm{d}\varphi\right)^2, \qquad (2.1)$$

where $(\rho, \zeta, \varphi, t)$ are Lewis-Papapetrou coordinates and t and φ are adapted to the Killing vectors, such that

$$\boldsymbol{\xi} = \frac{\partial}{\partial t} \quad \text{and} \quad \boldsymbol{\eta} = \frac{\partial}{\partial \varphi}. \qquad (2.2)$$

As a consequence, the metric functions f, h, W and a depend on the coordinates ρ and ζ only. Instead of f and h we will also make use of the functions U and k, where

$$f = e^{2U} \quad \text{and} \quad h = e^{2k}. \qquad (2.3)$$

Note that U can be interpreted as a generalized Newtonian potential and we call a the gravitomagnetic potential.

The timelike Killing vector $\boldsymbol{\xi}$ is normalized at spatial infinity according to

$$\xi^i\xi_i \to -1 \quad \text{for } \rho^2 + \zeta^2 \to \infty \qquad (2.4)$$

---

[2]An additional requirement for this Lewis-Papapetrou line element is a "circularity condition" which, given the two Killing vectors $\boldsymbol{\eta} = \frac{\partial}{\partial \varphi}$ and $\boldsymbol{\xi} = \frac{\partial}{\partial t}$, demands that the four-velocity of the fluid and the electromagnetic four-current density are of the form: $u^i = (0, 0, u^\varphi, u^t)$ and $j^i = (0, 0, j^\varphi, j^t)$ [18]. This, however, is satisfied for the charged rotating disc of dust, see eqs. (2.16) and (2.18).

and the spacelike Killing vector $\boldsymbol{\eta}$ vanishes along the symmetry axis $\mathcal{A}$:

$$\boldsymbol{\eta} = 0 \quad \text{at } \mathcal{A}. \tag{2.5}$$

Furthermore, orbits of $\boldsymbol{\eta}$ are closed and have a periodicity of 2π.

Evaluating the scalar products of the Killing vectors allows for a coordinate independent characterization of the metric functions f, W and a:

$$\xi^i \xi_i = g_{tt} = -f, \quad \eta^i \eta_i = g_{\varphi\varphi} = f^{-1}W^2 - fa^2, \quad \eta^i \xi_i = g_{\varphi t} = -fa. \tag{2.6}$$

As depicted in fig. 2.1, the symmetry axis $\mathcal{A}$ is identified (without loss of generality) with the ζ-axis. In other words, $\rho = 0$ characterizes $\mathcal{A}$ and ρ and ζ define a half-plane:

$$0 \le \rho < \infty, \quad -\infty < \zeta < \infty. \tag{2.7}$$

It can be shown that the following conditions hold on the axis of symmetry, see Stephani et al. [18]:

$$\rho \to 0: \quad a \to 0, \ W \to 0, \ \frac{W}{\rho\sqrt{h}} \to 1. \tag{2.8}$$

Axisymmetry and stationarity also apply to the electromagnetic field. In summary, expressed in terms of Lie-derivatives, we can state for both the gravitational and the electromagnetic field (see also [15]):

$$\mathcal{L}_{\boldsymbol{\xi}} g_{ik} = 0, \quad \mathcal{L}_{\boldsymbol{\eta}} g_{ik} = 0, \quad \mathcal{L}_{\boldsymbol{\xi}} F_{ik} = 0, \quad \mathcal{L}_{\boldsymbol{\eta}} F_{ik} = 0. \tag{2.9}$$

Using Lorenz-gauge the electromagnetic four-potential A_a takes the form:

$$A_a = (0, 0, A_\varphi, A_t), \tag{2.10}$$

where A_φ and A_t depend on the coordinates ρ and ζ only. As usual, the field strength tensor F_{ab} is expressed in terms of the four-potential A_a:

$$F_{ab} = A_{b;a} - A_{a;b} = A_{b,a} - A_{a,b}. \tag{2.11}$$

The electromagnetic field, as well as the gravitational, needs to vanish at spatial infinity, since the disc is understood as an isolated body[3]. We therefore demand

$$\rho^2 + \zeta^2 \to \infty: \quad A_\varphi \to 0, \ A_t \to 0 \tag{2.12}$$

and asymptotic flatness, i.e. that eq. (2.1) attains the Minkowski metric in cylindrical

---

[3]The concept of an isolated body relies on the assumption of an isotropic outside world, see e.g. [12].

2 Formulation of the disc problem within Einstein-Maxwell theory

coordinates ρ, ζ and φ,

$$\rho^2 + \zeta^2 \to \infty : \quad f \to 1\,, \; h \to 1\,, \; W \to \rho\,, \; a \to 0\,. \tag{2.13}$$

With $\rho = r\sin\theta$, $\zeta = r\cos\theta$, the following asymptotic behaviour results [15, 21]:

$$A_\varphi = \frac{D\sin^2\theta}{r} + \mathcal{O}\left(r^{-2}\right)\,, \quad A_t = -\frac{Q}{r} + \mathcal{O}\left(r^{-2}\right)\,, \tag{2.14}$$

$$f = 1 - \frac{2M}{r} + \mathcal{O}\left(r^{-2}\right)\,, \quad a = \frac{2J\sin^2\theta}{r} + \mathcal{O}\left(r^{-2}\right)\,, \tag{2.15}$$

where M is the gravitational mass, J the angular momentum, Q the electric charge and D the magnetic dipole moment.[4]

A stationary and rigidly rotating perfect fluid has a four-velocity given by:

$$u^i = e^{-\mathcal{V}}\left(\xi^i + \Omega\,\eta^i\right)\,, \quad \Omega = \text{const.}\,, \tag{2.16}$$

where $\Omega = \frac{\mathrm{d}\varphi}{\mathrm{d}t} = \frac{u^\varphi}{u^t}$ is the angular velocity measured by an observer at spatial infinity. Evaluating the normalization condition $u^i u_i = -1$ reveals the function $\mathcal{V}$:

$$\begin{aligned} e^{2\mathcal{V}} &= -\left(\xi^i + \Omega\,\eta^i\right)\left(\xi_i + \Omega\,\eta_i\right) \\ &= f\left[(1+\Omega a)^2 - \Omega^2 W^2 f^{-2}\right]\,. \end{aligned} \tag{2.17}$$

As electric currents are generated solely by the circular motion of the charged dust particles of the disc (the electrical conductivity of the disc is zero), we have a purely convective four-current density:

$$j^a = \rho_{\text{el}} u^a = \epsilon\mu u^a\,. \tag{2.18}$$

It should be noted that the mass density μ is related to the surface mass density σ via

$$\mu = \frac{f}{h}\sigma(\rho)\delta(\zeta)\,, \quad \text{for } 0 \le \rho \le \rho_0\,. \tag{2.19}$$

For $\rho > \rho_0$, σ and μ are identical to zero. In general, the baryonic mass density does not agree with the mass (or energy) density, however, as we will see in the next section, for dust they actually do. For this reason, we use the same notation for both here. A coordinate independent representation of σ is given in terms of the proper surface mass density

$$\sigma_{\text{p}} = \sqrt{\frac{f}{h}}\sigma\,. \tag{2.20}$$

Due to the rotation of the disc, in many situations it might be beneficial to discuss

---

[4]A fascinating feature of the charged rotating disc of dust is that, in contrast to the uncharged disc, even the baryonic mass M_{b} can be read off from the asymptotic behaviour via $M_{\text{b}} = \frac{Q}{\epsilon}$.

the geometrical and physical aspects in a co-rotating frame of reference rather than in the non-rotating frame described by $(\rho, \zeta, \varphi, t)$. Thanks to the rigid rotation we can globally introduce the co-rotating frame via

$$\rho' = \rho, \quad \zeta' = \zeta, \quad \varphi' = \varphi - \Omega t, \quad t' = t. \tag{2.21}$$

Thereupon, the covariance of the metric and the four-potential imply the following transformation laws:

$$f' = f\left[(1 + \Omega a)^2 - \Omega^2 W^2 f^{-2}\right], \quad (1 - \Omega a') f' = (1 + \Omega a) f, \tag{2.22a}$$

$$\frac{h'}{f'} = \frac{h}{f}, \quad W' = W, \tag{2.22b}$$

$$A'_{\varphi'} = A_\varphi, \quad A'_t = \Omega A_\varphi + A_t. \tag{2.22c}$$

Note that with eq. (2.22) the line element (2.1) retains its form. An immediate consequence of the transformation law for f is that the function $\mathcal{V}$ coincides with the co-rotating potential U':

$$\mathcal{V} = U'. \tag{2.23}$$

Notice, furthermore, that the four-velocity

$$u^i = \left(0, 0, \Omega e^{-\mathcal{V}}, e^{-\mathcal{V}}\right) = \left(0, 0, \Omega e^{-U'}, e^{-U'}\right), \tag{2.24}$$

see eq. (2.16), takes the simple form

$$u'^i = \left(0, 0, 0, e^{-\mathcal{V}}\right) = \left(0, 0, 0, e^{-U'}\right) \tag{2.25}$$

in the co-rotating frame.

2.2 Energy-momentum tensor

There are two contributions to the energy-momentum tensor of the charged rotating disc of dust. On one hand we have the perfect fluid part with

$$T_{ab}^{(\mathrm{dust})} = \mu u_a u_b \tag{2.26}$$

and on the other hand the electromagnetic part with

$$T_{ab}^{(\mathrm{em})} = \frac{1}{4\pi}\left(F_{ac}F_b{}^c - \frac{1}{4}g_{ab}F_{cd}F^{cd}\right). \tag{2.27}$$

2 Formulation of the disc problem within Einstein-Maxwell theory

Note that μ is the energy or mass density here and dust has zero pressure. Due to the rigidly rotating charged dust, with purely convective currents, both contributions can simply be added.[5] The total energy-momentum tensor for the disc thus reads:

$$
\begin{aligned}
T_{ab} &= T_{ab}^{(\mathrm{dust})} + T_{ab}^{(\mathrm{em})} \\
&= \mu u_a u_b + \frac{1}{4\pi}\left(F_{ac}F_b{}^c - \frac{1}{4}g_{ab}F_{cd}F^{cd}\right).
\end{aligned}
\tag{2.28}
$$

It should be noted that outside of the disc there is electro-vacuum and the only contribution to the energy-momentum tensor comes from the electromagnetic part, since $\mu = 0$ there.

As the electromagnetic energy-momentum tensor is traceless, the trace of T_{ab}, using $u^i u_i = -1$, is simply:

$$
T := T^a{}_a = g_{ab}T^{ab} = -\mu.
\tag{2.29}
$$

Of course, local energy-momentum conservation must be fulfilled in the disc:

$$
T^{ab}{}_{;b} = 0.
\tag{2.30}
$$

The Lorentz force density is given by[6]

$$
f_L^a := F^{ab}j_b = -T^{(\mathrm{em})\,ab}{}_{;b}.
\tag{2.31}
$$

For the energy-momentum conservation law therefore follows[7]:

$$
\mu_{;b}u^a u^b + \mu u^a{}_{;b}u^b + \mu u^a u^b{}_{;b} - f_L^a = 0.
\tag{2.32}
$$

It can easily be checked (using the antisymmetry of the field strength tensor) that the Lorentz force density is perpendicular to the four-velocity:

$$
f_L^a u_a = 0.
\tag{2.33}
$$

Applying $-u_a$ to eq. (2.32), using eq. (2.33), results in:

$$
(\mu u^a)_{;a} = 0.
\tag{2.34}
$$

This is the local mass conservation law or, in other words, due to the constant specific

---

[5]In general, this is not true.

[6]For the second equality one has make use of the Maxwell equations.

[7]Generally, the hydrodynamic energy-momentum balance equation is $T^{(\mathrm{perfect\ fluid})\,ab}{}_{;b} = f^a$, where f^a is an external force density. In case of the charged rotating disc of dust, the only acting force is the Lorentz force: $f^a = f_L^a$. Thus, together with the electromagnetic balance equation, $T^{(\mathrm{em})\,ab}{}_{;b} = -f_L^a$, one evidently obtains $T^{ab}{}_{;b} = 0$.

charge ϵ, this is equally also the continuity equation[8]:

$$j^a{}_{;a} = 0 \,. \tag{2.35}$$

Due to eq. (2.34), we can identify (as claimed in the previous section) the mass (or energy) density with the baryonic mass density.[9] Nevertheless, the baryonic mass does not agree with the gravitational mass, of course![10]

By applying the projection tensor $h_{ca} := g_{ca} + u_c u_a$ to eq. (2.32) we obtain:

$$\frac{\mathrm{D}u^a}{\mathrm{d}\tau} = \epsilon F^{ab} u_b \,, \tag{2.36}$$

where $\frac{\mathrm{D}u^a}{\mathrm{d}\tau} = u^a{}_{;b} u^b$ and $u^a = \frac{\mathrm{d}x^a}{\mathrm{d}\tau}$. As a result, the charged dust particles move under the influence of gravity and the Lorentz force. In the limit of vanishing charge ($\epsilon = 0$), the dust particles move along geodesics.

2.3 Boundary value problem

Expressed in terms of Lewis-Papapetrou coordinates $(\rho, \zeta, \varphi, t)$, the domain of the charged disc of dust (with coordinate radius ρ_0) is the following two-dimensional surface Σ_2,

$$\Sigma_2 : \quad \zeta = 0 \quad (0 \leq \rho \leq \rho_0) \,, \quad t = \mathrm{const.}\,. \tag{2.37}$$

The central equations describing the problem of a rotating disc made of charged dust in the framework of general relativity are, of course, the Einstein equations

$$R_{ab} - \frac{1}{2} R \, g_{ab} = 8\pi T_{ab} \,, \tag{2.38}$$

where R_{ab} and R are the Ricci-tensor and the Ricci-scalar, respectively, and the covariant Maxwell equations

$$F^{ab}{}_{;b} = 4\pi j^a \,. \tag{2.39}$$

Those are coupled via the metric tensor g_{ab}.

Using eq. (2.29), the Einstein equations can equally be written in the form

$$R_{ab} = 8\pi \left(T_{ab} + \frac{1}{2} \mu g_{ab} \right) \,. \tag{2.40}$$

Based on the Lewis-Papapetrou metric, eq. (2.1), one can evaluate eq. (2.40) (or

---

[8]The continuity equation also follows from the Maxwell equations, of course.

[9]This simply means that for dust the internal energy density is zero.

[10]Note that also the gravitational binding energy and the electromagnetic field energy contribute to the gravitational mass.

equally eq. (2.38)) and eq. (2.39) and explicitly write down the resulting coupled Einstein-Maxwell equations.

One of the electro-vacuum equations one finds is (see also [12] and [22]):

$$W_{,\rho\rho} + W_{,\zeta\zeta} = 0\,. \tag{2.41}$$

Obviously, if eq. (2.41) holds, so does

$$\tilde{W}_{,\rho\rho} + \tilde{W}_{,\zeta\zeta} = 0\,, \quad \text{with} \quad \tilde{W} := W - \rho\,. \tag{2.42}$$

Given eqs. (2.8) and (2.13) and another boundary condition, which can be derived from eq. (2.42) for the domain of the disc (by means of a "pill-box integration"[11], details follow later), we get:

$$\rho = 0: \qquad \tilde{W} = 0\,, \tag{2.43a}$$
$$\rho^2 + \zeta^2 \to \infty: \quad \tilde{W} \to 0\,, \tag{2.43b}$$
$$\Sigma_2: \qquad \tilde{W}_{,\zeta}\big|_{\zeta=0^\pm} = 0\,. \tag{2.43c}$$

The only possible solution of the Laplace equation eq. (2.42) that is regular and fulfils all conditions (2.43) is $\tilde{W} \equiv 0$, i.e.

$$W \equiv \rho\,. \tag{2.44}$$

As a consequence, the line element can be expressed globally in terms of Weyl-Lewis-Papapetrou coordinates:

$$ds^2 = f^{-1}\left[h\left(d\rho^2 + d\zeta^2\right) + \rho^2 d\varphi^2\right] - f\left(dt + a\,d\varphi\right)^2\,. \tag{2.45}$$

In the electro-vacuum domain this can always be achieved, however, for the rigidly rotating disc of charged dust the Weyl-Lewis-Papapetrou coordinates can even be introduced globally.[12]

To simplify further calculations we set $W = \rho$ from now on. Recall that $f = e^{2U}$ and $h = e^{2k}$. The remaining Einstein-Maxwell equations, expressed in the co-rotating

---

[11]Notice that $\tilde{W}_{,\rho\rho} + \tilde{W}_{,\zeta\zeta} = 0$ is equivalent to $\nabla \cdot \left(\rho^{-1}\nabla\tilde{W}\right) = 0$.

[12]The same is true for the uncharged rotating disc of dust.

frame, are as follows (see also [8] and [22]):

$$0 = \nabla \cdot \left[\frac{1}{\rho^2} e^{2U'} \left(\nabla A'_{\varphi'} - a' \nabla A'_t \right) \right] , \tag{2.46a}$$

$$4\pi\epsilon\sigma e^{-U'}\delta(\zeta) = \nabla \cdot \left[\frac{1}{\rho^2} e^{2U'} a' \left(\nabla A'_{\varphi'} - a' \nabla A'_t \right) + e^{-2U'} \nabla A'_t \right] , \tag{2.46b}$$

$$0 = \nabla \cdot \left[\frac{1}{\rho^2} e^{4U'} \nabla a' - \frac{4}{\rho^2} e^{2U'} A'_t \left(\nabla A'_{\varphi'} - a' \nabla A'_t \right) \right] , \tag{2.46c}$$

$$4\pi\sigma\delta(\zeta) = \Delta U' + \frac{1}{2\rho^2} e^{4U'} \left(\nabla a' \right)^2 - e^{-2U'} \left(\nabla A'_t \right)^2 - \frac{1}{\rho^2} e^{2U'} \left(\nabla A'_{\varphi'} - a' \nabla A'_t \right)^2 , \tag{2.46d}$$

$$k'_{,\rho} = \rho \left[\left(U'_{,\rho} \right)^2 - \left(U'_{,\zeta} \right)^2 \right] - \frac{1}{4\rho} e^{4U'} \left[\left(a'_{,\rho} \right)^2 - \left(a'_{,\zeta} \right)^2 \right] + \frac{1}{\rho} e^{2U'} \left[\left(A'_{\varphi',\rho} \right)^2 - \left(A'_{\varphi',\zeta} \right)^2 \right]$$
$$- \frac{1}{\rho} e^{-2U'} \left(\rho^2 - e^{4U'} a'^2 \right) \left[\left(A'_{t,\rho} \right)^2 - \left(A'_{t,\zeta} \right)^2 \right] - \frac{2}{\rho} e^{2U'} a' \left(A'_{\varphi',\rho} A'_{t,\rho} - A'_{\varphi',\zeta} A'_{t,\zeta} \right) , \tag{2.46e}$$

$$k'_{,\zeta} = 2\rho U'_{,\rho} U'_{\zeta} - \frac{1}{2\rho} e^{4U'} a'_{,\rho} a'_{,\zeta} + \frac{2}{\rho} e^{2U'} \left(A'_{\varphi',\rho} - a' A'_{t,\rho} \right) \left(A'_{\varphi',\zeta} - a' A'_{t,\zeta} \right)$$
$$- 2\rho e^{-2U'} A'_{t,\rho} A'_{t,\zeta} , \tag{2.46f}$$

where ∇ and Δ are meant as operators in 3-dimensional Euclidean space, with cylindrical coordinates ρ, ζ and φ, acting on φ-independent functions. In particular, for functions $f_1 = f_1(\rho, \zeta)$, $f_2 = f_2(\rho, \zeta)$ and a vector $\boldsymbol{F} = (F_\rho(\rho, \zeta), F_\zeta(\rho, \zeta), F_\varphi(\rho, \zeta))$ holds:

$$\Delta f_1 = \nabla \cdot \nabla f_1 = \left(\partial_\rho^2 + \frac{1}{\rho} \partial_\rho + \partial_\zeta^2 \right) f_1 , \tag{2.47}$$

$$\nabla f_1 \cdot \nabla f_2 = \partial_\rho f_1 \partial_\rho f_2 + \partial_\zeta f_1 \partial_\zeta f_2 , \tag{2.48}$$

$$\nabla \cdot \boldsymbol{F} = \frac{1}{\rho} \partial_\rho \left(\rho F_\rho \right) + \partial_\zeta F_\zeta . \tag{2.49}$$

Of the above equations, the first two, eqs. (2.46a) and (2.46b), are the Maxwell equations and the remaining, eqs. (2.46c) to (2.46f), are the Einstein equations. Strictly speaking, however, eq. (2.46c) is not a "pure" Einstein equation, since eq. (2.46a) was used to write it in the present form.

On the left hand side of equation (2.46a), $-4\pi\epsilon\sigma u'^\varphi \delta(\zeta)$ is actually written, where $u'^\varphi = 0$ in the co-rotating frame. In the non-rotating frame, $u^\varphi \neq 0$, however! Correspondingly in (2.46c) the left hand side actually reads $16\pi\epsilon\sigma u'^\varphi A'_t \delta(\zeta)$.

By restoring the left hand sides of eqs. (2.46a) and (2.46c) accordingly, eqs. (2.46a) to (2.46f) can trivially be transformed to the non-rotating frame by simply removing the primes from all the quantities, due to the covariance of the Einstein-Maxwell equations.

In the electro-vacuum region, however, both in the co-rotating and the non-rotating

frame all left hand sides of (2.46a) to (2.46d) vanish, since σ is identical to zero there.

Using eq. (2.49), we can rewrite the first of the above listed Einstein-Maxwell equation, eq. (2.46a), as

$$0 = \left[\frac{1}{\rho} e^{2U'} \left(A'_{\varphi',\rho} - a' A'_{t,\rho} \right) \right]_{,\rho} + \left[\frac{1}{\rho} e^{2U'} \left(A'_{\varphi',\zeta} - a' A'_{t,\zeta} \right) \right]_{,\zeta} . \qquad (2.50)$$

This equation can be read as an integrability condition for a potential β' defined via

$$\beta'_{,\rho} = \frac{1}{\rho} e^{2U'} \left(A'_{\varphi',\zeta} - a' A'_{t,\zeta} \right) , \quad \beta'_{,\zeta} = -\frac{1}{\rho} e^{2U'} \left(A'_{\varphi',\rho} - a' A'_{t,\rho} \right) . \qquad (2.51)$$

Accordingly, eq. (2.46c) can be put into the form

$$0 = \left[\frac{1}{\rho} e^{4U'} a'_{,\rho} - 2 \left(A'_{t,\zeta} \beta' - A'_t \beta'_{,\zeta} \right) \right]_{,\rho} + \left[\frac{1}{\rho} e^{4U'} a'_{,\zeta} + 2 \left(A'_{t,\rho} \beta' - A'_t \beta'_{,\rho} \right) \right]_{,\zeta} \qquad (2.52)$$

motivating the introduction of a new potential b' defined by

$$b'_{,\rho} = -\frac{1}{\rho} e^{4U'} a'_{,\zeta} - 2 \left(A'_{t,\rho} \beta' - A'_t \beta'_{,\rho} \right) , \quad b'_{,\zeta} = \frac{1}{\rho} e^{4U'} a'_{,\rho} - 2 \left(A'_{t,\zeta} \beta' - A'_t \beta'_{,\zeta} \right) . \qquad (2.53)$$

Note that the defining equations for β' and b', eqs. (2.51) and (2.53), expressed in the co-rotating frame are valid globally, i.e. for both the disc and the electro-vacuum regime. However, in the non-rotating frame these equations only hold in electro-vacuum. They, furthermore, retain their form by transforming to the non-rotating frame.

For the following discussion, the idea is now to bring the electro-vacuum Einstein-Maxwell equations into a more elegant form, utilizing the newly introduced potentials β and b, and to derive boundary value conditions for the domain of the disc. In other words, we want to reduce the disc problem to a boundary value problem for the electro-vacuum Einstein-Maxwell equations.

Starting with the electro-vacuum equations, we introduce the so-called Ernst potentials

$$\mathcal{E} = \left(f - |\Phi|^2 \right) + \mathrm{i} b \quad \text{and} \quad \Phi = \alpha + \mathrm{i} \beta , \qquad (2.54)$$

with $\alpha := -A_t$. Now it can be shown that for axistationary spacetimes the coupled Einstein-Maxwell equations in electro-vacuum, more specifically eqs. (2.46a) to (2.46d), can be reduced to the Ernst equations [23]:

$$\left(\mathrm{Re}\,\mathcal{E} + |\Phi|^2 \right) \Delta \mathcal{E} = \left(\nabla \mathcal{E} + 2\bar{\Phi} \nabla \Phi \right) \cdot \nabla \mathcal{E} , \qquad (2.55\mathrm{a})$$

$$\left(\mathrm{Re}\,\mathcal{E} + |\Phi|^2 \right) \Delta \Phi = \left(\nabla \mathcal{E} + 2\bar{\Phi} \nabla \Phi \right) \cdot \nabla \Phi . \qquad (2.55\mathrm{b})$$

The Ernst equations (as they are derived from the Einstein-Maxwell equations) are covariant and thus retain their form in the co-rotating frame.

Once the solutions to the Ernst equations are available, eqs. (2.51) and (2.53) (in the non-rotating frame) may be used to obtain a and A_φ by a path-independent line integration. The metric function $h = e^{2k}$ can then be determined by a path-independent line integration, using eq. (2.46e) or (2.46f) (in the non-rotating frame), from the other functions as well.

Next, we derive boundary conditions for the domain of the disc, Σ_2. To do this, we first need to discuss reflection symmetry. Obviously, the reflection symmetric nature of the disc problem must be reflected in the metric functions and consequently, via the inhomogeneous Maxwell equation (2.46b), also in the electromagnetic four-potential:

$$f(\rho, -\zeta) = f(\rho, \zeta)\,, \quad a(\rho, -\zeta) = a(\rho, \zeta)\,, \quad h(\rho, -\zeta) = h(\rho, \zeta)\,, \qquad (2.56)$$

$$A_\varphi(\rho, -\zeta) = A_\varphi(\rho, \zeta)\,, \quad A_t(\rho, -\zeta) = A_t(\rho, \zeta)\,. \qquad (2.57)$$

Their derivatives with respect to ζ are odd functions in ζ. Based on eqs. (2.51) and (2.53), this therefore also applies to the potentials β and b:

$$\beta(\rho, -\zeta) = -\beta(\rho, \zeta)\,, \quad b(\rho, -\zeta) = -b(\rho, \zeta)\,. \qquad (2.58)$$

For the complex Ernst potentials then follows:

$$\mathcal{E}(\rho, -\zeta) = \bar{\mathcal{E}}(\rho, \zeta)\,, \quad \Phi(\rho, -\zeta) = \bar{\Phi}(\rho, \zeta)\,, \qquad (2.59)$$

where the bar denotes complex conjugation. Notice that reflection symmetry translates (via the transformation laws) to the co-rotating metric functions and potentials as well.

In the limit $\zeta \to 0$, eqs. (2.56) and (2.57) imply continuity of the metric functions and the electromagnetic four-potential:

$$\{f, a, h, A_\varphi, A_t\}\big|_{\zeta=0^+} = \{f, a, h, A_\varphi, A_t\}\big|_{\zeta=0^-}\,. \qquad (2.60)$$

Whereas their normal derivatives have a jump on the disc layer Σ_2:

$$\{f_{,\zeta}, a_{,\zeta}, h_{,\zeta}, A_{\varphi,\zeta}, A_{t,\zeta}\}\big|_{\zeta=0^+} = -\{f_{,\zeta}, a_{,\zeta}, h_{,\zeta}, A_{\varphi,\zeta}, A_{t,\zeta}\}\big|_{\zeta=0^-}\,. \qquad (2.61)$$

In the electro-vacuum regime their normal derivatives vanish at $\zeta = 0$, however! (These statements about the limiting behaviour for $\zeta \to 0^\pm$ stay valid in the co-rotating frame.)

Analogous to the procedure for surface charge densities in electrostatics, we can derive junction conditions via a so-called "pill-box integration" of the Einstein-Maxwell equations. For this an integration over a small cylinder centred around a section on the disc surface is performed. By applying Gauss's theorem the volume integral can be reduced to an integration over the surface of the cylinder. In the limiting case where

the height of the cylinder shrinks to zero and its upper side encloses the disc from above and its lower side encloses it from below the only remaining contributions to the surface integral come from the area elements above and below the disc, $\mathrm{d}\boldsymbol{A}^{(\text{above})} = \mathrm{d}A\,\boldsymbol{n}$ and $\mathrm{d}\boldsymbol{A}^{(\text{below})} = \mathrm{d}A\,(-\boldsymbol{n})$, respectively. The unit normal vectors to the area elements, $\pm\boldsymbol{n}$, point in $\pm\zeta$-direction ($n_i = e^{U-k}\delta_i^\zeta$) and thus single out the ζ-component of the integrand.[13]

Performing such a "pill-box integration" of the first Einstein-Maxwell equation, eq. (2.46a), therefore delivers the following junction condition:

$$0 = \left(A'_{\varphi',\zeta} - a' A'_{t,\zeta} \right)\big|_{\zeta=0^+} - \left(A'_{\varphi',\zeta} - a' A'_{t,\zeta} \right)\big|_{\zeta=0^-} . \tag{2.62}$$

Alternatively, one can simply integrate eq. (2.46a) over an infinitesimal ζ-interval from $-\delta$ to $+\delta$, with $\delta \to 0$, to obtain the above junction condition. With the help of reflection symmetry we can state:

$$\zeta = 0 : \quad \left(A'_{\varphi',\zeta} - a' A'_{t,\zeta} \right)\big|_{\zeta=0} = 0 , \tag{2.63}$$

where "$\zeta = 0$" should indicate that this boundary condition holds in the entire ζ-plane, including the disc (Σ_2) and the domain beyond it ($\rho > \rho_0, \zeta = 0$).

Similarly, we obtain from eq. (2.46c) via a "pill-box integration" (or by means of $\lim_{\delta\to0}\int_{-\delta}^{+\delta}\mathrm{d}\zeta$) and reflection symmetry:

$$\zeta = 0 : \quad a'_{,\zeta}\big|_{\zeta=0} = 0 . \tag{2.64}$$

To arrive at eq. (2.64), eq. (2.63) was also used.

From eq. (2.46d) one can derive (with eqs. (2.63) and (2.64)) the boundary condition

$$\Sigma_2 : \quad U'_{,\zeta}\big|_{\zeta=0^\pm} = \pm 2\pi\sigma . \tag{2.65}$$

This means that the surface mass density σ is determined by the jump of the normal derivative of the co-rotating potential U' and cannot be chosen freely. At the rim of the disc ($\rho = \rho_0, \zeta = 0$), the surface mass density has to be regular. As it turns out, this regularity condition causes the surface mass density σ to vanish at the rim.

The second Einstein-Maxwell equation, eq. (2.46b), (together with eq. (2.63) and (2.65)) implies

$$\Sigma_2 : \quad \left(A'_t - \epsilon e^{U'} \right)_{,\zeta}\bigg|_{\zeta=0} = 0 . \tag{2.66}$$

A little detour back to $R_{11} = 8\pi(T_{11} - \frac{1}{2}Tg_{11})$ reveals (using eq. (2.65)) another

---

[13]The unit normal vector to a hypersurface characterized by $\mathcal{F}(x^i) = 0$ is defined as: $n_i = \dfrac{\mathcal{F}_{,i}}{\sqrt{|g^{kl}\mathcal{F}_{,k}\mathcal{F}_{,l}|}}$.
Here, $\mathcal{F} = \zeta = 0$.

boundary condition:

$$\zeta = 0: \quad k'_{,\zeta}\big|_{\zeta=0} = 0. \tag{2.67}$$

Finally, eq. (2.46f) (with the help of eqs. (2.63), (2.64), (2.66) and (2.67)) delivers a sixth boundary condition:

$$\Sigma_2: \quad \left(e^{U'} - \epsilon A'_t\right)_{,\rho}\Big|_{\zeta=0} = 0. \tag{2.68}$$

Based on the definitions of the introduced potentials β and b, we can also immediately infer from eqs. (2.63) and (2.64) that

$$\zeta = 0: \quad \beta'_{,\rho}\big|_{\zeta=0} = 0 \quad \text{and} \quad b'_{,\rho}\big|_{\zeta=0} = 0. \tag{2.69}$$

Choosing the integration constants to be zero, such that continuity at $\rho = \rho_0$ is ensured, as β and b are odd functions in ζ, thus implies

$$\zeta = 0: \quad \beta'\big|_{\zeta=0} = 0 \quad \text{and} \quad b'\big|_{\zeta=0} = 0. \tag{2.70}$$

This concludes the derivation of the boundary conditions from the Einstein-Maxwell equations in the co-rotating frame.

In summary, the Ernst equations (2.55) together with the (in this regard relevant) boundary conditions on the disc,

$$\Sigma_2: \quad b'\big|_{\zeta=0} = 0, \quad \beta'\big|_{\zeta=0} = 0, \quad \left(e^{U'} - \epsilon A'_t\right)_{,\rho}\Big|_{\zeta=0} = 0, \quad \left(A'_t - \epsilon e^{U'}\right)_{,\zeta}\Big|_{\zeta=0} = 0, \tag{2.71}$$

as well as the condition of asymptotic flatness (which means for the Ernst potentials that $\mathcal{E} \to 1$ and $\Phi \to 0$ for $\rho^2 + \zeta^2 \to \infty$) and the regularity condition of the surface mass density at the rim of the disc, form a well-defined boundary value problem for the charged rotating disc of dust (see also [8, 14]).

As already mentioned before, once the solution to the boundary value problem is determined, the functions a, A_φ and $h = e^{2k}$ can be calculated from the found Ernst potentials $\mathcal{E}$ and Φ by a path-independent line integration.

Physically, the first two boundary conditions of eq. (2.71) together ensure that there is no local surface mass flux density and surface current density in the co-rotating frame (i.e. there are only purely convective currents) [22]. The third boundary condition of eq. (2.71) represents the ρ-component of the equation of motion (2.36). Moreover, in the Newtonian limit holds $U' = U - \frac{1}{2}\Omega^2\rho^2$ and $A'_t = A_t = -U^{\mathrm{E}}$, where U is the gravitational and U^{E} the electric potential. Thus, the third boundary condition of

eq. (2.71) reduces in the Newtonian limit to

$$\epsilon U^{\mathrm{E}}{}_{,\rho} = -\left(U - \frac{1}{2}\Omega^2\rho^2\right)_{,\rho}. \tag{2.72}$$

Each dust particle in the disc is therefore in an equilibrium of electric, gravitational and centrifugal force. (Further details follow in subsections 5.2.2 and 6.4.2). Finally, the last boundary condition of eq. (2.71) establishes a relationship between the surface charge density and the surface mass density, which results from the introduction of the constant specific charge $\epsilon = \frac{\rho_{\mathrm{el}}}{\mu}$ (see also [22]).

2.4 Inverse scattering method

The "inverse scattering method" or "inverse scattering transform" is a powerful tool for solving nonlinear partial differential equations that was developed in the context of soliton theory. A general introduction to the method can be found, e.g., in [24]. Within soliton theory, it can be used to tackle initial value problems for nonlinear partial differential equations of the so-called AKNS class [25]. The method was first applied to the Korteweg-de Vries equation (which belongs to the AKNS class):

$$q_{,t} + q_{,xxx} + 6qq_{,x} = 0. \tag{2.73}$$

An essential requirement for the method is that there is a linear problem,

$$\mathbf{Y}_{,x} = \mathbf{U}\mathbf{Y}, \tag{2.74a}$$

$$\mathbf{Y}_{,t} = \mathbf{V}\mathbf{Y}, \tag{2.74b}$$

with a corresponding integrability condition $\mathbf{Y}_{,xt} = \mathbf{Y}_{,tx}$ that is equivalent to the nonlinear partial differential equation. $\mathbf{Y}$, $\mathbf{U}$ and $\mathbf{V}$ are matrices in general and they are functions of the coordinates x and t and a spectral parameter k.[14] Instead of solving the nonlinear partial differential equation directly - which might be very difficult or even impossible - it can thus be translated to a linear problem. Typically, it is comparatively much easier to gain a solution on the level of the linear problem. The solution can then be transformed back to the original nonlinear partial differential equation. In this sense, the inverse scattering method can be understood schematically as a nonlinear analogue of the Fourier transform.[15]

In the specific case of the Korteweg-de Vries equation, the associated linear problem is such that it implies the one-dimensional time-independent Schrödinger equation,

---

[14]The matrix $\mathbf{U}$ of the linear problem and the metric potential U (where $f = e^{2U}$) should not be confused.

[15]Another method from soliton theory with a similar procedure is the Bäcklund transformation.

where $-q(x,0)$ is the potential and k^2 the energy. (Note, however, that the parameter t has nothing to do with the time coordinate from quantum mechanics.) It is a standard problem of quantum mechanics to derive the corresponding "scattering data" from the potential. This can then be evolved in time. Finally, $q(x,t)$ can be determined from the (time-evolved) scattering data via the solution of the Gel'fand-Levitan-Marchenko integral equation, representing the inverse problem (i.e. the back transformation). The term "inverse scattering method" goes back to the described solution procedure for the initial value problem of the Korteweg-de Vries equation.

In case of axisymmetry and stationarity, the inverse scattering method can also be applied to boundary value problems for the exterior Einstein and Einstein-Maxwell equations. For the former, see e.g. [26] and [27].

The linear problem for a boundary value problem within Einstein-Maxwell theory can be stated in the following form [15]:

$$\mathbf{Y}_{,z} = \left\{ \begin{pmatrix} b_1 & 0 & c_1 \\ 0 & a_1 & 0 \\ d_1 & 0 & 0 \end{pmatrix} + \lambda \begin{pmatrix} 0 & b_1 & 0 \\ a_1 & 0 & -c_1 \\ 0 & d_1 & 0 \end{pmatrix} \right\} \mathbf{Y} , \tag{2.75a}$$

$$\mathbf{Y}_{,\bar{z}} = \left\{ \begin{pmatrix} b_2 & 0 & c_2 \\ 0 & a_2 & 0 \\ d_2 & 0 & 0 \end{pmatrix} + \frac{1}{\lambda} \begin{pmatrix} 0 & b_2 & 0 \\ a_2 & 0 & -c_2 \\ 0 & d_2 & 0 \end{pmatrix} \right\} \mathbf{Y} , \tag{2.75b}$$

with

$$a_1 = \bar{b}_2 = \frac{\mathcal{E}_{,z} + 2\bar{\Phi}\,\Phi_{,z}}{2f} , \quad a_2 = \bar{b}_1 = \frac{\mathcal{E}_{,\bar{z}} + 2\bar{\Phi}\,\Phi_{,\bar{z}}}{2f} , \tag{2.76}$$

$$c_1 = f\bar{d}_2 = \Phi_{,z} , \quad c_2 = f\bar{d}_1 = \Phi_{,\bar{z}} , \tag{2.77}$$

$$\lambda = \sqrt{\frac{K - \mathrm{i}\bar{z}}{K + \mathrm{i}z}} \tag{2.78}$$

and complex coordinates

$$z = \rho + \mathrm{i}\zeta , \quad \bar{z} = \rho - \mathrm{i}\zeta . \tag{2.79}$$

Here, the 3×3-matrix $\mathbf{Y}$ depends on z, $\bar{z}$ and λ and the complex parameter K is the spectral parameter. This is a modified version of the linear problem published by Neugebauer and Kramer [28].

It can be shown that the integrability condition $\mathbf{Y}_{,z\bar{z}} = \mathbf{Y}_{,\bar{z}z}$ is indeed equivalent to the Ernst equations (2.55) [15, 28]. On the other hand, if $\mathcal{E}$ and Φ solve the Ernst equations, $\mathbf{Y}_{,z\bar{z}} = \mathbf{Y}_{,\bar{z}z}$ holds and thus $\mathbf{Y}$ does not depend on the integration path. The general idea is now to derive $\mathbf{Y}$ as a holomorphic function in λ (or alternatively in K) and subsequently to deduce the entries of the matrices $\mathbf{U} = \mathbf{Y}^{-1}\mathbf{Y}_{,z}$ and $\mathbf{V} = \mathbf{Y}^{-1}\mathbf{Y}_{,\bar{z}}$.

2 Formulation of the disc problem within Einstein-Maxwell theory

They then reveal the solutions for the Ernst potentials $\mathcal{E}$ and Φ [12, 26].[16]

A first step in order to solve the boundary value problem of the charged rotating disc of dust[17] is to integrate the linear problem along the path $\mathcal{A}^+\mathcal{C}\mathcal{A}^-$ to determine a general[18] solution for $\mathbf{Y}$ on $\mathcal{A}^\pm$, where $\mathcal{A}^\pm$ denotes the upper/lower part of the symmetry axis $\mathcal{A}$ and $\mathcal{C}$ represents spatial infinity, see fig. 2.2. A useful, resulting property is that the holomorphic structure of $\mathbf{Y}(z, \bar{z}, \lambda)$ in fact remains unchanged by an analytic extension to the entire ρ, ζ-plane (with $0 \leq \rho \leq \rho_0$, $\zeta = 0$ being excluded). This gives the solution of the Ernst potentials $\mathcal{E}$ and Φ in the entire electro-vacuum region in the end.
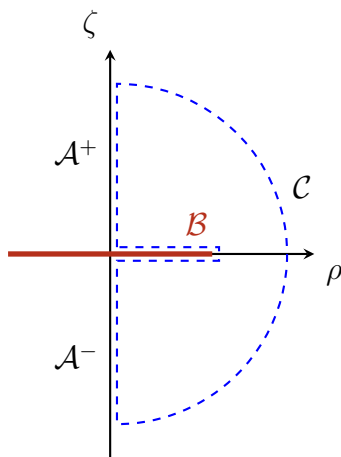

Figure 2.2: Integration of the linear problem along the path $\mathcal{A}^+\mathcal{C}\mathcal{A}^-\mathcal{B}$ (after [12]).

In the second step, the integration of the linear problem has to be performed along the surface of the disc, $\mathcal{B}$, defined by $\rho \leq \rho_0$, $\zeta = 0^\pm$. Here, the information about the boundary values of the disc is incorporated into the solution. However, this alone is not sufficient to determine the coefficients in the linear problem. Due to the fact that the domain of the disc is a non-(electro-)vacuum region, for which the Ernst equations are not valid, the linear problem fails at $\rho \leq \rho_0$, $\zeta = 0$. This implies that $\mathbf{Y}$ jumps along the contours $\Gamma_{u/l} : \operatorname{Re} K = 0$, $-\rho_0 \leq \operatorname{Im} K \leq \rho_0$ in the upper/lower sheet of the two-sheeted Riemann K-surface, see fig. 2.3.[19] Off the contour(s), $\mathbf{Y}$ is a regular

---

[16]In fact (in a specific case), one may not even need to determine the solution for $\mathbf{Y}$ completely, instead one can simply discuss $\mathbf{Y}$ as a holomorphic function in λ (or K) and then calculate the entries of $\mathbf{U}$ and $\mathbf{V}$ directly.

[17]Due to the generally similar procedure for solving the boundary value problem, the remainder of this section is partly orientated on [12, 26].

[18]This step does not yet involve any specific knowledge about the body.

[19]Note that $\lambda = \sqrt{\frac{K - \mathrm{i}\bar{z}}{K + \mathrm{i}z}}$ is double-valued.

function in K. Therefore, $\mathbf{Y}$ satisfies the (general) Riemann-Hilbert problem:

$$
\begin{aligned}
K \in \Gamma_{\mathrm{u}} : \quad & \mathbf{Y}_- = \mathbf{Y}_+ \mathcal{D}_{\mathrm{u}}(K) \,, \\
K \in \Gamma_{\mathrm{l}} : \quad & \mathbf{Y}_- = \mathbf{Y}_+ \mathcal{D}_{\mathrm{l}}(K) \,, \\
K \notin \Gamma_{\mathrm{u/l}} : \quad & \mathbf{Y} \text{ analytic in } K \,,
\end{aligned}
\tag{2.80}
$$

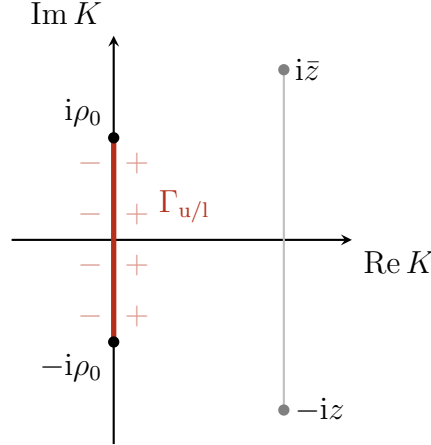where $\mp$ specifies the left and right side of the contour(s), respectively.

Figure 2.3: Two-sheeted K-surface with the contour(s) $\Gamma_{\mathrm{u/l}}$ and branch points $\mathrm{i}\bar{z}$ and $-\mathrm{i}z$ (after [29]).

By choosing the branch points as $K_{\mathrm{B}} = \pm\mathrm{i}\rho_0$, the corresponding branch cut between the two branch points coincides with contours $\Gamma_{\mathrm{u/l}}$, which thus merge into one contour Γ. Ideally, based on the linear problem (and by also utilising reflection symmetry), a concrete Riemann-Hilbert problem for the charged rotating disc of dust can then be constructed.[20] Solving this Riemann-Hilbert problem leads to linear integral equations from which $\mathcal{E}$ and Φ can ultimately be gained.

Note that in this very brief overview of the inverse scattering method (with respect to both the Korteweg-de Vries equation and, in particular, to the charged rotating disc of dust), many technical and rather involved details are omitted.

In the case of the uncharged rotating disc of dust, the inverse scattering method could be applied successfully and an exact solution to the corresponding boundary value problem could be found [26, 29]. The solution is given in terms of hyperelliptic theta functions [6, 7].

However, transferring the solution procedure to the problem of the charged rotating disc of dust has not yet been successful. Unfortunately, it has not yet been possible to formulate an associated Riemann-Hilbert problem.

---

[20]The Riemann-Hilbert problem generally involves free functions that need to be fixed in such a way that the Riemann-Hilbert problem yields the same solution as the linear problem.

3 Post-Newtonian expansion

Although it has not yet been possible to successfully apply the inverse scattering method to the charged rotating disc of dust, the corresponding boundary value problem could be solved in terms of a post-Newtonian expansion up to tenth order [8, 9].

While an exact analytic solution might be more appealing from a mathematical point of view, in a lot of situations it is actually more practical to have a semi-analytic solution in terms of such an expansion.[12]

3.1 Relativity parameter

The post-Newtonian expansion used for the charged rotating disc of dust relies on a relativity parameter γ, originally introduced by Bardeen and Wagoner [30]:

$$\gamma := 1 - \sqrt{f_c}, \quad \text{with} \quad f_c := f(\rho = 0, \zeta = 0) \,. \tag{3.1}$$

Equivalently, γ can be expressed in terms of the redshift, z_c, of a photon emitted at $\rho = 0$, $\zeta = 0$ and observed at $\rho^2 + \zeta^2 \to \infty$:

$$\gamma = \frac{z_c}{1 + z_c} \,, \tag{3.2}$$

where $z_c = e^{-U_c} - 1$. From both expressions, (3.1) and (3.2), it is evident that γ takes values between 0 and 1. For $\gamma \ll 1$ one obtains a Newtonian solution and $\gamma \to 1$ corresponds to the ultra-relativistic limit in which we assume black hole formation [9]. It should be recalled that U, appearing in $f_c = e^{2U_c}$, can be interpreted as a generalized Newtonian potential (see also [8]).

The parameter space of the disc solution is spanned by $g \in [0, 1]$, $\epsilon \in [0, 1]$ and the coordinate radius ρ_0, where $g := \sqrt{\gamma}$. Why in fact g is the correct expansion parameter instead of γ will become clear in section 3.3. Without loss of generality we restrict to positive charges and ρ_0 serves as a scaling parameter. All physical parameters describing the disc, such as the angular velocity Ω, the gravitational mass M and the

---

[1]However, in order to make rigorous statements about a (presumed) black hole limit and in particular to prove that cosmic censorship indeed holds for the charged rotating disc of dust in an ultra-relativistic limit, one needs an exact solution.

[2]The discussion in this chapter partly follows [10] and [11].

angular momentum J, are functions of g, ϵ and ρ_0 only.[3]

3.2 Elliptic coordinates

A convenient choice of coordinates for solving the boundary value problem of the charged rotating disc of dust, derived in section 2.3, is given in terms of elliptic coordinates η and ν, defined through

$$\rho = \rho_0 \sqrt{\left(1 - \eta^2\right)\left(1 + \nu^2\right)}\,, \quad \zeta = \rho_0 \eta \nu\,, \tag{3.3}$$

with $\eta \in [-1, 1]$ and $\nu \in [0, \infty]$. Additionally normalizing all dimensioned quantities with suitable powers of ρ_0 leads to a dimensionless formulation of the disc problem. The normalized quantities are denoted by *, e.g.,

$$a^* = \frac{a}{\rho_0}\,, \quad A^*_\varphi = \frac{A_\varphi}{\rho_0} \quad \text{or} \quad \Omega^* = \rho_0\Omega\,.[4] \tag{3.4}$$

Note that in elliptical coordinates Δf_1 and $\nabla f_1 \cdot \nabla f_2$, where f_1 and f_2 are φ-independent functions, read:

$$\Delta f_1 = \nabla \cdot \nabla f_1 = \frac{1}{\rho_0^2 \left(\eta^2 + \nu^2\right)} \left[\left(1 - \eta^2\right)\partial_\eta^2 f_1 - 2\eta\partial_\eta f_1 + \left(1 + \nu^2\right)\partial_\nu^2 f_1 + 2\nu\partial_\nu f_1\right]\,, \tag{3.5}$$

$$\nabla f_1 \cdot \nabla f_2 = \frac{1 - \eta^2}{\rho_0^2 \left(\eta^2 + \nu^2\right)}\partial_\eta f_1 \partial_\eta f_2 + \frac{1 + \nu^2}{\rho_0^2 \left(\eta^2 + \nu^2\right)}\partial_\nu f_1 \partial_\nu f_2\,. \tag{3.6}$$

With eqs. (3.5) and (3.6) the Ernst equations (2.55) (in the non-rotating frame) take the form (see also [22][5]):

$$\left(\operatorname{Re}\mathcal{E} + |\Phi|^2\right)\left[\left(1 - \eta^2\right)\mathcal{E}_{,\eta\eta} - 2\eta\mathcal{E}_{,\eta} + \left(1 + \nu^2\right)\mathcal{E}_{,\nu\nu} + 2\nu\mathcal{E}_{,\nu}\right]$$
$$= \left(1 - \eta^2\right)\left(\mathcal{E}_{,\eta} + 2\bar{\Phi}\Phi_{,\eta}\right)\mathcal{E}_{,\eta} + \left(1 + \nu^2\right)\left(\mathcal{E}_{,\nu} + 2\bar{\Phi}\Phi_{,\nu}\right)\mathcal{E}_{,\nu}\,, \tag{3.7a}$$
$$\left(\operatorname{Re}\mathcal{E} + |\Phi|^2\right)\left[\left(1 - \eta^2\right)\Phi_{,\eta\eta} - 2\eta\Phi_{,\eta} + \left(1 + \nu^2\right)\Phi_{,\nu\nu} + 2\nu\Phi_{,\nu}\right]$$
$$= \left(1 - \eta^2\right)\left(\mathcal{E}_{,\eta} + 2\bar{\Phi}\Phi_{,\eta}\right)\Phi_{,\eta} + \left(1 + \nu^2\right)\left(\mathcal{E}_{,\nu} + 2\bar{\Phi}\Phi_{,\nu}\right)\Phi_{,\nu}\,. \tag{3.7b}$$

Additionally, the defining equations for the potentials β and b, eqs. (2.51) and (2.53),

---

[3]Alternatively, other dimensioned parameters such as the baryonic mass M_b, the gravitational mass M or the total proper radius R_0 (introduced in chapter 5) can be used as scaling parameter instead of the coordinate radius ρ_0. Rather unsuitable for our purposes is the angular velocity Ω, as it is often interesting to compare disc configurations with different rotation speeds.

[4]See also [8].

[5]There are typos in the reference [22] concerning the formulas expressed in elliptic coordinates.

read:

$$\left(1 - \eta^2\right) \beta_{,\eta} = -f \left(A^*_{\varphi,\nu} + a^* \alpha_{,\nu}\right) , \tag{3.8}$$

$$\left(1 + \nu^2\right) \beta_{,\nu} = f \left(A^*_{\varphi,\eta} + a^* \alpha_{,\eta}\right) \tag{3.9}$$

and

$$\left(1 - \eta^2\right) b_{,\eta} = f^2 a^*_{,\nu} - 2 \left(1 - \eta^2\right) \left(\alpha \beta_{,\eta} - \beta \alpha_{,\eta}\right) , \tag{3.10}$$

$$\left(1 + \nu^2\right) b_{,\nu} = -f^2 a^*_{,\eta} - 2 \left(1 + \nu^2\right) \left(\alpha \beta_{,\nu} - \beta \alpha_{,\nu}\right) . \tag{3.11}$$

In elliptical coordinates, the metric function $h = e^{2k}$ can be derived from

$$
\begin{aligned}
&\left(1 - \eta^2\right) \left(\eta^2 + \nu^2\right) k_{,\eta} \\
&= -\frac{1}{4f^2} \left(1 - \eta^2\right) \left(1 + \nu^2\right) \left[\eta \left(1 - \eta^2\right) \left(f_{,\eta}\right)^2 - \eta \left(1 + \nu^2\right) \left(f_{,\nu}\right)^2 - 2\nu \left(1 - \eta^2\right) f_{,\eta} f_{,\nu}\right] \\
&\quad + \frac{f^2}{4} \left[\eta \left(1 - \eta^2\right) \left(a^*_{,\eta}\right)^2 - \eta \left(1 + \nu^2\right) \left(a^*_{,\nu}\right)^2 - 2\nu \left(1 - \eta^2\right) a^*_{,\eta} a^*_{,\nu}\right] \\
&\quad - f \left[\eta \left(1 - \eta^2\right) \left(A^*_{\varphi,\eta}\right)^2 - \eta \left(1 + \nu^2\right) \left(A^*_{\varphi,\nu}\right)^2 - 2\nu \left(1 - \eta^2\right) A^*_{\varphi,\eta} A^*_{\varphi,\nu}\right] \\
&\quad + \frac{1}{f} \left[\left(1 - \eta^2\right) \left(1 + \nu^2\right) - f^2 a^{*2}\right] \\
&\qquad \cdot \left[\eta \left(1 - \eta^2\right) \left(A_{t,\eta}\right)^2 - \eta \left(1 + \nu^2\right) \left(A_{t,\nu}\right)^2 - 2\nu \left(1 - \eta^2\right) A_{t,\eta} A_{t,\nu}\right] \\
&\quad + 2fa^* \left[\eta \left(1 - \eta^2\right) A^*_{\varphi,\eta} A_{t,\eta} - \eta \left(1 + \nu^2\right) A^*_{\varphi,\nu} A_{t,\nu} - \nu \left(1 - \eta^2\right) \left(A^*_{\varphi,\eta} A_{t,\nu} + A^*_{\varphi,\nu} A_{t,\eta}\right)\right] .
\end{aligned}
\tag{3.12}
$$

Finally, the line element (2.45), expressed in elliptical coordinates, takes the form:

$$
\begin{aligned}
\mathrm{d}s^2 = f^{-1} &\left[\rho_0^2 \left(\eta^2 + \nu^2\right) h \left(\frac{\mathrm{d}\eta^2}{1 - \eta^2} + \frac{\mathrm{d}\nu^2}{1 + \nu^2}\right) + \rho_0^2 \left(1 - \eta^2\right) \left(1 + \nu^2\right) \mathrm{d}\varphi^2\right] \\
&- f \left(\mathrm{d}t + \rho_0 a^* \mathrm{d}\varphi\right)^2 .
\end{aligned}
\tag{3.13}
$$

where f, h and a^* are functions of η and ν now.

3.3 Expansion

As a starting point of the post-Newtonian expansion we utilize the relation

$$\gamma = -U_N(\rho = 0, \zeta = 0) = \frac{\Omega^{*\,2}_N}{1 - \epsilon^2} , \tag{3.14}$$

between the Newtonian potential U_N and the angular frequency Ω_N that holds in Newtonian limit only. A derivation of this relation follows in subsection 5.2.2. Beyond

the Newtonian limit we therefore get $\Omega^{*2} = (1 - \epsilon^2)\,\gamma + \mathcal{O}(\gamma^2)$. Expanding this relation implies that Ω^* is an odd function in $g := \sqrt{\gamma}$, i.e.

$$\Omega^* = \sum_{k=0}^{\infty} \Omega_{2k+1}^* g^{2k+1}\,, \tag{3.15}$$

where Ω_{2k+1}^* is a function of η and ν and $\Omega_1^* = \sqrt{1 - \epsilon^2}$.[6]

All the discussed potentials and metric functions can be expanded in Ω^*. Examining their symmetry properties reveals a purely symmetric or antisymmetric behaviour under the transformation $\Omega^* \to -\Omega^*$ that changes the sense of rotation. Therefore, they can also be written as a series in g, containing only even or odd powers of g, respectively. It follows that the real parts of the Ernst potentials are even and the imaginary parts are odd functions:

$$f = 1 + \sum_{k=1}^{\infty} f_{2k} g^{2k}\,, \quad \alpha = \sum_{k=1}^{\infty} \alpha_{2k} g^{2k}\,, \quad b = \sum_{k=1}^{\infty} b_{2k+1} g^{2k+1}\,, \quad \beta = \sum_{k=1}^{\infty} \beta_{2k+1} g^{2k+1}\,. \tag{3.16}$$

For the remaining functions we get:

$$h = 1 + \sum_{k=2}^{\infty} h_{2k} g^{2k}\,, \quad a^* = \sum_{k=1}^{\infty} a_{2k+1}^* g^{2k+1}\,, \quad A_\varphi^* = \sum_{k=1}^{\infty} A_{\varphi\,2k+1}^* g^{2k+1}\,. \tag{3.17}$$

All the coefficient functions f_{2k}, α_{2k}, b_{2k+1}, ... depend on the coordinates η and ν only. (See also [8] and [22].)

By means of an iterative procedure it is possible, with the help of a computer algebra system, to derive solutions for the Ernst potentials of, in principle, arbitrarily high order. In fact, the boundary value problem for the charged rotating disc of dust at first order ($k = 1$) is relatively simple and can be solved. With the obtained solution one can then solve the boundary value problem at second order ($k = 2$). These solutions can in turn be inserted into the third order boundary value problem, and so on. In reality, of course, this cannot be continued indefinitely, since the computational effort and thus also the computing time increases exponentially.[7]

Via this iterative procedure Palenta and Meinel [8] were able to obtain analytic solutions for those coefficient functions up to eighth order and Breithaupt et al. [9] later on even up to tenth. The subsequent calculations and discussions of the present thesis build on Breithaupt's semi-analytic solution of the charged rotating disc of dust.[8]

To get an idea of these solutions, the metric functions evaluated on the disc, i.e. for

---

[6]It turns out that Ω (appropriately normalized, e.g. by R_0 introduced in section 5.1) increases monotonically with g and decreases monotonically with ϵ. (For both $g = 0$ and $\epsilon = 1$ it vanishes.)

[7]A detailed description of the solution algorithm can be found in [8] and [22].

[8]Petroff and Meinel also provided a post-Newtonian expansion up to arbitrary order of the uncharged rotating disc of dust [31].

$\nu = 0$, are listed below up to second order[9]:

$$f(\eta, 0) = 1 - (1 + \eta^2) g^2 - \frac{1}{24} \left((45\epsilon^2 - 48) \eta^4 - (34\epsilon^2 - 12) \eta^2 - 11\epsilon^2 + 12 \right) g^4$$
$$+ \mathcal{O}(g^6) , \tag{3.18}$$

$$h(\eta, 0) = 1 - \frac{1}{2\pi^2} (1 - \epsilon^2) (1 - \eta^2) \left((\pi^2 + 16) \eta^2 - \pi^2 + 16 \right) g^4 + \mathcal{O}(g^6) , \tag{3.19}$$

$$a^*(\eta, 0) = \frac{3}{2} \sqrt{1 - \epsilon^2} (1 - \eta^2) \left(\eta^2 + \frac{1}{3} \right) g^3 + \frac{1}{192\pi^2} \sqrt{1 - \epsilon^2} (1 - \eta^2) \left[\left((377\epsilon^2 + 192) \eta^4 \right. \right.$$
$$\left. - (334\epsilon^2 - 888) \eta^2 - 99\epsilon^2 + 360 \right) \pi^2 + \frac{1024}{3} (\epsilon^2 - 4) (\eta^4 + \eta^2 + 1) \right] g^5$$
$$+ \mathcal{O}(g^7) . \tag{3.20}$$

Worth mentioning are the global prefactors of the expansions (see also [8] and [22]):

$$\Omega^* \sim \sqrt{1 - \epsilon^2} , \tag{3.21}$$

$$\alpha \sim \epsilon , \quad b \sim \sqrt{1 - \epsilon^2} \eta , \quad \beta \sim \epsilon \sqrt{1 - \epsilon^2} \eta , \tag{3.22}$$

$$a^* \sim \sqrt{1 - \epsilon^2} (1 - \eta^2) , \quad A_\varphi^* \sim \epsilon \sqrt{1 - \epsilon^2} (1 - \eta^2) . \tag{3.23}$$

First of all, we see from eq. (3.21) that disc configurations with $\epsilon = 0$ rotate with maximal angular velocity and ones with $\epsilon = 1$ have no rotation at all. This becomes obvious in the Newtonian limit where each dust particle in the disc is in an equilibrium of gravitational, electric and centrifugal force (see section 2.3). The prefactors ensure that all electromagnetic quantities, i.e. α, β and A_φ^*, vanish for $\epsilon = 0$ and that all quantities related to rotation, i.e. b, β, a^*, A_φ^* and of course Ω^*,[10] become zero for $\epsilon = 1$ (no rotation).

Furthermore, as it should be, on the axis of symmetry ($\eta = \pm 1$) a^* and A_φ^* vanish and in the equatorial plane outside the disc ($\eta = 0$) b and β.

---

[9]The evaluation on the disc reduces the length of the expansions significantly.

[10]Note that the magnetic field is determined by A_φ^* and is induced by the rotating charged dust particles (whereas the electric field is derived from A_t). The gravitomagnetic potential a^* also vanishes in the static case.

4 Ehrenfest's paradox within special relativity

In 1909 Ehrenfest formulated a famous paradox concerning a rigidly rotating disc (or a cylinder in the original version) within special relativity [32]. He pointed out that special relativistic rigidity, introduced by Born [33], easily leads to two contradicting statements about radius and circumference measured by a non-rotating observer before and after the disc is set into rotation.

The paradox gave rise to a long lasting debate on how to resolve it, see, e.g., [34]. Numerous physicists came up with solution approaches, however, they turned out to be wrong in most cases. Grøn presented in 1975 a resolution solely based on kinematics [35]. Initially, it was not clear whether this would be sufficient or whether a dynamical treatment would be necessary to solve the problem completely. Today, most physicists (including the author of this dissertation) accept Grøn's kinematic considerations as the correct way to resolve Ehrenfest's paradox.[1]

4.1 Ehrenfest's paradox

Ehrenfest showed that rigid rotation of discs (or cylinders) within special relativity involving a period of angular acceleration inevitably leads to a paradox [32].

The concept of rigidity was originally introduced by Born in the context of special relativity, however, it is also compatible with general relativity. Born rigidity is defined for an arbitrarily moving body as follows:
The distance between any two infinitesimally close points of the body, as measured by instantaneous inertial observers at those points, remains constant during the motion. Equivalently, for each pair of infinitesimally close particles of the body, the distance between the corresponding world lines, measured orthogonally to one of the two world lines, stays constant along it [33, 36–38].

Relying on this definition, Ehrenfest formulated a paradox: A relativistic cylinder with radius R is given a rotating motion about its axis, which finally becomes constant - while satisfying Born rigidity at all times. Let R'' be the radius of the constantly

---

[1]This chapter is partly orientated on [10].

rotating cylinder measured, like R, by an observer at rest, then two contradicting requirements need to be fulfilled:

(i) $2\pi R'' < 2\pi R$,

(ii) $R'' = R$.

As each element of the circumference is parallel to the direction of motion of the disc, the circumference must be Lorentz contracted relative to its rest length $2\pi R$. The radius, on the other hand, is not contracted, since each element is perpendicular to the direction of motion.

At first glance, this might seem like a simple problem. However, this paradox and related questions led to decades of intensive discussions involving many famous physicists such as Planck [39], Einstein [40], Lorentz [41], Eddington [42], Rosen [43] and many others.

One particular problem was the correct description of rotating platforms in the framework of special relativity. Another issue was whether and how to incorporate material properties into the solution. Furthermore, there was simply no concrete and physically relevant disc solution available to calculate circumference and radius and check what actually happens when the disc is set into rotation. In connection with the original paradox, there is also the question of what co-rotating observers would measure for circumference and radius compared to non-rotating observers and what the spatial geometry of the disc would look like accordingly.

4.2 Kinematic resolution

While to this day there is still no common agreement on the solution of Ehrenfest's paradox, there is a kinematic resolution by Grøn that most physicists indeed accept [34, 35, 44]. This section is dedicated to this resolution.

Grøn introduces three different types of observers:

a) an inertial observer S at rest relative to axis of rotation,

b) observers S' co-rotating to the disc and

c) inertial observers S_k $(k = 1, ..., n)$ instantaneously at rest relative points on the periphery of the disc.

Additionally, on the disc's periphery n light emitters are installed. The instantaneous inertial observers and the light emitters are arranged alternately along the periphery, see fig. 4.1. It is assumed that $n \gg 1$, such that the inertial observers are infinitesimally close to each other.

An essential requirement of Ehrenfest's paradox is Born rigidity. However, as e.g. Cavalleri and Spinelli [45] pointed out, Born rigidity is not a material property, but the result of a carefully designed sequence of acting forces to set a body in motion without inducing any stresses into the material. Therefore, a rigid motion according to Born, in which the disc is set in rotation, should be realizable by a sequence of simultaneous blows at each point on the disc, measured by inertial observers (since each infinitesimal patch on the disc must remain undeformed).
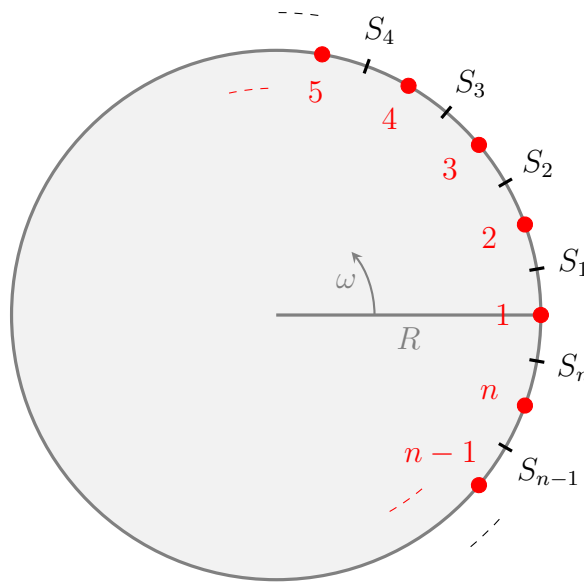

Figure 4.1: On the rotating disc there are alternately n light emitters and n inertial frames momentarily at rest around the periphery (based on [35]).

We now address the question of whether simultaneity (with regard to the blows) can be established in a consistent way among the inertial observers. For simplicity we restrict the discussion to the periphery of the disc and thus to the inertial observers S_k. However, the conclusion that is drawn is generally valid.

The blows act on the same points where the light emitters are installed and with each blow we associate the emission of light.

Assuming that such a simultaneity can be achieved, observer S_1 measures the light emission events 1 and 2 simultaneously, observer S_2 the events 2 and 3, and so on, until observer S_n who perceives the events n and 1 as simultaneous. As each inertial observer S_k receives the light signals simultaneously, they must also be emitted in his/her inertial frame at the same time.

In contrast, from the point of view of the laboratory observer S the events 1 to n happen not simultaneously. For S to observe the arrival of the light signals from event k and $k+1$ at S_k at the same time, the event k has to occur before the event $k+1$, since due to the rotation of the disc, S_k moves towards the light signal from $k+1$ and away from the one from k. Hence, for S the event 1 happens earlier than 2, 2 earlier than 3, and so on, up to $n-1$ that happens earlier than n. However, the event n

would need to occur before event 1, which would contradict the just established order of events, as seen by S, i.e. $1 < 2 < 3 < ... < n - 1 < n$.

In conclusion, it is kinematically impossible to synchronize clocks of successive instantaneous inertial observers S_k, and thus the blows, around the periphery of the disc. Setting a disc into rotation while satisfying Born's rigidity condition at all times is therefore impossible. This represents Grøn's kinematic resolution of the Ehrenfest paradox.

4.3 Proper distances

In general relativity one is free to choose any coordinate system $x^i = (x^\alpha, t)$ that is most suitable to describe a given physical scenario. Associated coordinate intervals $\mathrm{d}x^i$, however, do not correspond to actual physical distance or time intervals. To obtain a physically sensible notion of distance, more precisely a proper distance, we follow a derivation by Landau and Lifshitz [46]. As we will see, this method does not only apply to general relativity, but also to rotating frames in special relativity.

First, proper time intervals are defined in the usual way. For an observer at rest relative to the coordinate frame, i.e. $\mathrm{d}x^\alpha = 0$, we obtain

$$\mathrm{d}\tau^2 = -\mathrm{d}s^2 = -g_{44}\mathrm{d}t^2 \tag{4.1}$$

and thus

$$\mathrm{d}\tau = \sqrt{-g_{44}}\mathrm{d}t, \quad \text{for} \quad g_{44} < 0. \tag{4.2}$$

If the condition $g_{44} < 0$ is violated, the reference system cannot be realized by real bodies.

The proper distance between point A at x^α and point B at $x^\alpha + \mathrm{d}x^\alpha$ is determined via the so-called "radar method". For this, a light signal is transmitted from B to A, reflected there and sent back to B along the same path. At point B the proper time $\mathrm{d}\tau$ is measured for this process. Accordingly, the proper distance between the two infinitesimal close points is then defined as

$$\mathrm{d}\sigma = \frac{\mathrm{d}\tau}{2}. \tag{4.3}$$

To determine the proper distance $\mathrm{d}\sigma$ we write the line element as:

$$\mathrm{d}s^2 = g_{\alpha\beta}\mathrm{d}x^\alpha\mathrm{d}x^\beta + 2g_{\alpha 4}\mathrm{d}x^\alpha\mathrm{d}t + g_{44}\mathrm{d}t^2. \tag{4.4}$$

As $\mathrm{d}s^2 = 0$ for light signals, we obtain two possible solutions corresponding two forward

and backward propagation:

$$dt^{(1/2)} = \frac{1}{g_{44}} \left(-g_{\alpha 4} dx^\alpha \pm \sqrt{(g_{\alpha 4} g_{\beta 4} - g_{\alpha\beta} g_{44}) \, dx^\alpha dx^\beta} \right). \tag{4.5}$$

Let $t^\star$ be the moment at which the reflection of the light signal at A takes place, then the total time at B, between emission at $t^\star + dt^{(1)}$ and absorption at $t^\star + dt^{(2)}$, is:

$$dt^{(2)} - dt^{(1)} = -\frac{2}{g_{44}} \sqrt{(g_{\alpha 4} g_{\beta 4} - g_{\alpha\beta} g_{44}) \, dx^\alpha dx^\beta}. \tag{4.6}$$

With eqs. (4.2) and (4.3), we then immediately obtain the proper spatial line element:

$$d\sigma^2 = \gamma_{\alpha\beta} dx^\alpha dx^\beta, \quad \text{where} \quad \gamma_{\alpha\beta} := g_{\alpha\beta} - \frac{g_{\alpha 4} g_{\beta 4}}{g_{44}}. \tag{4.7}$$

An integration of $d\sigma$, however, is only meaningful in case of a time-independent metric.

Note that the quadratic form (4.7) has to be positive definite, which is satisfied if:

$$\gamma_{11} > 0, \quad \det \begin{pmatrix} \gamma_{11} & \gamma_{12} \\ \gamma_{21} & \gamma_{22} \end{pmatrix} > 0, \quad \det \begin{pmatrix} \gamma_{11} & \gamma_{12} & \gamma_{13} \\ \gamma_{21} & \gamma_{22} & \gamma_{23} \\ \gamma_{31} & \gamma_{32} & \gamma_{33} \end{pmatrix} > 0. \tag{4.8}$$

Using eq. (4.7), the 4-dimensional line element can be expressed as follows [43, 47, 48]:

$$ds^2 = d\sigma^2 - dT^2, \quad \text{with} \quad dT := \sqrt{-g_{44}} \left(dt + \frac{g_{\alpha 4}}{g_{44}} dx^\alpha \right). \tag{4.9}$$

dT corresponds to an infinitesimal time interval measured in a local inertial frame instantaneously at rest relative to point B (e.g. on an arbitrarily moving object).

Via the same light sending procedure the clocks of A and B can be synchronized. The moment $t^\star$ at A and

$$t^\star + dt_s := t^\star + \frac{1}{2} \left(dt^{(2)} + dt^{(1)} \right),$$
$$\text{with} \quad dt_s = -\frac{g_{\alpha 4}}{g_{44}} dx^\alpha, \tag{4.10}$$

at B, i.e. halfway between emission and reception of the light signal, are defined as simultaneous. This is referred to as Einstein synchronization.

According to eqs. (4.9) and (4.10), the clocks of points A and B are Einstein synchronized if and only if $dT = 0$. Therefore, by sending a one-way light signal between the Einstein synchronized points A and B (by construction of the Einstein synchronization the speed of light is isotropic between those points), their proper spatial distance is measured. (Instead of first synchronizing the clocks and then measuring the distance, however, it is more practical to use the "radar method" directly to obtain the proper

spatial distance.)

Moreover, in an instantaneous local inertial frame equipped with Einstein synchronized clocks, proper spatial distances are measured as well. On the other hand, simultaneity defined by $\mathrm{d}t = 0$ does not lead to the proper spatial line element, but simply to the spatial part of the 4-dimensional metric, $g_{\alpha\beta}\mathrm{d}x^{\alpha}\mathrm{d}x^{\beta}$.

It should be stressed that $\mathrm{d}T$ is not a perfect differential. In general, it is therefore not possible to integrate $\mathrm{d}T$ around a closed curve. As a consequence, in case of the rotating disc, the surface represented by $\mathrm{d}T = 0$, i.e. the surface characterized by $\mathrm{d}\sigma^2$, is discontinuous. This also prevents the Einstein synchronization of clocks momentarily at rest around the periphery of the rotating disc discussed in section 4.2.

4.4 Spatial geometry

With the radar method, introduced in the previous section, we are well equipped to determine the proper spatial geometry of a rotating disc within special relativity. Grøn also discusses the spatial geometry in [35] (in addition to the kinematic resolution of Ehrenfest's paradox). We assume that the disc is put into rotation in an arbitrary way.

To describe the spatial geometry, we need to transform to the co-rotating frame of the disc via $\varphi' = \varphi - \omega t$, where ω is the disc's constant angular velocity. Note that this is a Galilean and not a Lorentz transformation. As opposed to the relative character of the (constant) linear velocity, the angular velocity is an absolute quantity that can be measured locally by Foucault's pendulum and by Sagnac's experiment [49].

Starting from the non-rotating frame of reference furnished with the Minkowski line element (evaluated on the disc),

$$\mathrm{d}s^2\big|_{\mathrm{disc}} = \mathrm{d}r^2 + r^2\mathrm{d}\varphi^2 - \mathrm{d}t^2 \,, \tag{4.11}$$

and applying the transformation to the co-rotating frame, results in [35]:

$$\mathrm{d}s^2\big|_{\mathrm{disc}} = \mathrm{d}r^2 + r^2\mathrm{d}\varphi'^2 + 2\omega r^2\mathrm{d}\varphi'\mathrm{d}t - \left(1 - \omega^2 r^2\right)\mathrm{d}t^2 \,. \tag{4.12}$$

Co-rotating observers can then apply the radar method of section 4.3 to locally determine the proper spatial geometry of the disc. The resulting proper spatial line element, using eq. (4.7), reads [35]:

$$\mathrm{d}\sigma^2\big|_{\mathrm{disc}} = \mathrm{d}r^2 + \frac{r^2}{1 - \omega^2 r^2}\,\mathrm{d}\varphi'^2 \,. \tag{4.13}$$

Notice that eq. (4.13) is not just the spatial part of metric (4.12). In fact, this would only be the case if the off-diagonal term in eq. (4.12) would be zero.

The conditions of positive definiteness, eq. (4.8), translate to $\gamma_{rr} > 0$ and $\gamma_{\varphi'\varphi'} > 0$,

and thus to $|\omega r| < 1$. This simply means that no particle in the disc can rotate with a velocity greater than or equal to the speed of light and that the disc has a maximal possible size, depending on ω.

Integration of eq. (4.13) reveals the proper radius

$$R' = r \,, \tag{4.14}$$

the proper circumference

$$C' = \frac{2\pi r}{\sqrt{1 - \omega^2 r^2}} \tag{4.15}$$

and the proper area

$$A' = 2\pi \frac{1 - \sqrt{1 - \omega^2 r^2}}{\omega^2} \,. \tag{4.16}$$

Non-rotating observers could also apply the radar method to determine the proper spatial geometry of their own "rest space" (which differs from the proper spatial geometry of the disc measured by co-rotating observers). However, as there is no off-diagonal term in the line element (4.11), the proper spatial line element, based on eq. (4.7), immediately reduces to the spatial part of eq. (4.11). A non-rotating observer thus measures the radius

$$R = r \,, \tag{4.17}$$

the circumference

$$C = 2\pi r \tag{4.18}$$

and the area

$$A = \pi r^2 \,. \tag{4.19}$$

Notice that the measurement of the radius, as one would expect, agrees in both frames of reference: $R' = R = r$.

While a non-rotating observer describes the spatial geometry of his/her own "rest space" as Euclidean,

$$\frac{C}{R} = \frac{C}{r} = 2\pi \,, \tag{4.20}$$

the co-rotating observers in fact measure a non-Euclidean proper spatial geometry for the disc,

$$\frac{C'}{R'} = \frac{C'}{r} = \frac{2\pi}{\sqrt{1 - \omega^2 r^2}} \,. \tag{4.21}$$

It is also worth mentioning that statements (i) and (ii) of Ehrenfest's paradox can be read as a violation of the Euclidean spatial geometry that must be measured in the inertial frame of the non-rotating observer. Eqs. (4.20) and (4.21) indeed resolve this contradiction. Only co-rotating observers see a non-Euclidean geometry, but never (independent of the rotational state of the disc) a non-rotating observer. The co-

rotating frame of reference is not an inertial frame, so the measurement of a non-Euclidean geometry is not forbidden.

Already in 1916, Einstein pointed out in his famous article on the general theory of relativity [40] that observers co-moving to a rotating disc (which is arbitrarily set into rotation) no longer see Euclidean geometry. Observed in the non-rotating frame, not the circumference of the disc is being contracted due to rotation (as might be implied by Ehrenfest's paradox), but the infinitesimal measuring rods placed along the circumference. Measuring rods arranged along the radius are perpendicular to the direction of motion and are therefore not contracted. As a consequence, observers on the rotating disc measure a circumference to radius ratio larger than 2π (they have to use more measuring rods along the circumference), while in the non-rotating frame a ratio of exactly 2π is obtained.

In fact, the Ehrenfest paradox and the realisation of the necessity of a non-Euclidean geometry for rotating systems inspired Einstein, due to the equivalence principle, to consider gravity as a geometrical theory.

5 Geometry

Grøn's resolution of the Ehrenfest paradox based on kinematic considerations is accepted by most physicists nowadays. As noted in section 4.4, he also gave a mathematical description of the spatial geometry of rotating discs within special relativity. However, it lacks any kind of material properties that are to be found in real discs. While it is fine to solve the Ehrenfest paradox from a purely kinematic point of view, for related questions about the spatial geometry, material properties are expected to have a non-negligible influence - especially during the phase in which the disc is set into rotation.

So the question arises as to how the ratio of circumference to radius of a more realistic disc solution is observed from the point of view of non-rotating and co-rotating observers, how those measurements change when the rotation speed is altered and how the material properties affect that disc.

As the charged rotating disc of dust is a concrete, physically relevant solution of the Einstein-Maxwell equations, with material-like properties as we will see, we can tackle the questions related to the geometry, based on this solution, in a very direct way. This is particularly interesting as the post-Newtonian expansion allows us to go beyond special relativity and to also study the influence of general relativistic effects. With the specific charge parameter ϵ we can, furthermore, effectively regulate the rotation speed of the disc.

Inspired by those geometric investigations, it is obvious to also explore the intrinsic curvature of the charged rotating disc of dust. Of particular interest is how the intrinsic curvature, which is simply the Gaussian curvature for a two-dimensional disc, changes as the specific charge ϵ is altered.

This chapter is based on [10] by Rumler et al..[1]

5.1 Related questions to Ehrenfest's paradox

As described in chapter 4, Ehrenfest stated in his famous paradox within special relativity that setting a disc (or cylinder) in rotation while satisfying Born's rigidity condition necessarily leads to two contradicting requirements on the disc's radius and circumference. Furthermore, Grøn presented a kinematic resolution of the paradox

---

[1]`http://creativecommons.org/licenses/by/4.0/`

most physicists agree with. He demonstrated that it is impossible to consistently synchronize clocks of instantaneous inertial rest frames around the periphery of the rotating disc.

Despite its resolution, there are still interesting questions related to Ehrenfest's paradox:

1) How does the spatial geometry of an accelerated disc which is initially at rest evolve as measured by non-rotating and co-rotating observers?

2) What is the spatial geometry of a disc that is already set into rotation as seen by non-rotating and co-rotating observers?

3) A real disc has material properties, how do they influence the rotating disc?

While those questions were partly addressed by Grøn from a purely kinematic point of view, see [35, 48], they are most interesting for more realistic disc models that have some material properties.

Not surprisingly, as a concrete and physically meaningful solution, the charged rotating disc of dust is a good candidate for answering these questions. (We will see that it does indeed have material-like properties.) Even though the questions will only be addressed for this particular disc model, the results and conclusions might still be generally valid (at least to some extent).

5.1.1 Proper spatial line element

In the present section we want to analyse geometric quantities like the proper radius and the proper circumference of the charged rotating disc of dust and address the above posed questions. For this purpose, we introduce the following line element:

$$\mathrm{d}\sigma^2 = h_{ik}\mathrm{d}x^i\mathrm{d}x^k\,, \tag{5.1}$$

where

$$h_{ik} = g_{ik} + u_i u_k \tag{5.2}$$

is the projection tensor used in section 2.2. The original line element $\mathrm{d}s^2 = g_{ik}\mathrm{d}x^i\mathrm{d}x^k$ can then be written as

$$\mathrm{d}s^2 = \mathrm{d}\sigma^2 - u_i u_k \mathrm{d}x^i\mathrm{d}x^k\,. \tag{5.3}$$

Note that, by construction, for an infinitesimal displacement vector $\mathrm{d}x^i$ orthogonal to u^i the line element (5.3) reduces to $\mathrm{d}s^2 = \mathrm{d}\sigma^2$ and for $\mathrm{d}x^i = u^i\mathrm{d}\tau$ to $\mathrm{d}s^2 = -\mathrm{d}\tau^2$ (where τ is the proper time). As a result, $\mathrm{d}\sigma^2$ can be utilised to measure infinitesimal proper distances on the disc. Indeed, in the co-rotating frame of the disc, where only

the fourth component of the four-velocity field is non-vanishing (the same applies to the four-velocity of the co-rotating observers), we recover with

$$d\sigma^2 = h'_{\alpha\beta}\,dx'^\alpha dx'^\beta = \left(g'_{\alpha\beta} - \frac{g'_{\alpha 4}g'_{\beta 4}}{g'_{44}}\right)dx'^\alpha dx'^\beta\,, \quad \text{where} \quad \alpha, \beta = 1, 2, 3\,, \qquad (5.4)$$

the line element (4.7) derived by Landau and Lifshitz [46] using the "radar method". Since the spacetime is stationary and the four-velocity field shares this symmetry, the projection tensor $h'_{\alpha\beta}$ is time-independent and eq. (5.4) can be used to calculate finite proper spatial distances via integration. However, it should be stressed that the four-velocity field is not hypersurface-orthogonal and the 3-space characterized globally by the line element (5.4) is not a hypersurface of spacetime either.

From now on we are only interested in the proper spatial geometry of the disc itself, as a 2-dimensional object - described by the line element $d\sigma^2\big|_{\text{disc}} = \big\{h'_{\alpha\beta}\,dx'^\alpha dx'^\beta\big\}\big|_{\text{disc}}$. This is the geometry observed by a family of "residents" of the disc who apply the radar method.

In elliptic coordinates the 2-dimensional proper spatial line element of the metric (3.13) takes the form

$$d\sigma^2\Big|_{\nu=0} = f'^{-1}h'\rho_0^2\frac{\eta^2}{1-\eta^2}d\eta^2 + f'^{-1}\rho_0^2(1-\eta^2)d\varphi'^2\,. \qquad (5.5)$$

Note that, since $\nu = 0$ on the disc, the elliptic coordinates η and ν decouple and $d\rho^2 = \rho_0^2\frac{\eta^2}{1-\eta^2}d\eta^2$ and $\rho^2 = \rho_0^2(1-\eta^2)$.

Integration of the line element (5.5) then gives the proper circumference

$$C'(\eta) = 2\pi\rho_0\sqrt{1-\eta^2}f'^{-1/2}\,, \qquad (5.6)$$

the proper area

$$A'(\eta) = 2\pi\rho_0^2\int_\eta^1 d\tilde{\eta}\,\tilde{\eta}\,f'^{-1}h'^{1/2} \qquad (5.7)$$

and the proper radius

$$R'(\eta) = \rho_0\int_\eta^1 d\tilde{\eta}\,\frac{\tilde{\eta}}{\sqrt{1-\tilde{\eta}^2}}\left(f'^{-1}h'\right)^{1/2} \qquad (5.8)$$

of the rotating disc of charged dust. By inserting the post-Newtonian expansions of the metric functions in the co-rotating frame, using eqs. (3.15) to (3.17) and (2.22), also eqs. (5.6) to (5.8) can be written as series expansions in g.

Accordingly, in the non-rotating frame of reference the disc's circumference, area and radius are given by $C(\eta) = 2\pi\rho_0\sqrt{1-\eta^2}f^{-1/2}$, $A(\eta) = 2\pi\rho_0^2\int_\eta^1 d\tilde{\eta}\,\tilde{\eta}\,f^{-1}h^{1/2}$ and $R(\eta) = \rho_0\int_\eta^1 d\tilde{\eta}\,\frac{\tilde{\eta}}{\sqrt{1-\tilde{\eta}^2}}\left(f^{-1}h\right)^{1/2}$, respectively.

Using the transformation law $f'^{-1}h' = f^{-1}h$, it follows trivially:

$$R'(\eta) = R(\eta).\tag{5.9}$$

In agreement with a special relativistic disc, see section 4.4, both co-rotating and non-rotating observers obtain the same result for the measurement of the radius.

When it is stated that the geometry is "seen" or "measured" by co-rotating observers, it is actually meant that the co-rotating observers apply the radar method to measure distances. Since they are at rest relative to the rotating disc (and their four-velocity field, in accordance with the four-velocity field of fixed particles in the disc, has only a fourth component in the co-rotating frame), they measure the proper spatial geometry of the disc. In the non-rotating frame, on the other hand, the non-rotating observers also use the radar method. However, they are at rest relative to the non-rotating frame (with a four-velocity field that has vanishing spatial components in the non-rotating frame) and consequently do not measure the proper spatial geometry of the disc, but the proper spatial geometry of their own "rest space".

5.1.2 Newtonian limit

In order to compare the results for C', A' and R of the charged rotating disc of dust with those of a rotating disc within the framework of special relativity (SR), discussed in section 4.4, we have to take the Newtonian limit. Thus, we require that both the metric deviate only slightly from the Minkowski metric and that the rotational velocities be small compared to the speed of light.

Charged disc of dust (Newtonian limit):

$$C' = 2\pi\rho_0 \left[\rho^* + \left(\frac{1}{2}\Omega_1^{*2}\rho^{*2} - \frac{1}{2}f_2 \right) \rho^* g^2 \right],$$

$$A' = \pi\rho_0^2 \left[\rho^{*2} + \left(\frac{1}{4}\Omega_1^{*2}\rho^{*2} + \frac{1}{2}(2 - f_2) \right) \rho^{*2} g^2 \right],$$

$$R = \rho_0 \left[\rho^* + \frac{1}{6}(4 - f_2)\rho^* g^2 \right].$$

Disc within SR (Newtonian limit):

$$C' = 2\pi r \left[1 + \frac{1}{2}(\omega r)^2 \right],$$

$$A' = \pi r^2 \left[1 + \frac{1}{4}(\omega r)^2 \right],$$

$$R = r.$$

Crucial to the discussion of Ehrenfest's paradox and the closely related geometric questions is the ratio of circumference to radius as seen from co-rotating and non-rotating observers.

Charged disc of dust (Newtonian limit):

$$\frac{C'}{R'} = 2\pi \left[1 + \left(\frac{1}{2}\Omega_1^{*2}\rho^{*2} - \frac{1}{3}(2 + f_2) \right) g^2 \right],$$

$$\frac{C}{R} = 2\pi \left[1 - \frac{1}{3}(2 + f_2) g^2 \right].$$

Disc within SR (Newtonian limit):

$$\frac{C'}{r} = 2\pi \left[1 + \frac{1}{2}(\omega r)^2 \right],$$

$$\frac{C}{r} = 2\pi.$$

The first-order ($k = 1$) coefficient function f_2 is given by $f_2(\eta, 0) = -1 - \eta^2$ and $\rho^* = \frac{\rho}{\rho_0} = \sqrt{1 - \eta^2}$.[2]

It should be noted that the above expansions utilise different expansion parameters. A post-Newtonian expansion in g is used for the disc of dust (see section 3.1) and for the SR-disc we have an expansion around small rotational velocities ωr compared to the speed of light c. Therefore, only in the Newtonian limit, where both $g \approx \frac{\sqrt{-U_c}}{c} \ll 1$ and $\frac{\omega r}{c} \ll 1$, a comparison is meaningful.

Grøn discusses only kinematic aspects of the disc and material properties are absent in [35, 44, 48]. The same is true, of course, for the special relativistic disc studied in section 4.4. (It is exactly the same disc.) However, a real disc is held together by attractive forces originating from the rigid material itself. In case of the disc of dust attractive gravitational forces, mediated through the terms involving f_2, play the role of those material forces.

Taking the different expansions and the appearance of the terms with f_2 into account, the disc of dust agrees with the special relativistic disc in the Newtonian limit.

Furthermore, an interesting observation can be made. The quantities C', A' and R of the disc of dust are all larger than those of the special relativistic disc (for $\eta^2 < 1$ and $r > 0$). Although dust is by definition a pressure-less fluid without any elastic properties, the rotating disc of dust nevertheless behaves to some extent as if it had material properties, resulting in a kind of "elastic" expansion.
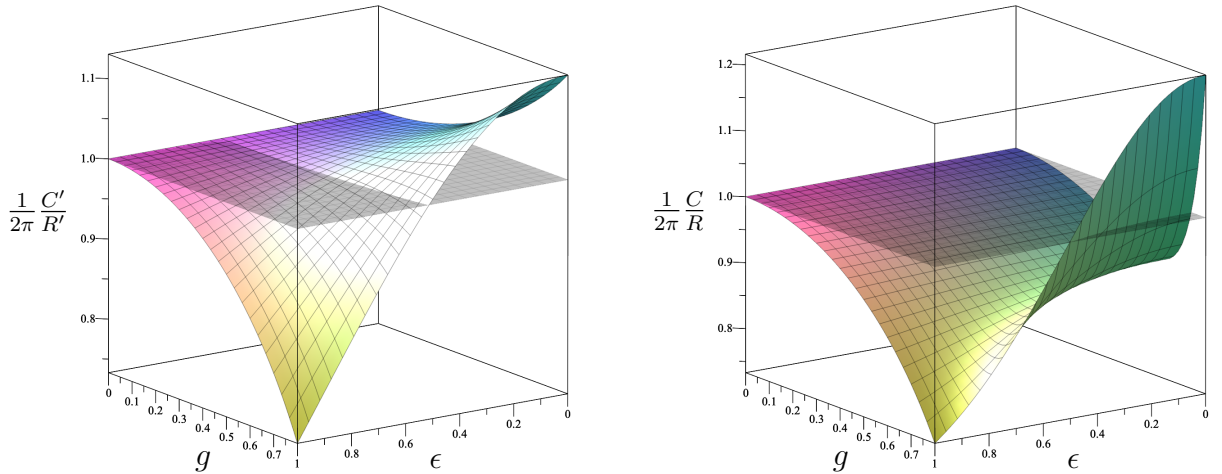

Figure 5.1: Normalized ratio of circumference to radius in the co-rotating (left) and non-rotating frame (right) as a function of the specific charge ϵ and the relativity parameter g, plotted for $\eta = 0$ (after [10]).

Explicitly writing out the ratios of circumference to radius leads to:

---

[2] C', A', R, etc. of the special relativistic disc are derived from the corresponding expressions from section 4.4 by an expansion in ωr.

$$\frac{C'}{R'} = 2\pi \left[1 + \frac{1}{6} \left(1 - \eta^2 \right) \left(1 - 3\epsilon^2 \right) g^2 \right] , \qquad (5.10)$$

$$\frac{C}{R} = 2\pi \left[1 - \frac{1}{3} \left(1 - \eta^2 \right) g^2 \right] . \qquad (5.11)$$

Remarkably, for $\eta^2 < 1$, there is a geometrical transition induced by an alteration of the specific charge: $\frac{C'}{R'} \gtrless 2\pi$ for $\epsilon^2 \lessgtr \frac{1}{3}$. This transition is also present beyond the Newtonian limit, as can be seen in fig. 5.1 (left). All figures in this thesis are created using all available (exact) orders.[3] For vanishing charge the ratio of proper circumference to proper radius becomes larger than 2π, just as in the case of the special relativistic disc.

In the non-rotating frame there is no such transition, instead the ratio of circumference to radius is always smaller than 2π, independent of the specific charge (excluding $\eta = \pm 1$). This also stays true beyond the Newtonian limit (apart from high values of g), see fig. 5.1 (right). Within special relativity the ratio is exactly equal to 2π. Those results, however, do not contradict each other, since values smaller than 2π are caused by the gravitational correction term involving f_2. As discussed above, the kinematic analysis of the rotating disc within special relativity does not involve corresponding terms.

5.1.3 Answering related questions

Now, let us address the questions raised in the beginning of this section, starting with the first one. As discussed in section 3.3, changing the specific charge parameter ϵ directly affects the rotational velocity Ω of the disc. In particular, by decreasing ϵ form 1 to 0 we can transition from disc configurations with zero angular velocity to configurations with maximum rotation speed. This, however, is achieved in a quasi-stationary way and cannot be seen as setting the disc into rotation, as we alter the specific charge of the disc and thus the disc itself. Nevertheless, we can compare disc configurations with increasing rotational velocities with each other and examine the effect on the spatial geometry. As can be seen in fig. 5.1 (left), for co-rotating observers the geometric ratio $\frac{C'}{R'}$ monotonically increases from values smaller to greater than 2π. In fact, as will be shown in section 5.2, there is also an almost simultaneous transition from positive to negative curvature. Non-rotating observers also measure increasing values of $\frac{C}{R}$, see fig. 5.1 (right). They, however, remain below 2π, apart from high values of g due to the emergence of an ergosphere (see section 6.3).[4]

Concerning the second question, we have seen that the ratio $\frac{C'}{R'}$, that characterizes the proper spatial geometry and is measured by co-rotating observers, can be less than,

---

[3]With the exception of section 6.4, all quantities calculated in this thesis are given by expansions up to $k = 10$.

[4]Note that inside an ergosphere non-rotating (with respect to infinity) observers no longer exist.

equal to or greater than 2π depending on the specific charge ϵ. For a ratio equal to 2π the critical value of the specific charge is $\epsilon_{\mathrm{crit}} = \frac{1}{\sqrt{3}}$ in the Newtonian limit. With growing g, ϵ_{crit} decreases slightly and becomes dependent on the radial coordinate η (see fig. 5.9). Non-rotating observers, on the other hand, always perceive smaller values than 2π for $\frac{C}{R}$ (again, apart from high values of g).
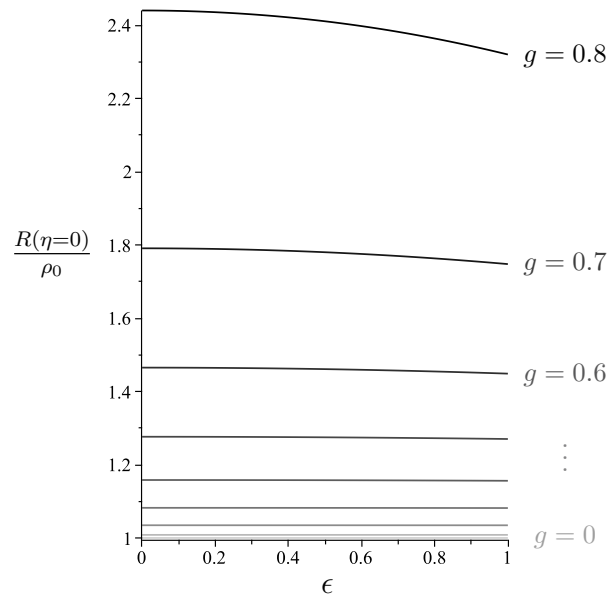

Figure 5.2: Normalized proper radius, evaluated at the rim of the disc, as a function of ϵ (after [10]).

Finally, the third question resolves around the influence of material properties present in a real rotating disc. Indeed, as we have already seen in the Newtonian limit, the disc of dust mimics "elastic" material properties and shows an "elastic" expansion as response to the rotational motion. But also beyond Newtonian physics, according to fig. 5.2, the disc's total proper radius $R_0 := R(\eta = 0)$ (measured in units of ρ_0) grows with decreasing specific charge ϵ and in turn increasing rotational velocities Ω.[5] The more relativistic the disc, the more pronounced is the effect.

5.2 Curvature

Motivated by the found geometric transition induced by a change of the specific charge ϵ, we now examine the intrinsic curvature of rotating discs more closely.

As the domain of a rotating disc is simply a two-dimensional spatial surface, denoted by Σ_2, the geometric quantity that describes its intrinsic curvature is the Gaussian curvature K.

In the following subsections the Gaussian curvature of the charged rotating disc of

---

[5]Notice that $R_0 = \int_0^{\rho_0} \sqrt{g_{\rho\rho}} \, \mathrm{d}\rho$.

dust (using the post-Newtonian expansion up to $k = 10$) and various analytic limiting cases will be calculated. The findings will be compared and reviewed.

5.2.1 Gaussian curvature of the charged disc of dust

By using the derived expressions for the proper radius R and the proper circumference C', eqs. (5.6) and (5.8), the proper spatial line element of the charged rotating disc of dust can be written in the following instructive and simple way:

$$d\sigma^2\Big|_{\Sigma_2} = dR^2 + \left(\frac{C'(R)}{2\pi}\right)^2 d\varphi'^2, \tag{5.12}$$

where at least formally $C'(R) = C'(\eta(R))$.

The Gaussian curvature K is an intrinsic and coordinate independent measure of the curvature of a 2-dimensional surface embedded in $\mathbb{R}^3$. In two dimensions, the sectional curvature, which is generally defined for a plane spanned by two tangent vectors on a n-dimensional Riemannian manifold, is equivalent to the Gaussian curvature. Exploiting this relation, the Gaussian curvature can be calculated via

$$K = \frac{R^{(2)}_{1212}}{\det\left(g^{(2)}_{ab}\right)}, \tag{5.13}$$

where both the Riemann curvature tensor $R^{(2)}_{abcd}$ and the metric $g^{(2)}_{ab}$ correspond to the 2-dimensional surface. Alternatively, the Gaussian curvature can also be calculated by means of the principle curvatures κ_1 and κ_2: $K = \kappa_1\kappa_2$. For more details see, e.g., [50].

With the above version of the proper spatial line element the Gaussian curvature takes a very simply form, i.e.

$$K = -\frac{C'(R)_{,RR}}{C'(R)}. \tag{5.14}$$

It thus follows immediately that the Gaussian curvature of the charged rotating disc of dust is determined primarily by the second derivative of the proper circumference C' with respect to the proper radius R.

Even though the above formula for K, eq. (5.14), is quite insightful, it is not that practical, since we do not know the functional dependence of C' on R. By using the chain rule we can, however, transform formula (5.14) into the slightly less appealing but all the more useful form

$$K = \frac{1}{C'(\eta)}\left(\frac{dR}{d\eta}\right)^{-3}\left[\frac{d^2R}{d\eta^2}C'(\eta)_{,\eta} - \frac{dR}{d\eta}C'(\eta)_{,\eta\eta}\right]. \tag{5.15}$$

Inserting the solutions for the post-Newtonian expansion leads to

$$K = \frac{1}{\rho_0^2} \left[\left(3\epsilon^2 - 1\right) g^2 \right.$$

$$+ \left(\left(6\eta^2 - 5\right) \epsilon^4 + \left(\frac{7}{6} - 8\eta^2\right) \epsilon^2 + 3\eta^2 + \frac{1}{2} + \frac{16\eta^2}{\pi^2}\left(\epsilon^2 - 1\right) \right) g^4$$

$$\left. + \mathcal{O}\left(g^6\right) \right]. \tag{5.16}$$

As can be seen in fig. 5.3 (left), there is a characteristic transition curve in the parameter space where the curvature K changes its sign. The same transition curve appears in fig. 5.1 (left) depicting $\frac{C'}{R'}$. Explicitly written out expansions up to fifth order of $\frac{C'}{R'}$ and $R_0^2 K$ are listed in appendix A.1.
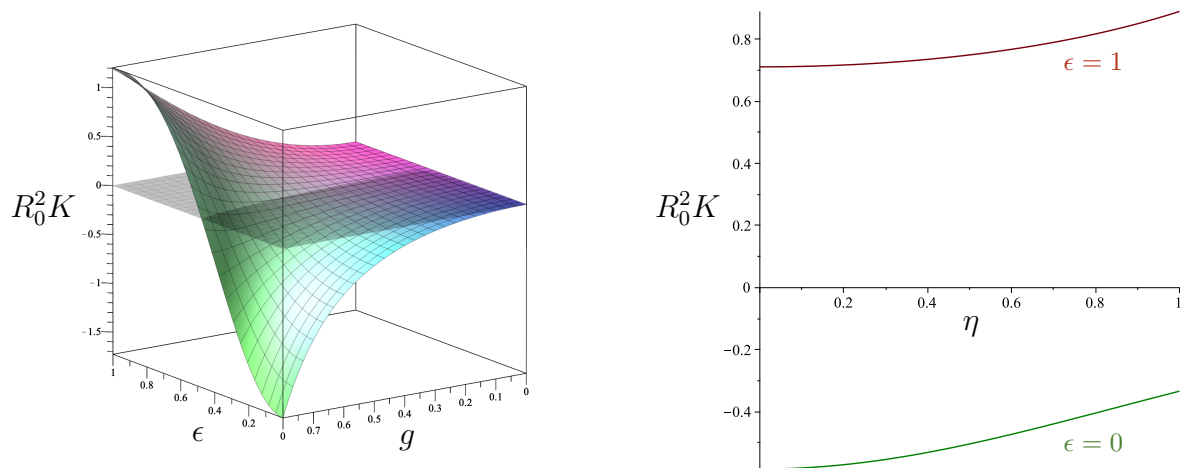
Figure 5.3: *Left panel*: Gaussian Curvature K normalized by the total proper radius R_0, shown for $\eta = 0$ (after [10]). *Right panel*: Radial dependence of the normalized Gaussian curvature for the special cases $\epsilon = 0$ and $\epsilon = 1$, where $g = 0.6$ (after [10]).

The right panel of fig. 5.3 shows the radial dependence of $R_0^2 K$ for the special cases $\epsilon = 1$ and $\epsilon = 0$. In case of maximal charge, i.e. $\epsilon = 1$, the disc has no rotation at all and general relativistic effects cause positive curvature. For $\epsilon = 0$ the rotation is maximal and special relativistic effects are dominant and lead, in accordance with the special relativistic disc [34], to negative curvature. In both cases the curvature K gets more positive towards the centre of the disc (where $\eta = 1$). This is expected, since in the non-rotating case general relativistic effects increase towards the centre of a massive object, where the gravitational potential is the deepest. At maximal rotation, on the other hand, the rotational speed decreases towards the centre while general relativistic effects increase.

Interesting to the current discussion is also the functional dependence of C' on R that is visualized in terms of parametric plots (including appropriate normalizations)
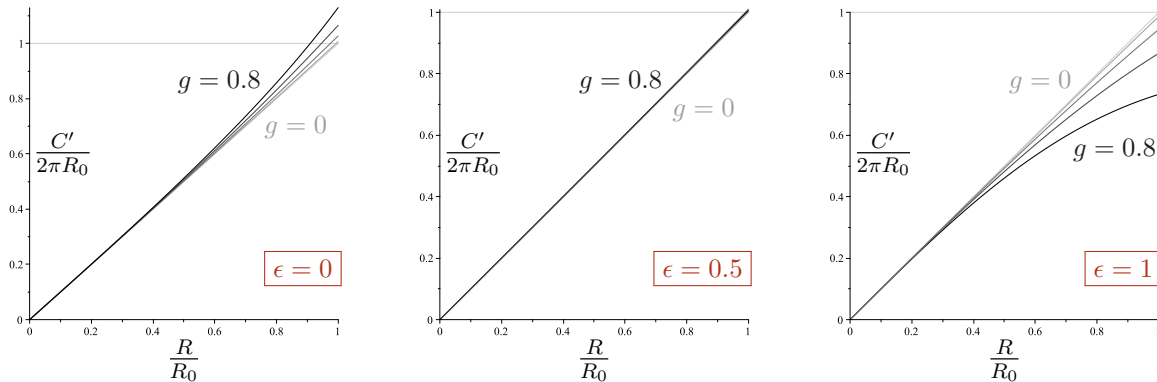
Figure 5.4: Functional dependence of C' (normalized by $2\pi R_0$) on R (normalized by R_0) plotted for $g \in \{0, 0.2, 0.4, 0.6, 0.8\}$ and $\epsilon = 0$ (left), $\epsilon = 0.5$ (middle) and $\epsilon = 1$ (right) (after [10]).

in fig. 5.4. As can be observed there, $C'_{,RR} > 0$ for small ϵ and $C'_{,RR} < 0$ for large ϵ. In between there is a transition. Considering formula (5.14), this perfectly coincides with the plot of the normalized curvature in fig. 5.3 (left). The plots in fig. 5.4 also clearly show that $\frac{C'}{R'}$ is greater than 2π for small values of ϵ and less than 2π for large values, just like in fig. 5.1 (left). Figure 5.4 thus explains the relationship between the plots of $\frac{C'}{R'}$ and K (left panels of figs. 5.1 and 5.3).

5.2.2 Newtonian theory: Maclaurin discs and their Gaussian curvature

In the Newtonian limit Einstein and Maxwell equations decouple and reduce to the Poisson equations for the gravitational and the electric potential. Thus, in Newtonian theory the disc of dust is fully described by

$$\Delta U = 4\pi \mu^{\mathrm{Mld}}, \quad \text{with} \quad \mu^{\mathrm{Mld}} = \begin{cases} \sigma^{\mathrm{Mld}}(\rho)\delta(\zeta) & \text{for } 0 \le \rho \le \rho_0 \\ 0 & \text{otherwise} \end{cases}, \tag{5.17}$$

$$\Delta U^{\mathrm{E}} = -4\pi\epsilon\mu^{\mathrm{Mld}}, \tag{5.18}$$

and

$$\epsilon U^{\mathrm{E}}_{,\rho} = -\left(U - \frac{1}{2}\Omega^2\rho^2\right)_{,\rho}, \tag{5.19}$$

where U is the gravitational and $U^{\mathrm{E}} := \alpha = -A_t$ the electric potential. Eq. (5.19) shows (as already mentioned in section 2.3) that the dust particles in the disc are in an equilibrium of electric, gravitational and centrifugal force.

Rotating discs in the framework of Newtonian theory characterized by eqs. (5.17) to (5.19) are also known as charged Maclaurin discs.

The solution for the exterior Newtonian gravitational potential of Maclaurin spher-

oids, in terms of elliptic coordinates, is given by [12]:

$$U = -\frac{M}{\rho_0} \left\{ \operatorname{arccot} \nu + \frac{3}{4} \left[\nu - \left(\nu^2 + \frac{1}{3} \right) \operatorname{arccot} \nu \right] \left(1 - 3\eta^2 \right) \right\} . \tag{5.20}$$

In the limit where the spheroid shrinks to a disc, this potential is given everywhere. As before, we are interested in the solution on the disc itself. On Σ_2, where $\nu = 0$, the gravitational potential reduces to

$$U|_{\nu=0} = \frac{1}{2} U_c \left(1 + \eta^2 \right) , \tag{5.21}$$

with $U_c = -g^2$ in the Newtonian limit. According to eqs. (5.17) and (5.18), U^{E} trivially follows from eq. (5.21): $U^{\mathrm{E}} = -\epsilon U$.

Furthermore, using the solution for U, eq. (5.19) can be rewritten to the already known equation,

$$U_c = -\frac{\Omega^2 \rho_0^2}{1 - \epsilon^2} , \tag{5.22}$$

that was used as a starting point for the post-Newtonian expansion.

Integrating eq. (5.17) over an infinitesimal ζ-interval and exploiting reflection symmetry reveals the surface mass density

$$\sigma^{\mathrm{Mld}} = \frac{1}{2\pi} U_{,\zeta}\Big|_{\zeta=0^+} = \frac{3M}{2\pi \rho_0^2} \eta , \tag{5.23}$$

where M is the mass of the disc. It can be easily verified that

$$U' = U - \frac{1}{2} \Omega^2 \rho^2 \tag{5.24}$$

is the co-rotating potential in the Newtonian limit.

By understanding the Newtonian theory as a limit of the full general relativistic theory we can reuse the line element. The 4-dimensional line element in the Newtonian limit, evaluated on the disc, reads

$$\mathrm{d}s^2\Big|_{\nu=0} = (1 - 2U)\, \rho_0^2 \frac{\eta^2}{1 - \eta^2} \mathrm{d}\eta^2 + (1 - 2U)\, \rho_0^2 \left(1 - \eta^2 \right) \mathrm{d}\varphi'^2$$
$$+ 2\Omega \rho_0^2 \left(1 - \eta^2 \right) \mathrm{d}\varphi' \mathrm{d}t - (1 + 2U')\mathrm{d}t^2 . \tag{5.25}$$

Using eq. (5.4), the proper spatial line element of the Maclaurin disc follows immediately:

$$d\sigma^2\Big|_{\nu=0} = \left[1 + \left(1 + \eta^2 \right) g^2 \right] \rho_0^2 \frac{\eta^2}{1 - \eta^2} \mathrm{d}\eta^2$$
$$+ \left[1 + \left(2 - \epsilon^2 \left(1 - \eta^2 \right) \right) g^2 \right] \rho_0^2 \left(1 - \eta^2 \right) \mathrm{d}\varphi'^2 . \tag{5.26}$$

As expected, the Gaussian curvature of the Maclaurin disc resulting from eq. (5.26) is given by:

$$K^{\text{Mld}} = \frac{1}{\rho_0^2} \left(3\epsilon^2 - 1\right) g^2 \,. \tag{5.27}$$

In conclusion, the Gaussian curvature of the charged Maclaurin disc is in perfect agreement with the Gaussian curvature of the disc of dust in the Newtonian limit.

5.2.3 Gaussian curvature of a specific ECD-disc configuration

For general (not necessarily disc-) configurations with $\epsilon = \pm 1$ one obtains electrically counterpoised dust (ECD), see, e.g., [51]. Those solutions are static. The Papapetrou-Majumdar class [52, 53] contains such static solutions to the Einstein-Maxwell equations and the corresponding line element is of the form[6]

$$\mathrm{d}s^2 = f^{-1} \left[\left(\mathrm{d}\rho^2 + \mathrm{d}\zeta^2\right) + \rho^2 \mathrm{d}\varphi^2\right] - f \mathrm{d}t^2 \,, \tag{5.28}$$

where

$$f^{1/2} = e^U = 1 - \epsilon\alpha \tag{5.29}$$

is the defining relation between the metric function f and the electrostatic potential α. Due to the static spacetime the electromagnetic four-potential has only one non-vanishing component:

$$A_a = \left(0, 0, 0, -\alpha\right) \,. \tag{5.30}$$

Starting from line element (5.28), the Einstein-Maxwell equations reduce to the surprisingly simple equation

$$\Delta e^{-U} = -4\pi\mu^{\text{ECD}} e^{-3U} \,. \tag{5.31}$$

By introducing a new potential V and a redefined mass density $\mu_{\text{st}}^{\text{ECD}}$ as

$$V := 1 - e^{-U} \quad \text{and} \quad \mu_{\text{st}}^{\text{ECD}} := \mu^{\text{ECD}} e^{-3U} \,, \tag{5.32}$$

eq. (5.31) can be transformed into the Poisson equation

$$\Delta V = 4\pi\mu_{\text{st}}^{\text{ECD}} \,. \tag{5.33}$$

It is a remarkable property of ECD-configurations that the nonlinear Einstein-Maxwell equations reduce to a single linear Poisson equation and thus a linear superposition of solutions on the level of the Poisson equation is possible.

---

[6]General ECD-configurations do not need to be axisymmetric. However, with regard to an ECD-disc, this form of the line element is chosen nevertheless.

The solution of eq. (5.33) can be represented as a Poisson integral and based on its asymptotic behaviour we can identify the mass[7]:

$$M = \int \mu_{\text{st}}^{\text{ECD}}(\rho, \zeta) \, \rho \, \mathrm{d}\rho \, \mathrm{d}\varphi \, \mathrm{d}\zeta \, . \tag{5.34}$$

For ECD the mass density $\mu_{\text{st}}^{\text{ECD}}$ is not predetermined by the theory, but can rather be freely chosen. As a physically motivated toy model, we consider a specific ECD-disc configuration equipped with the mass density of a Maclaurin disc:

$$\mu_{\text{st}}^{\text{ECD}} = \mu^{\text{Mld}} \, . \tag{5.35}$$

Note, that this means $\mu_{\text{st}}^{\text{ECD}} = e^{2U} \sigma_{\text{st}}^{\text{ECD}}(\rho)\delta(\zeta) = \sigma^{\text{Mld}}(\rho)\delta(\zeta)$. Choosing the mass density in this way is justified, since then the mass of the ECD-disc also coincides with the one of the Maclaurin disc: $M = \int \mu_{\text{st}}^{\text{ECD}}(\rho, \zeta) \, \rho \, \mathrm{d}\rho \, \mathrm{d}\varphi \, \mathrm{d}\zeta = \int \mu^{\text{Mld}}(\rho, \zeta) \, \rho \, \mathrm{d}\rho \, \mathrm{d}\varphi \, \mathrm{d}\zeta$.

In case of the Maclaurin disc, the equation of motion $\Delta U = 4\pi\mu^{\text{Mld}}$ leads to the solution $U|_{\nu=0} = \frac{1}{2}U_c\left(1 + \eta^2\right)$, see eqs. (5.17) and (5.21). Analogously, for ECD the solution of eq. (5.33) with the chosen mass density (5.35) is given by

$$V|_{\nu=0} = \frac{1}{2}V_c\left(1 + \eta^2\right) \, . \tag{5.36}$$

However, now we get $V_c = -\frac{g^2}{1-g^2}$.

The proper spatial line element, stemming from eq. (5.28), for the chosen ECD-disc configuration in terms of elliptic coordinates then reads

$$\mathrm{d}\sigma^2\Big|_{\nu=0} = f^{-1}\Big|_{\nu=0} \left(\rho_0^2 \frac{\eta^2}{1-\eta^2}\mathrm{d}\eta^2 + \rho_0^2\left(1 - \eta^2\right)\mathrm{d}\varphi^2\right) \, , \tag{5.37}$$

where

$$f^{-1/2} = 1 - V \, , \quad V|_{\nu=0} = -\frac{1}{2}\frac{g^2}{1 - g^2}\left(1 + \eta^2\right) \, .$$

It implies the following Gaussian curvature:

$$K^{\text{ECD}} = \frac{1}{\rho_0^2} \frac{32\left(1 - g^2\right)^2 g^2}{\left[2 - \left(1 - \eta^2\right) g^2\right]^4} \, . \tag{5.38}$$

The corresponding plot of the normalized Gaussian curvature can be found in fig. 5.5. There we introduced $R_0^{\text{ECD}} := R^{\text{ECD}}(\eta = 0) = \rho_0 \frac{6 - g^2}{6(1 - g^2)}$.

Interestingly, in contrast to the charged rotating disc of dust for $\epsilon = 1$ (see fig. 5.3 (right)), the chosen ECD-disc configuration possesses higher (positive) curvature at the

---

[7]Note that for ECD-configurations, the gravitational mass M is equal to the baryonic mass M_{b}, since the the gravitational binding energy is compensated by the electromagnetic field energy. Indeed, it holds: $M_{\text{b}} = \int \mu^{\text{ECD}}\sqrt{f^{-3}\rho^2} \, \mathrm{d}\rho \, \mathrm{d}\varphi \, \mathrm{d}\zeta = \int \mu_{\text{st}}^{\text{ECD}}\rho \, \mathrm{d}\rho \, \mathrm{d}\varphi \, \mathrm{d}\zeta = M$.
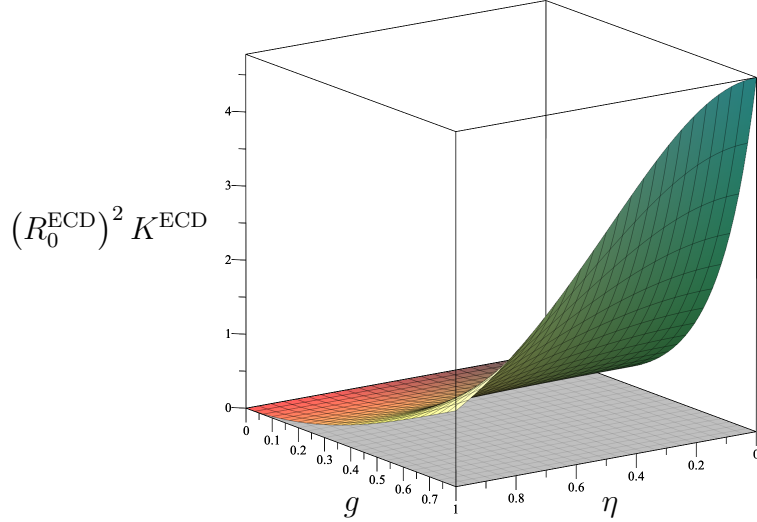
Figure 5.5: Normalized Gaussian Curvature of the chosen ECD-configuration (after [10]).

rim of the disc and lower at the centre. But nevertheless, it has a positive curvature in agreement with the $\epsilon = 1$-limit of the charged rotating disc of dust.

To gain a better understanding of this radial curvature behaviour, we investigate and compare the proper surface mass densities of the so far discussed discs. The resulting proper surface mass densities are

$$
\begin{aligned}
\sigma_{\mathrm{p}} &= \sigma \sqrt{f h^{-1}} = \left. \frac{1}{2\pi} U'_{,\zeta} \right|_{\zeta = 0^+} \sqrt{f h^{-1}} \\
&= \frac{2}{\pi^2 \rho_0} \left[\eta g^2 + \frac{1}{6} \left(\left(\frac{23}{3} \eta^2 - 5 \right) \epsilon^2 - 7 \eta^2 \right) \eta g^4 + \mathcal{O}\left(g^6 \right) \right],
\end{aligned}
\tag{5.39}
$$

$$
\begin{aligned}
\sigma_{\mathrm{p}}^{\mathrm{Mld}} &= \sigma^{\mathrm{Mld}} \\
&= \frac{2}{\pi^2 \rho_0} g^2 \eta,
\end{aligned}
\tag{5.40}
$$

$$
\begin{aligned}
\sigma_{\mathrm{p}}^{\mathrm{ECD}} &= \sigma^{\mathrm{ECD}} e^U \\
&= \frac{2}{\pi^2 \rho_0} \left[1 + \frac{1}{2} \frac{g^2}{1 - g^2} \left(1 + \eta^2 \right) \right]^{-2} \frac{g^2}{1 - g^2} \eta \\
&= \frac{2}{\pi^2 \rho_0} \left[\eta g^2 - \eta^3 g^4 + \mathcal{O}\left(g^6 \right) \right].
\end{aligned}
\tag{5.41}
$$

As it should be, $\sigma_{\mathrm{p}}^{\mathrm{Mld}}$ represents the Newtonian limit of σ_{p} and $\sigma_{\mathrm{p}}^{\mathrm{ECD}}$.

On the left panel of fig. 5.6 all three normalized proper surface mass densities are plotted and on the right panel $R_0 \sigma_{\mathrm{p}}|_{\epsilon = 1}$ and $R_0^{\mathrm{ECD}} \sigma_{\mathrm{p}}^{\mathrm{ECD}}$ are depicted for different values of the relativity parameter g.

From fig. 5.6 (right) it is evident that $\sigma_{\mathrm{p}}^{\mathrm{ECD}}$ (for fixed R_0^{ECD}) is denser at the rim and less dense at the centre compared to $\sigma_{\mathrm{p}}|_{\epsilon = 1}$ (for fixed $R_0|_{\epsilon = 1}$). The higher g, the more extreme is this behaviour of the chosen ECD-configuration. This dominance of
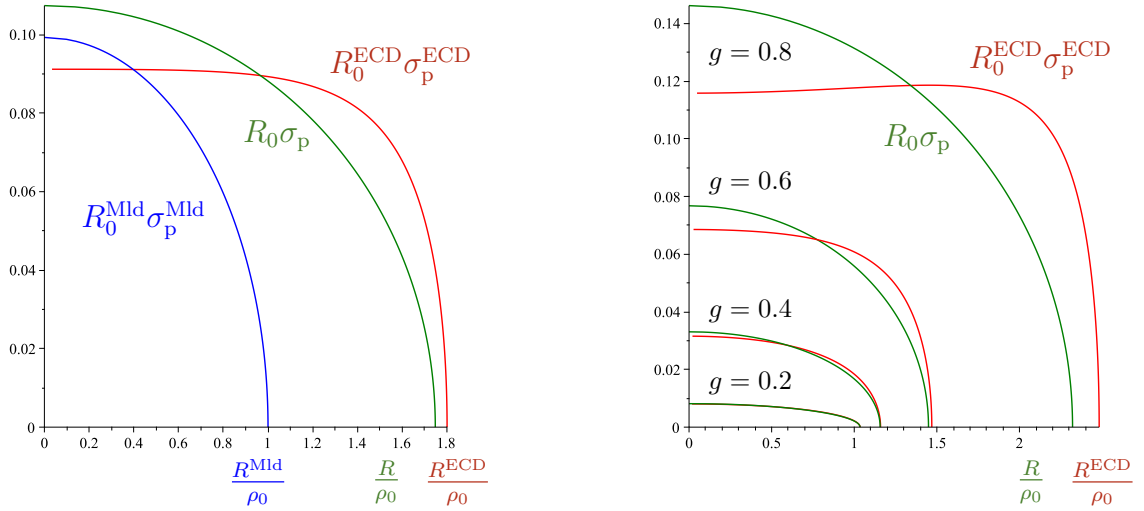
Figure 5.6: *Left panel*: Comparison of the normalized proper surface mass densities $R_0^{\mathrm{Mld}}\sigma_{\mathrm{p}}^{\mathrm{Mld}}$, $R_0\sigma_{\mathrm{p}}$ and $R_0^{\mathrm{ECD}}\sigma_{\mathrm{p}}^{\mathrm{ECD}}$ for $g = 0.7$ and $\epsilon = 1$ (after [10]). *Right panel*: Comparison of the normalized proper surface mass densities $R_0\sigma_{\mathrm{p}}$ and $R_0^{\mathrm{ECD}}\sigma_{\mathrm{p}}^{\mathrm{ECD}}$ for different values of g and $\epsilon = 1$ (after [10]).

the proper surface mass density $\sigma_{\mathrm{p}}^{\mathrm{ECD}}$ at the rim as opposed to the centre (compared to $\sigma_{\mathrm{p}}|_{\epsilon=1}$) leads to the observed higher curvature K^{ECD} at the rim. In contrast, the curvature $K|_{\epsilon=1}$ generated by the surface mass density $\sigma_{\mathrm{p}}|_{\epsilon=1}$ of the maximally charged disc of dust increases towards the centre.

5.2.4 Gaussian curvature of the uncharged disc of dust

By means of the inverse scattering method that originates from soliton theory, the global problem of the uniformly rotating disc of dust without charge was solved rigorously by Neugebauer and Meinel [6, 7, 12], see section 2.4.

As outlined, an essential part of this method is to formulate and to solve a Riemann-Hilbert problem. It turns out that this Riemann-Hilbert problem has a unique solution in the parameter region $0 < \mu < \mu_0 := 4.629...$, where $\mu := 2\,(\rho_0\Omega)^2\,e^{-2\mathcal{V}_0}$ and $\mathcal{V}_0 := \mathcal{V}(\rho = 0, \zeta = 0) = U'(\rho = 0, \zeta = 0)$.[8] Here $\mu \to 0$ corresponds to the Newtonian limit and for $\mu \to \mu_0$ the formation of a Kerr-black hole was proven [6, 7], see also [54].

Analogous to the charged disc, the line element can globally be written in Weyl-Lewis-Papapetrou form:

$$\mathrm{d}s^2 = e^{-2U'}\left[e^{2k'}\left(\mathrm{d}\rho^2 + \mathrm{d}\zeta^2\right) + \rho^2\mathrm{d}\varphi'^2\right] - e^{2U'}\left(\mathrm{d}t + a\,\mathrm{d}\varphi'\right)^2 . \tag{5.42}$$

Denoting $x := \frac{\rho}{\rho_0}$, as used in the literature above, the resulting proper spatial line element reads

$$\left.\mathrm{d}\sigma^2\right|_{\Sigma_2} = e^{-2(U-k)}\rho_0^2\,\mathrm{d}x^2 + e^{-2\mathcal{V}_0}\rho_0^2 x^2\mathrm{d}\varphi'^2 , \tag{5.43}$$

---

[8]In this subsection, μ is exceptionally not the mass density.

utilising the boundary condition $e^{2U'} = e^{2\mathcal{V}_0}$ and the transformation law $k' - U' = k - U$.

For the associated Gaussian curvature we obtain the compact formula

$$K^{\text{uncharged}} = -\frac{1}{2\rho_0^2 x}\frac{\partial}{\partial x}e^{2(U-k)} = -\frac{1}{2\rho_0^2 x}\frac{\partial}{\partial x}e^{2(\mathcal{V}_0-k')}\,. \tag{5.44}$$

The normalized Gaussian curvature shown in fig. 5.7 (left) can, therefore, be computed by

$$\left(R_0^{\text{uncharged}}\right)^2 K^{\text{uncharged}}(g,x) = -2\mu k'_{,\tilde{\mu}}(\tilde{\mu})\frac{\left[\int_0^1 dx\, e^{k'(\tilde{\mu})}\right]^2}{e^{2k'(\tilde{\mu})}}\,, \tag{5.45}$$

where $\tilde{\mu} := \mu(1-x^2)$ was introduced and the relation between the parameters g and μ is given by $g(\mu) = \sqrt{1 - e^{\mathcal{V}_0}(\mu)}$. In eq. (5.45), the only occurring metric potential k' can be determined from the Ernst potential $e^{2\mathcal{V}_0} + ib_0$ at $x = 0$ using

$$k'_{,\tilde{\mu}}(\tilde{\mu}) = \frac{1}{4}\frac{\left[e^{2\mathcal{V}_0}{}_{,\tilde{\mu}}(\tilde{\mu})\right]^2 + \left[b_{0,\tilde{\mu}}(\tilde{\mu})\right]^2}{e^{2\mathcal{V}_0}(\tilde{\mu})}\,. \tag{5.46}$$

Note that the solutions obtained for $e^{2\mathcal{V}_0}$ and b_0 are expressed in terms of Jacobian elliptic functions.
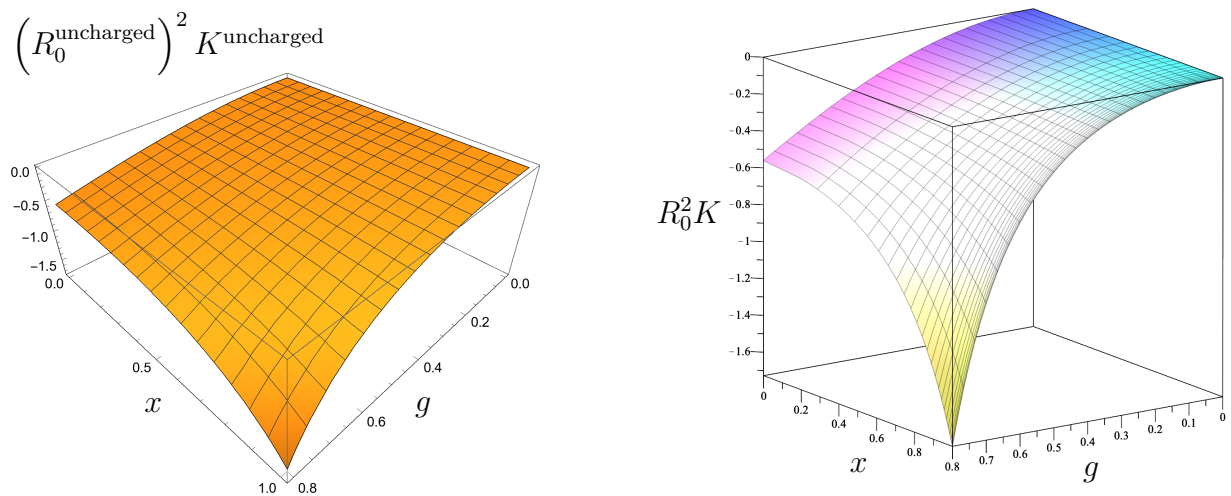
Figure 5.7: Normalized Gaussian curvature of the uncharged disc of dust (left) and of the charged disc of dust in the limit of vanishing charge (right) (after [10]).

Comparing the plot of the normalized Gaussian curvature of the uncharged disc (exact solution), fig. 5.7 (left panel), with the one of the charged disc evaluated at $\epsilon = 0$ (post-Newtonian expansion up to tenth order), fig. 5.7 (right panel), shows a good qualitative agreement.

Checking the more conclusive numerical values, certifies an excellent coincidence between the (exact) analytic and the semi-analytic solution for $\epsilon = 0$. Averaged over the disc (using $x = \{0, 0.3, 0.7, 1\}$), the relative error of $R_0^2 K|_{\epsilon=0}$ in relation to

Table 5.1: Gaussian curvature: uncharged disc (exact solution) versus charged disc in the limit $\epsilon \to 0$ (series expansion up to tenth order) (after [10]).

		$K^{\text{uncharged}} \left(R_0^{\text{uncharged}} \right)^2$	$\left. KR_0^2 \right|_{\epsilon \to 0}$
$g = 0.6$	$x = 0$	- 0.333602	- 0.333602
	$x = 0.3$	- 0.349614	- 0.349614
	$x = 0.7$	- 0.434073	- 0.434072
	$x = 1$	- 0.584301	- 0.584297
$g = 0.7$	$x = 0$	- 0.441980	- 0.441979
	$x = 0.3$	- 0.471784	- 0.471784
	$x = 0.7$	- 0.640493	- 0.640487
	$x = 1$	- 0.988126	- 0.987999
$g = 0.8$	$x = 0$	- 0.560113	- 0.560108
	$x = 0.3$	- 0.611598	- 0.611586
	$x = 0.7$	- 0.930419	- 0.930281
	$x = 1$	- 1.73047	- 1.72751

$\left(R_0^{\text{uncharged}} \right)^2 K^{\text{uncharged}}$ is 2.29×10^{-6} for $g = 0.6$, 3.50×10^{-5} for $g = 0.7$ and still only 4.72×10^{-4} for $g = 0.8$. See table 5.1 for the corresponding numerical values of the normalized Gaussian curvature.

5.2.5 Visualization

Similar to Flamm's paraboloid in case of Schwarzschild spacetime, we want to visualize the spatial curvature of the charged disc of dust by an isometric embedding.

The isometric embedding of the proper 2-dimensional disc space, characterized by eq. (5.12), into 3-dimensional Euclidean space, furnished with the line element $\mathrm{d}l^2 = \mathrm{d}r^2 + r^2\mathrm{d}\phi^2 + \mathrm{d}z^2$ is achieved by the identifications

$$\phi = \varphi' \,, \tag{5.47}$$

$$r = \frac{C'(R)}{2\pi} \,, \tag{5.48}$$

$$z(R) = \int_0^R \left[1 - \left(\frac{C'(\tilde{R})_{,\tilde{R}}}{2\pi} \right)^2 \right]^{1/2} \mathrm{d}\tilde{R} \,, \tag{5.49}$$

if the condition $C'(R)_{,R} \leq 2\pi$ is satisfied.

Consequently, this embedding only works for sufficiently high values of ϵ. Based on the fact that the curvature becomes first negative at the centre of the disc by lowering ϵ (if initially it is positive everywhere), see subsection 5.2.6, it can be shown that $K \geq 0$

(for all R) is not only a sufficient but also a necessary condition for the embedding constraint, $C'(R)_{,R} \leq 2\pi$ (for all R), to be fulfilled.
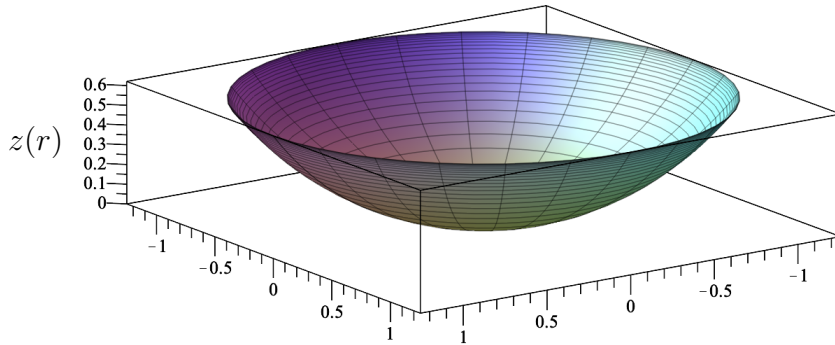

Figure 5.8: Isometric embedding of the proper 2-dimensional disc space into 3-dimensional Euclidean space for $g = 0.6$ and $\epsilon = 1$. The scaling parameter ρ_0 is set to 1 (after [10]).

In fig. 5.8 the embedding of the charged disc of dust is depicted for the values $g = 0.6$ and $\epsilon = 1$. The figure shows that for large values of ϵ the proper circumference $C'(R)$ is less than the corresponding Euclidean value $2\pi R$ and that this discrepancy grows with R, i.e. exactly what can be seen in fig. 5.4 (right).

5.2.6 Transition curves

In three different cases we have seen the occurrence of a transition curve in the parameter space (ϵ, g):

$$1) \; \frac{C'}{R'} = 2\pi \; , \qquad 2) \; K = 0 \; , \qquad 3) \; C'_{,R} = 2\pi \; .$$

It turns out that these transition curves look very similar, almost identical, as shown in fig. 5.9 (left).

The radial dependence of the transition curve $K = 0$ (the others being very similar) can be read off from the right panel of fig. 5.9. As can be seen there, changing ϵ does not cause a transition throughout the whole disc at the same time. In fact, by starting with positive curvature, i.e. high values of ϵ, the transition to negative curvature happens first at the centre and last at the rim.

5.3 Convergence estimate

When working with series expansions, it is essential to also check their convergence. For the post-Newtonian expansion used for the charged rotating disc of dust there is no general mathematical proof of the convergence yet [22]. However, to gain insight, we can estimate the convergence behaviour of each expanded quantity individually.
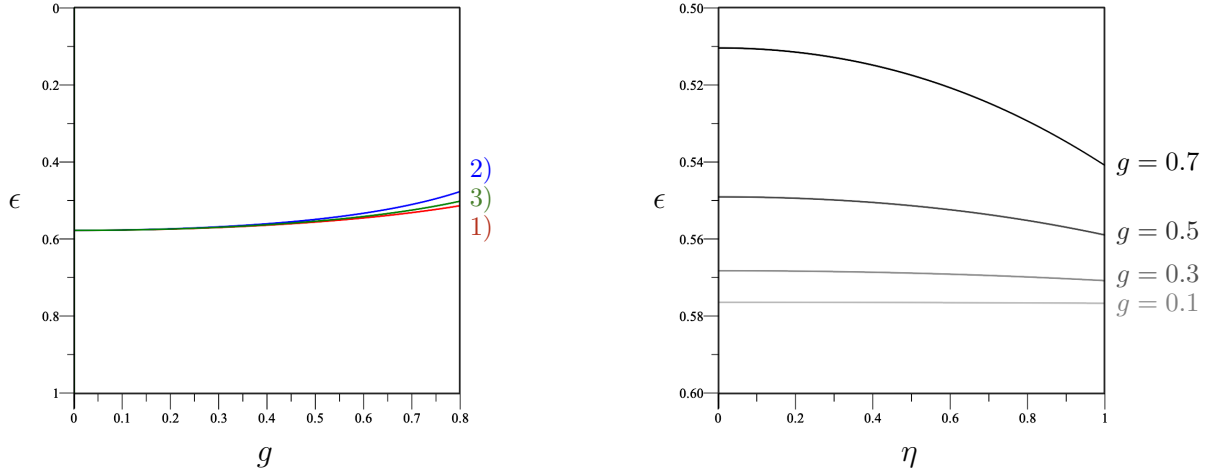
Figure 5.9: *Left panel*: Conditions 1), 2), and 3) lead to very similar transition curves in the parameter space, here depicted for $\eta = 0$ (after [10]). *Right panel*: Radial dependence of the curve $K = 0$ plotted for different values of the relativistic parameter g (after [10]).

Suppose we are interested in the convergence behaviour of a geometrical or physical quantity $\mathcal{X}$ of the charged rotating disc of dust. Due to the symmetry behaviour under the transformation $\Omega \to -\Omega$, $\mathcal{X}$ is either an even or odd series in g (see section 3.3):

$$\mathcal{X} = \sum_{k=0}^{10} \mathcal{X}_{2k} g^{2k} \quad \text{or} \quad \mathcal{X} = \sum_{k=0}^{10} \mathcal{X}_{2k+1} g^{2k+1} \,. \tag{5.50}$$

We denote the series truncated at order $k = \mathcal{K}$, where $\mathcal{K} \leq 10$, with:

$$\mathcal{X}_{|\mathcal{K}} := \sum_{k=0}^{\mathcal{K}} \mathcal{X}_{2k} g^{2k} \quad \text{or} \quad \mathcal{X}_{|\mathcal{K}} := \sum_{k=0}^{\mathcal{K}} \mathcal{X}_{2k+1} g^{2k+1} \,. \tag{5.51}$$

To understand whether and how well $\mathcal{X}$ converges, we determine at each order how much the series has effectively changed by adding the current order. So for each $\mathcal{K}$ we calculate the change that occurs when the $\mathcal{K}$th order is added to $\mathcal{X}_{|\mathcal{K}-1}$ relative to $\mathcal{X}_{|\mathcal{K}}$:

$$\delta\mathcal{X}_{|\mathcal{K}} := \frac{|\mathcal{X}_{|\mathcal{K}} - \mathcal{X}_{|\mathcal{K}-1}|}{|\mathcal{X}_{|\mathcal{K}}|} \,. \tag{5.52}$$

Fig. 5.10 shows the relative change by adding the current order (as defined in eq. (5.52)) for the area, the circumference, the radius and the ratio of circumference to radius of the charged rotating disc of dust as functions of $\mathcal{K}$ in the co-rotating (left) and the non-rotating frame (right). The relative change by adding the current order for the Gaussian curvature K and the normalized Gaussian curvature $R_0^2 K$ of the disc, can be read off from fig. 5.11.

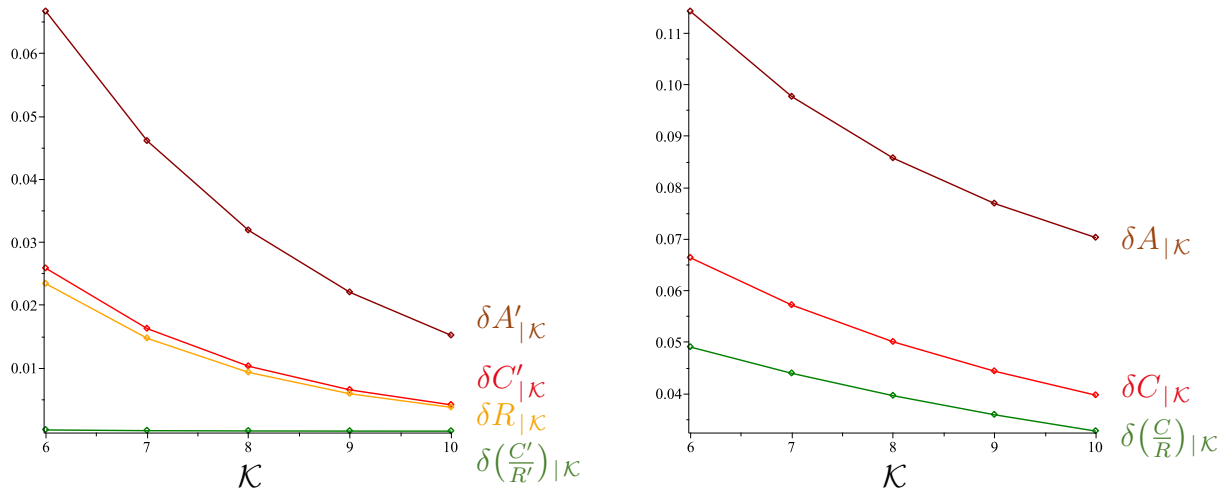As can clearly be seen, all the series expansions of the quantities in figs. 5.10 and 5.11

Figure 5.10: Convergence estimate of A', C', $R' = R$, $\frac{C'}{R'}$ (left) and A, C, $\frac{C}{R}$ (right) depending on $\mathcal{K}$, plotted for $g = 0.8$, $\epsilon = 0$ and $\eta = 0$.
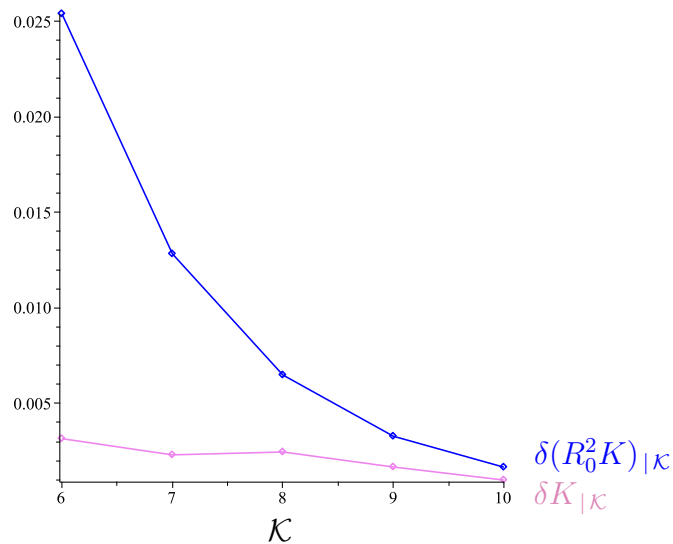

Figure 5.11: Convergence estimate of K and $R_0^2 K$ depending on $\mathcal{K}$, plotted for $g = 0.8$, $\epsilon = 0$ and $\eta = 0$.

change less and less with higher orders and the relative change becomes sufficiently small at order $\mathcal{K} = 10$. It can therefore be confirmed that the geometric quantities examined in this chapter indeed exhibit convergence behaviour. (The convergence of the area in the non-rotating frame is rather slow. However, this quantity does not play a decisive role in this chapter.)

Over all, the chosen parameters for the plots, i.e. $g = 0.8$, $\epsilon = 0$ and $\eta = 0$, lead to the worst results in most cases. It can furthermore be observed that the quantities in the co-rotating frame compared to the non-rotating frame have a significantly better convergence behaviour. This is consistent with the fact that they are also more relevant for describing the disc. From fig. 5.11 one might conclude that the normalized Gaussian curvature $R_0^2 K$ generally converges slower than the Gaussian curvature K. However,

this is not to true for all ϵ and η.

Notice that especially the quantities $\frac{C'}{R'}$ and $R_0^2 K$, which characterize the proper spatial geometry of the charged rotating disc of dust, have an excellent convergence behaviour. In particular, at tenth order the relative changes are $\delta\left(\frac{C'}{R'}\right)_{|10} = 7.6 \times 10^{-6}$ and $\delta(R_0^2 K)_{|10} = 1.7 \times 10^{-3}$ for $g = 0.8$, $\epsilon = 0$ and $\eta = 0$.

This procedure for estimating the convergence according to eq. (5.52) has proven to be useful for the geometric quantities of the disc and is therefore also applied in the subsequent chapter, which is devoted entirely to the physical aspects of the charged rotating disc of dust.

6 Physics

Inspired by the Ehrenfest paradox, a detailed analysis of the spatial geometry of the charged rotating disc of dust was carried out in chapter 5. In the present chapter, the focus is now on the physical aspects of the disc and the corresponding spacetime.

First, a closer examination of the proper surface mass density of the disc is carried out. With sufficiently relativistic and fast rotating disc configurations, an interesting effect arises.

A very convenient way to characterize the exterior spacetime of the charged rotating disc of dust is by means of multipole moments. The gravitational and electromagnetic multipole moments of the disc are calculated and discussed in detail. Moreover, a generalized multipole conjecture that could serve as a powerful tool to distinguish ordinary physical bodies from black holes is stated.

It turns out that for sufficiently relativistic disc configurations, an ergosphere of torus-like shape forms inside the disc. No static observers exist within such an ergosphere. Special attention is paid to the influence of the relativity parameter and the specific charge on the formation process of the ergosphere.

Finally, test particles are used to probe the exterior spacetime of the charged rotating disc of dust. The circular motion of neutral test particles in the equatorial plane of the disc is investigated. In this context, also general formulae for both neutral and charged test particles following equatorial circular orbits are derived.

6.1 Surface mass density

In section 2.1, the surface mass density σ was introduced according to the relation $\mu = \frac{f}{h}\sigma(\rho)\delta(\zeta)$, for $0 \leq \rho \leq \rho_0$, see eq. (2.19). The proportionality factor $\frac{f}{h}$ was chosen for later convenience such that with the boundary condition (2.65) we simply get:

$$\sigma = \frac{1}{2\pi}U'_{,\zeta}\big|_{\zeta=0^+} .$$
(6.1)

An invariant definition of the surface mass density is given by [12]:

$$\sigma_{\mathrm{p}} = \frac{1}{2\pi}\left(U'_{,i}n^i\right)\Big|_{\zeta=0^+} = \frac{1}{2\pi}e^{U-k}U'_{,\zeta}\big|_{\zeta=0^+} ,$$
(6.2)

where $n^i = e^{U-k}\delta^i_\zeta$ is the unit normal vector to the hypersurface $\zeta = 0$. Notice that the proper surface mass density (6.2) agrees with the one from section 2.1, see eq. (2.20).

In elliptic coordinates, eq. (3.3), the partial derivative ∂_ζ reads:

$$\partial_\zeta = \frac{\nu(1-\eta^2)}{\rho_0(\eta^2+\nu^2)}\partial_\eta + \frac{\eta(1+\nu^2)}{\rho_0(\eta^2+\nu^2)}\partial_\nu \,. \tag{6.3}$$

With the post-Newtonian expansions of U, k and U' follows, via eq. (6.2), the solution for the proper surface mass density $\sigma_{\rm p}$ of the charged rotating disc of dust.[1] In figs. 6.1 and 6.2 the normalized proper surface mass density $R_0\sigma_{\rm p}$ as a function of the normalized proper radius $\frac{R}{R_0}$ is plotted for different values of the relativity parameter g and the specific charge ϵ.
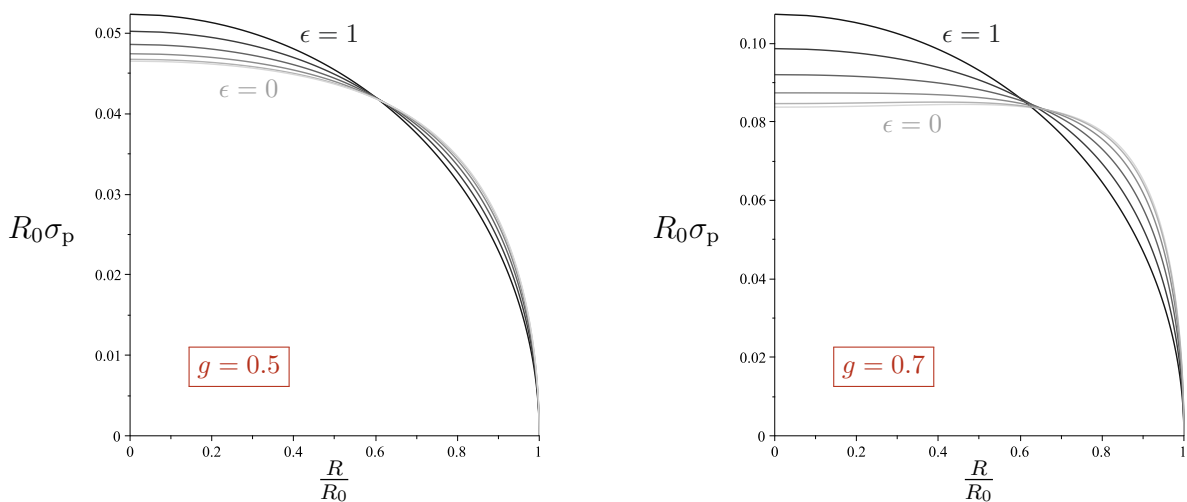
Figure 6.1: Normalized proper surface mass density $R_0\sigma_{\rm p}$ as a function of the normalized proper radius $\frac{R}{R_0}$, shown for $\epsilon \in \{0, 0.2, 0.4, 0.6, 0.8, 1\}$ and $g = 0.5$ (left) or $g = 0.7$ (right).

Remarkably, for $g \gtrsim 0.7$ and sufficiently low values of ϵ (depending on g) a global maximum forms near the rim of the disc. It is most pronounced for $\epsilon = 0$ and disappears for $\epsilon = 1$. This effect can be interpreted as follows. Disc configurations with $\epsilon = 1$ are static and by decreasing the specific charge ϵ from 1 to 0 the angular velocity of the corresponding configurations increases from zero to a maximum value. (In the previous chapter, this fact was exploited several times for the discussion of the spatial geometry of the disc.) With decreasing values of ϵ and thus increasing rotational speed, also the centrifugal force (in a Newtonian language) increases. So for sufficiently relativistic configurations the formation of a maximum near the rim is apparently a response to high rotational speeds.[2]

---

[1] See also [8].

[2] Note that proper surface mass density $R_0^{\rm ECD}\sigma_{\rm p}^{\rm ECD}$ has for sufficiently high g also a maximum near the rim, see fig. 5.6 (right). However this ECD-disc configuration is chosen rather artificially and has a higher curvature at the rim as opposed to the centre. It is by no means the $\epsilon=1$-limit of the
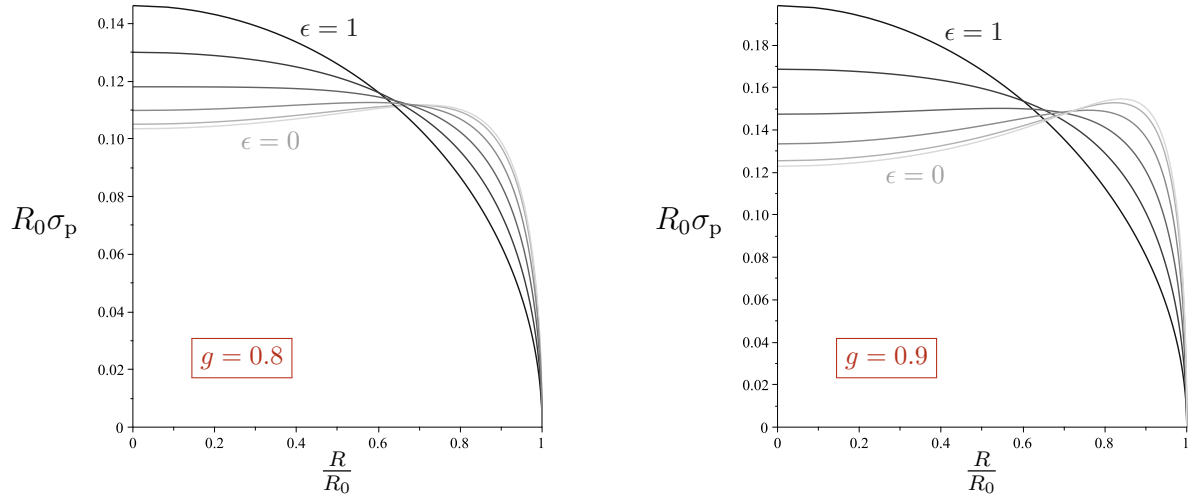
Figure 6.2: Normalized proper surface mass density $R_0\sigma_{\mathrm{p}}$ as a function of the normalized proper radius $\frac{R}{R_0}$, shown for $\epsilon \in \{0, 0.2, 0.4, 0.6, 0.8, 1\}$ and $g = 0.8$ (left) or $g = 0.9$ (right).

This also resembles the behaviour of viscous fluids or elastic materials (for fixed R_0). As already found in subsection 5.1.3, the charged rotating disc of dust mimics such a behaviour in some sense.

Ultimately, the in chapter 5 observed transition from positive curvature, for strongly charged disc configurations, to negative curvature, for weakly charged ones, manifests itself for sufficiently high values of g in the formation of a maximum in the normalized proper surface mass density near the rim of the disc.
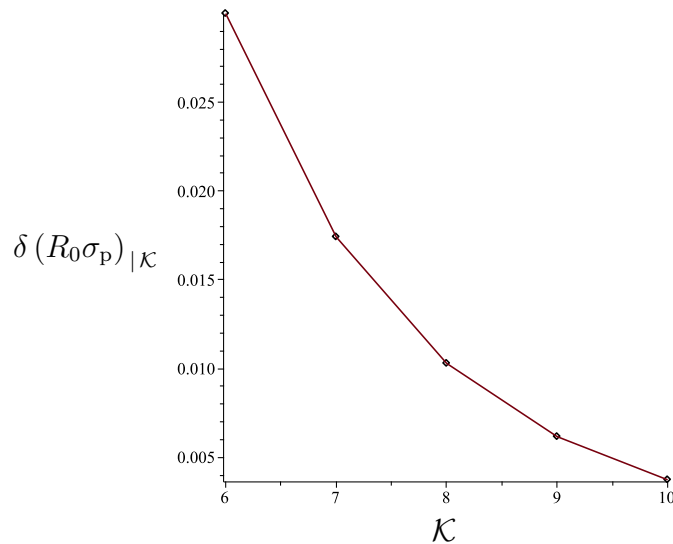
Figure 6.3: Convergence estimate of the normalized proper surface mass density $R_0\sigma_{\mathrm{p}}$ depending on $\mathcal{K}$, plotted for $g = 0.9$, $\epsilon = 0$ and $\eta = 0.2$.

As it turns out, the normalized proper surface mass density $R_0\sigma_{\mathrm{p}}$ exhibits a particu-

---

charged rotating disc of dust.

larly good convergence behaviour. Fig. 6.3 expresses this clearly. Here, the convergence was estimated using the same formula, eq. (5.52), as in the previous chapter. This justifies the discussion up to $g = 0.9$ in this section.

6.2 Multipole moments

The exterior spacetime of an astrophysical body can be characterized by its multipole moments. In 1970, Geroch introduced multipole moments in a coordinate independent way for static, asymptotically flat, vacuum spacetimes [55] and Hansen later generalized them to stationary (asymptotically flat, vacuum) spacetimes [56]. In case of axisymmetry, Hansen further showed that the multipole moment tensors can be represented by scalars P_n [56]. Relying on an asymptotic expansion of the Ernst potential on the symmetry axis, Fodor, Hoenselaers and Perjés presented, in 1989, an explicit algorithm to compute those scalar multipole moments [57].

A generalization to stationary, electro-vacuum spacetimes with gravitational and electromagnetic multipole moments was published by Simon [58] and a corresponding calculation scheme for scalars P_n and Q_n, in the axisymmetric case, was given by Hoenselaers and Perjés [59]. As it turned out, [59] contained two non-trivial mistakes, however. The first one was corrected by Sotiriou and Apostolatos [60] and the second one recently, in 2021, by Fodor et al. [61].

In this section the gravitational and electromagnetic multipole moments of the charged rotating disc of dust using the latest calculation procedure by Fodor et al. [61] are calculated and discussed.[3] A study of the multipole moments of the exact solution of the uncharged disc of dust [6, 7, 12] was published by Kleinwächter et al. [63]. Additionally, a generalized version of the multipole conjecture by Filter and Kleinwächter [64] is formulated and tested using the multipole moments of the charged rotating disc of dust.

This section is based on [11] by Rumler and Meinel.[4]

6.2.1 Derivation of multipole moments

In order to derive multipole moments, we introduce new potentials

$$\Xi := \frac{1 - \mathcal{E}}{1 + \mathcal{E}} \quad \text{and} \quad \Lambda := \frac{2\Phi}{1 + \mathcal{E}} \, . \tag{6.4}$$

---

[3]Interesting in this context is also the gyromagnetic factor, see [62].
[4]© 2023 American Physical Society

The Ernst equations (2.55) in terms of these potentials read [59]:

$$\left(|\Xi| - |\Lambda| - 1\right)\Delta\Xi = 2\left(\bar{\Xi}\nabla\Xi - \bar{\Lambda}\nabla\Lambda\right)\cdot\nabla\Xi\,, \tag{6.5a}$$

$$\left(|\Xi| - |\Lambda| - 1\right)\Delta\Lambda = 2\left(\bar{\Xi}\nabla\Xi - \bar{\Lambda}\nabla\Lambda\right)\cdot\nabla\Lambda\,. \tag{6.5b}$$

Ξ and Λ can be expressed as an asymptotic expansion on the upper symmetry axis:

$$\Xi_+ = \frac{1}{\zeta}\sum_{n=0}^{\infty}\frac{m_n}{\zeta^n}\,, \quad \Lambda_+ = \frac{1}{\zeta}\sum_{n=0}^{\infty}\frac{q_n}{\zeta^n}\,. \tag{6.6}$$

According to Fodor et al. [61] the gravitational and electromagnetic multipole moments, P_n and Q_n, respectively, of an axisymmetric and stationary spacetime can be obtained from the coefficients m_n and q_n by the following procedure:

$$P_0 = m_0\,, \tag{6.7}$$

$$P_1 = m_1\,, \tag{6.8}$$

$$P_2 = m_2\,, \tag{6.9}$$

$$P_3 = m_3 + \frac{1}{5}\bar{q}_0 S_{10}\,, \tag{6.10}$$

$$P_4 = m_4 - \frac{1}{7}\bar{m}_0 M_{20} + \frac{3}{35}\bar{q}_1 S_{10} + \frac{1}{7}\bar{q}_0\left(3S_{20} - 2H_{20}\right)\,, \tag{6.11}$$

$$P_5 = m_5 - \frac{1}{21}\bar{m}_1 M_{20} - \frac{1}{3}\bar{m}_0 M_{30} + \frac{1}{21}\bar{q}_2 S_{10} + \frac{1}{21}\bar{q}_1\left(4S_{20} - 3H_{20}\right)$$
$$+ \frac{1}{21}\bar{q}_0\left(\bar{q}_0 q_0 S_{10} - \bar{m}_0 m_0 S_{10} + 14S_{30} + 13S_{21} - 7H_{30}\right) \tag{6.12}$$

and

$$Q_0 = q_0\,, \tag{6.13}$$

$$Q_1 = q_1\,, \tag{6.14}$$

$$Q_2 = q_2\,, \tag{6.15}$$

$$Q_3 = q_3 - \frac{1}{5}\bar{m}_0 H_{10}\,, \tag{6.16}$$

$$Q_4 = q_4 + \frac{1}{7}\bar{q}_0 Q_{20} - \frac{3}{35}\bar{m}_1 H_{10} - \frac{1}{7}\bar{m}_0\left(3H_{20} - 2S_{20}\right)\,, \tag{6.17}$$

$$Q_5 = q_5 + \frac{1}{21}\bar{q}_1 Q_{20} + \frac{1}{3}\bar{q}_0 Q_{30} - \frac{1}{21}\bar{m}_2 H_{10} - \frac{1}{21}\bar{m}_1\left(4H_{20} - 3S_{20}\right)$$
$$+ \frac{1}{21}\bar{m}_0\left(\bar{m}_0 m_0 H_{10} - \bar{q}_0 q_0 H_{10} - 14H_{30} - 13H_{21} + 7S_{30}\right)\,, \tag{6.18}$$

where

$$M_{ij} = m_i m_j - m_{i-1} m_{j+1} \,, \quad Q_{ij} = q_i q_j - q_{i-1} q_{j+1} \,, \tag{6.19}$$

$$S_{ij} = m_i q_j - m_{i-1} q_{j+1} \,, \quad H_{ij} = q_i m_j - q_{i-1} m_{j+1} \,. \tag{6.20}$$

Higher multipole moments become increasingly complicated. The gravitational and electromagnetic multipole moments are closely related to each other. In fact, by interchanging $m_n \leftrightarrow q_n$ and $\bar{m}_n \leftrightarrow -\bar{q}_n$ (correspondingly $M_{ij} \leftrightarrow Q_{ij}$ and $S_{ij} \leftrightarrow H_{ij}$), P_n transforms into Q_n. This results from the exchange symmetry $\Xi \leftrightarrow \Lambda$, $\bar{\Xi} \leftrightarrow -\bar{\Lambda}$ of the Ernst equations (6.5).

As discussed in chapter 2, the disc of dust additionally obeys reflection symmetry. Expressed on the upper symmetry axis, reflection symmetry is equivalent to [65–69]

$$\mathcal{E}_+ (\zeta) \, \bar{\mathcal{E}}_+ (-\zeta) = 1 \,, \quad \Phi_+ (\zeta) = -\bar{\Phi}_+ (-\zeta) \, \mathcal{E}_+ (\zeta) \tag{6.21}$$

or in terms of the new potentials to

$$\Xi_+ (\zeta) = -\bar{\Xi}_+ (-\zeta) \,, \quad \Lambda_+ (\zeta) = -\bar{\Lambda}_+ (-\zeta) \,. \tag{6.22}$$

This means that P_n and Q_n are real for even n and imaginary for odd n. The real and imaginary parts of P_n are called mass and angular momentum moments and those of Q_n are referred to as electric and magnetic moments. We denote:

$$P_n = M_n + \mathrm{i} J_n \,, \tag{6.23}$$

$$Q_n = E_n + \mathrm{i} B_n \,, \tag{6.24}$$

where due to reflection symmetry,

$$\text{for even } n: \quad P_n = M_n \,, \quad Q_n = E_n \,, \tag{6.25}$$

$$\text{for odd } n: \quad P_n = \mathrm{i} J_n \,, \quad Q_n = \mathrm{i} B_n \,. \tag{6.26}$$

Note that on the upper symmetry axis $\eta = 1$, $\zeta = \rho_0 \nu$ and thus

$$\Xi_+ = \frac{1}{\nu} \sum_{n=0}^{\infty} \frac{m_n^*}{\nu^n} \,, \quad \Lambda_+ = \frac{1}{\nu} \sum_{n=0}^{\infty} \frac{q_n^*}{\nu^n} \tag{6.27}$$

with dimensionless $m_n^* := \frac{m_n}{\rho_0^{n+1}}$ and $q_n^* := \frac{q_n}{\rho_0^{n+1}}$. In order to obtain coordinate independent expressions for the multipole moments, we normalize m_n and q_n by the disc's total proper radius:

$$m_n^\circ := \frac{m_n}{R_0^{n+1}} \,, \quad q_n^\circ := \frac{q_n}{R_0^{n+1}} \,. \tag{6.28}$$

Accordingly, the normalized gravitational and electromagnetic multipole moments are given by

$$P_n^\circ := \frac{P_n}{R_0^{n+1}} \quad \text{and} \quad Q_n^\circ := \frac{Q_n}{R_0^{n+1}} \, . \tag{6.29}$$

The first multipole moments are the gravitational mass, $P_0 = M_0 = M$, the angular momentum, $P_1/\mathrm{i} = J_1 = J$, the electric charge, $Q_0 = E_0 = Q$, and the magnetic dipole moment, $Q_1/\mathrm{i} = B_1 = D$.

Inserting the potentials f, b, α and β, eq. (3.16), into Ξ and Λ, eq. (6.4), and applying the above mentioned procedure reveals the multipole moments of the charged rotating disc of dust in terms of a post-Newtonian expansions up to tenth order. The first multipole moments, normalized by the disc's total proper radius R_0, up to third order $(k = 3)$, read[5]:

$$M^\circ = \frac{4g^2}{3\pi} - \frac{4\left(\epsilon^2 - 1\right)g^4}{45\pi} + \frac{1}{30240\pi^3} \left(\left(2790\epsilon^4 - 23699\epsilon^2 + 20464\right)\pi^2 \right.$$
$$\left. - 35840\epsilon^4 + 247296\epsilon^2 - 211456\right)g^6 + \mathcal{O}\left(g^8\right) \, , \tag{6.30}$$

$$J^\circ = \sqrt{1 - \epsilon^2} \left[\frac{8g^3}{15\pi} - \frac{2\left(34\epsilon^2 - 7\right)g^5}{315\pi} + \frac{1}{453600\pi^3} \left(\left(59894\epsilon^4 - 40131\epsilon^2 - 126312\right)\pi^2 \right.\right.$$
$$\left.\left. - 322560\epsilon^4 + 207872\epsilon^2 + 1189888\right)g^7 + \mathcal{O}\left(g^9\right) \right] \, , \tag{6.31}$$

$$Q^\circ = \epsilon \left[\frac{4g^2}{3\pi} - \frac{16\left(\epsilon^2 - 1\right)g^4}{45\pi} + \frac{1}{30240\pi^3} \left(\left(5862\epsilon^4 - 32147\epsilon^2 + 25840\right)\pi^2 \right.\right.$$
$$\left.\left. - 35840\epsilon^4 + 247296\epsilon^2 - 211456\right)g^6 + \mathcal{O}\left(g^8\right) \right] \, , \tag{6.32}$$

$$D^\circ = \epsilon\sqrt{1 - \epsilon^2} \left[\frac{4g^3}{15\pi} - \frac{\left(34\epsilon^2 - 115\right)g^5}{315\pi} + \frac{1}{907200\pi^3} \left(\left(58614\epsilon^4 - 177091\epsilon^2 - 200232\right)\pi^2 \right.\right.$$
$$\left.\left. - 322560\epsilon^4 - 867328\epsilon^2 + 3340288\right)g^7 + \mathcal{O}\left(g^9\right) \right] \, . \tag{6.33}$$

Below, also the normalized gravitational and electromagnetic quadrupole and octupole

---

[5]Note that M and J can also be represented by Komar integrals, which allows for a direct calculation (see e.g. [70]). Q can be written completely analogously as such an integral (see e.g. [15]). These definitions can be arranged in such a way that they agree with the asymptotically derived quantities of this section.

moments (up to $k = 3$) of the charged rotating disc of dust are listed:

$$P_2^\circ = M_2^\circ$$
$$= -\frac{4g^2}{15\pi} + \frac{4\left(5\epsilon^2 + 8\right)g^4}{105\pi} + \frac{1}{453600\pi^3}\left(\left(-46258\epsilon^4 + 23337\epsilon^2 - 71376\right)\pi^2\right.$$
$$\left. + 107520\epsilon^4 + 68096\epsilon^2 - 175616\right)g^6 + \mathcal{O}\left(g^8\right), \tag{6.34}$$

$$\frac{P_3^\circ}{i} = J_3^\circ$$
$$= \sqrt{1 - \epsilon^2}\left[-\frac{8g^3}{35\pi} + \frac{2\left(68\epsilon^2 + 171\right)g^5}{945\pi} - \frac{1}{4989600\pi^3}\left(\left(449242\epsilon^4 + 1015547\epsilon^2\right.\right.\right.$$
$$\left.\left.\left. - 256536\right)\pi^2 - 1520640\epsilon^4 - 4764672\epsilon^2 + 10543104\right)g^7 + \mathcal{O}\left(g^9\right)\right], \tag{6.35}$$

$$Q_2^\circ = E_2^\circ$$
$$= \epsilon\left[-\frac{4g^2}{15\pi} + \frac{4\left(4\epsilon^2 + 9\right)g^4}{105\pi} - \frac{1}{453600\pi^3}\left(\left(36018\epsilon^4 - 26537\epsilon^2 + 84816\right)\pi^2\right.\right.$$
$$\left.\left. - 107520\epsilon^4 - 68096\epsilon^2 + 175616\right)g^6 + \mathcal{O}\left(g^8\right)\right], \tag{6.36}$$

$$\frac{Q_3^\circ}{i} = B_3^\circ$$
$$= \epsilon\sqrt{1 - \epsilon^2}\left[-\frac{4g^3}{35\pi} + \frac{\left(62\epsilon^2 + 51\right)g^5}{945\pi} - \frac{1}{9979200\pi^3}\left(\left(394522\epsilon^4 + 54107\epsilon^2\right.\right.\right.$$
$$\left.\left.\left. - 2568216\right)\pi^2 - 1520640\epsilon^4 - 9022464\epsilon^2 + 19058688\right)g^7 + \mathcal{O}\left(g^9\right)\right]. \tag{6.37}$$

The mass, angular momentum, electric and magnetic moments are alternating positive and negative, to be more precise,

$$\begin{aligned} \text{for } l = 0, 2, 4, \dots : \qquad && M_{2l} &\geq 0, & J_{2l+1} &\geq 0, \\ && E_{2l} &\geq 0, & B_{2l+1} &\geq 0, \qquad (6.38) \\ \text{for } l = 1, 3, 5, \dots : \qquad && M_{2l} &\leq 0, & J_{2l+1} &\leq 0, \\ && E_{2l} &\leq 0, & B_{2l+1} &\leq 0. \qquad (6.39) \end{aligned}$$

It should be emphasized that the global prefactors, whereby

$$J_n \sim \sqrt{1 - \epsilon^2}, \quad E_n \sim \epsilon, \quad B_n \sim \epsilon\sqrt{1 - \epsilon^2}, \tag{6.40}$$

ensure that for vanishing charge, i.e. $\epsilon = 0$, all electromagnetic multipole moments Q_n become zero and for vanishing rotation, i.e. $\epsilon = 1$, all angular momentum and magnetic

moments, J_n and B_n, respectively.

Additionally, mass and electric moments contain only even powers of g and angular momentum and magnetic moments only odd, due to a symmetric and antisymmetric transformation behaviour, respectively, under a change of sense of rotation.

The influence of the global prefactors is also reflected in figs. 6.4 and 6.5. There, the dependence of the multipole moments normalized by the total proper radius, M_n°, J_n°, E_n° and B_n°, on the specific charge ϵ is depicted for $n = 0, ..., 7$. The relativity parameter is set to $g = 0.6$.
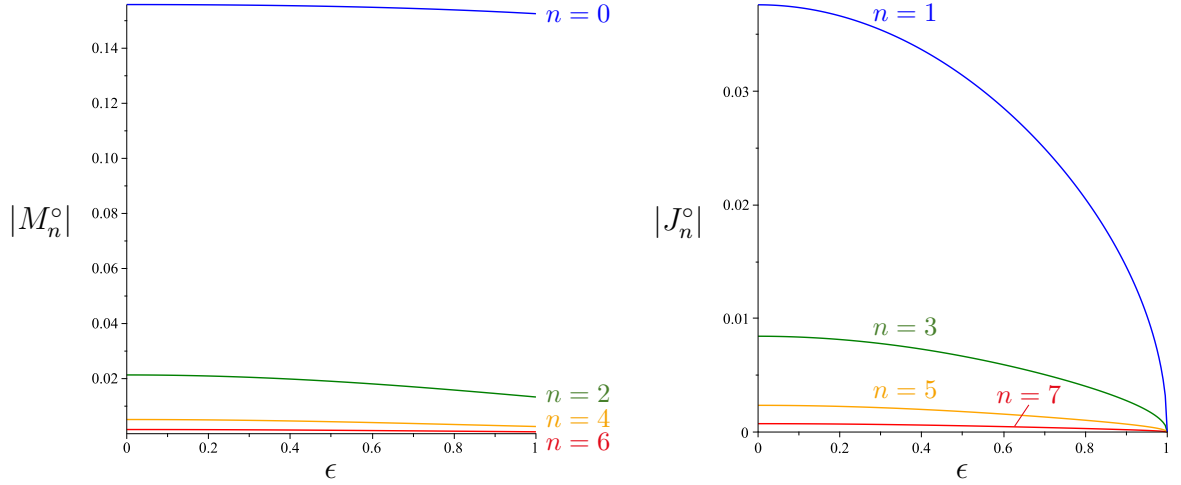
Figure 6.4: Normalized mass moments M_n° for $n \in \{0, 2, 4, 6\}$ (left) and normalized angular momentum moments J_n° for $n \in \{1, 3, 5, 7\}$ (right) as functions of the specific charge ϵ, plotted for $g = 0.6$ (after [11]).
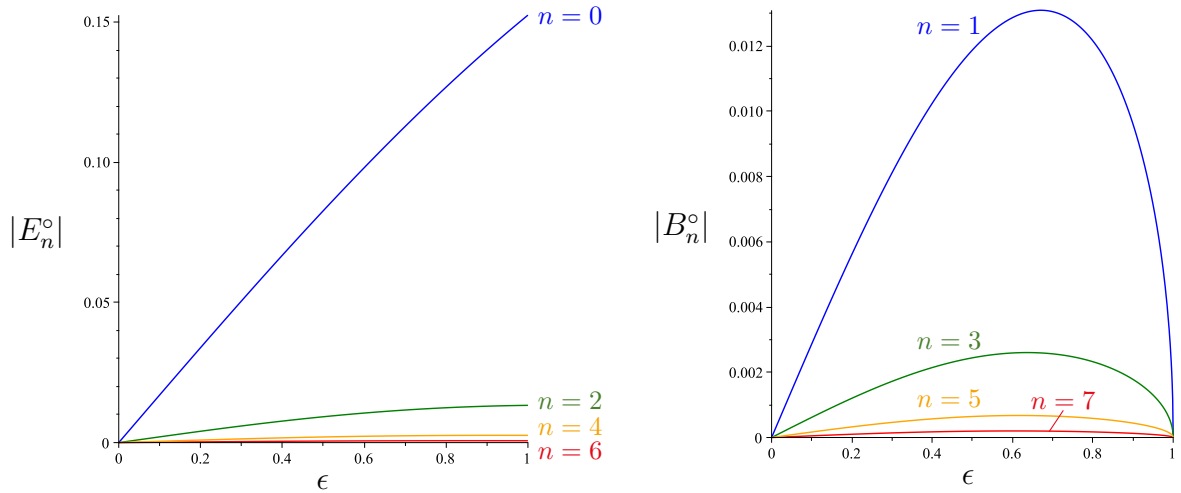
Figure 6.5: Normalized electric moments E_n° for $n \in \{0, 2, 4, 6\}$ (left) and normalized magnetic moments B_n° for $n \in \{1, 3, 5, 7\}$ (right) as functions of the specific charge ϵ, plotted for $g = 0.6$ (after [11]).

Fig. 6.6 shows the dependence of the normalized gravitational multipole moments on the relativity parameter g, where $\epsilon = 0.3$. As can be seen there, in the limit $g \to 0$
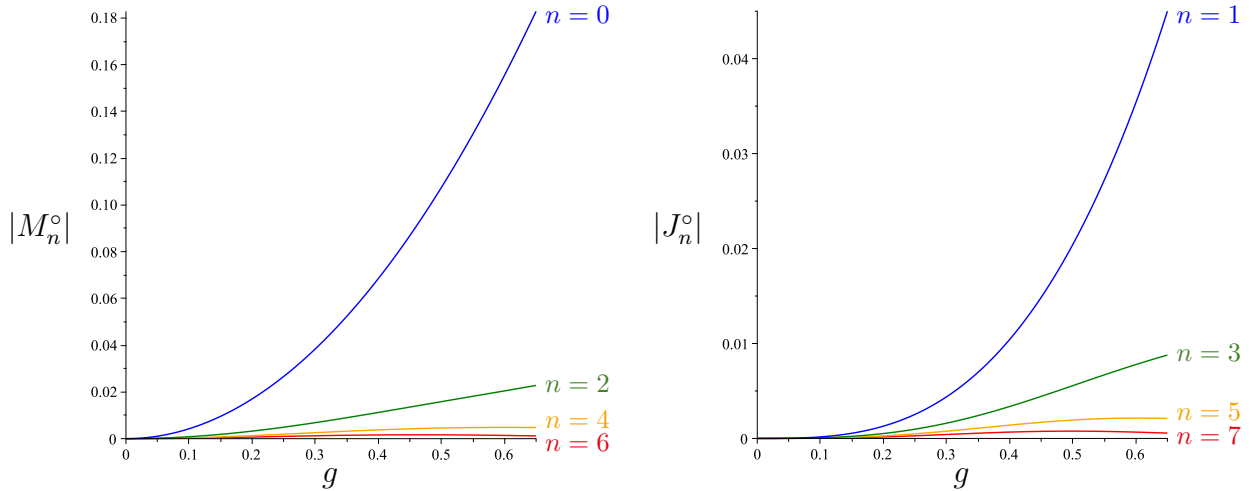
Figure 6.6: Normalized mass moments M_n° for $n \in \{0, 2, 4, 6\}$ (left) and normalized angular momentum moments J_n° for $n \in \{1, 3, 5, 7\}$ (right) as functions of the relativity parameter g, plotted for $\epsilon = 0.3$ (after [11]).

all gravitational multipole moments P_n° vanish and with increasing g the first ones (to be more precise, $n \leq 1$ for all ϵ) grow monotonically. The electromagnetic multipole moments Q_n show a completely analogous behaviour.

Remarkably, as can be seen in figs. 6.4 to 6.6, all multipole moments are perfectly ordered:

$$|M_n| \geq |M_{n+2}| \, , \tag{6.41}$$

$$|J_n| \geq |J_{n+2}| \, , \tag{6.42}$$

$$|B_n| \geq |B_{n+2}| \, , \tag{6.43}$$

$$|E_n| \geq |E_{n+2}| \, . \tag{6.44}$$

Notice that this ordering as well as the alternating sign can also be observed for the (exact) gravitational multipole moments of the uncharged disc of dust [63].

Interesting are also the ratios $\frac{P_n^\circ}{P_{n-2}^\circ}$ and $\frac{Q_n^\circ}{Q_{n-2}^\circ}$ of the individual moments. According to fig. 6.7, the absolute values of the ratios are greater, the higher the gravitational multipole moments are. The corresponding plots of the ratios of the electromagnetic multipole moments look almost identical to those of the gravitational moments and in fact agree at $g = 0$.[6] In addition, there is a pairwise agreement at $g = 0$: $\frac{P_3^\circ}{P_1^\circ} = \frac{P_4^\circ}{P_2^\circ} = -\frac{3}{7} \left(= \frac{Q_3^\circ}{Q_1^\circ} = \frac{Q_4^\circ}{Q_2^\circ} \right)$ and $\frac{P_5^\circ}{P_3^\circ} = \frac{P_6^\circ}{P_4^\circ} = -\frac{5}{9} \left(= \frac{Q_5^\circ}{Q_3^\circ} = \frac{Q_6^\circ}{Q_4^\circ} \right)$.

The decision to restrict our discussion to the first eight multipole moments P_n and Q_n and the relativity parameter to $g \leq 0.65$ is based on the convergence behaviour of the multipole moments. To estimate the convergence of, for example, the electric

---

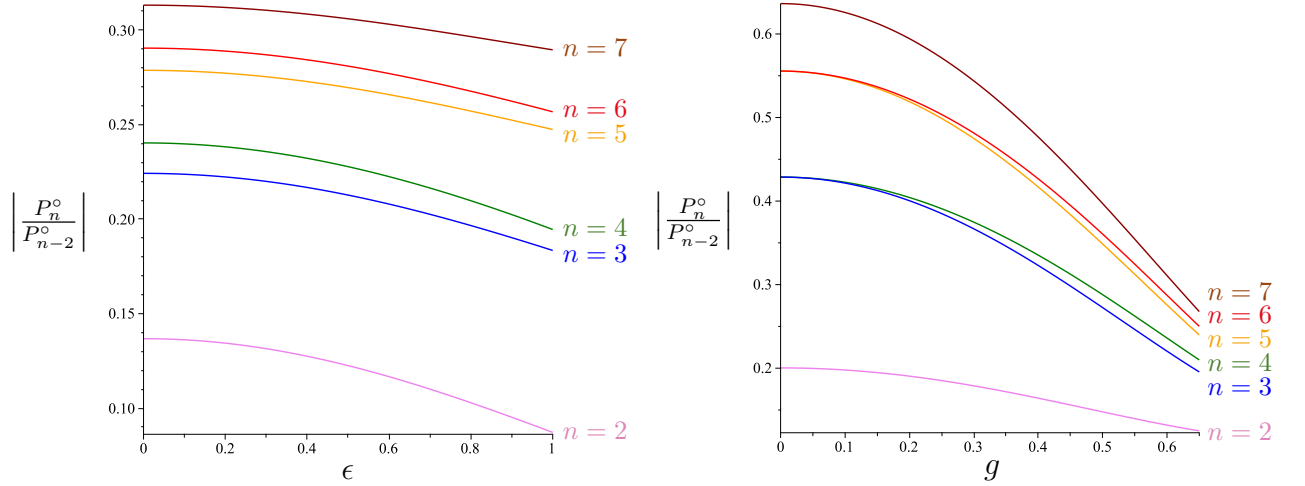[6]This is not a coincidence, as in the Newtonian limit $\Lambda = \epsilon \, \Xi$ holds, see subsection 6.2.3.

Figure 6.7: *Left panel*: Ratios $\frac{P_n^\circ}{P_{n-2}^\circ}$ for $n \in \{2, 3, ..., 7\}$ as functions of the specific charge ϵ, plotted for $g = 0.6$ (after [11]). *Right panel*: Ratios $\frac{P_n^\circ}{P_{n-2}^\circ}$ for $n \in \{2, 3, ..., 7\}$ as functions of the relativity parameter g, plotted for $\epsilon = 0.3$ (after [11]).

moments, we use eq. (5.52), i.e. for each $n = 0, ..., 6$:

$$\delta E_{n \,|\, \mathcal{K}}^\circ := \frac{\left| E_{n \,|\, \mathcal{K}}^\circ - E_{n \,|\, \mathcal{K}-1}^\circ \right|}{\left| E_{n \,|\, \mathcal{K}}^\circ \right|}, \quad \text{where} \quad E_{n \,|\, \mathcal{K}}^\circ := \sum_{k=1}^{\mathcal{K}} E_{n 2k}^\circ g^{2k}. \tag{6.45}$$

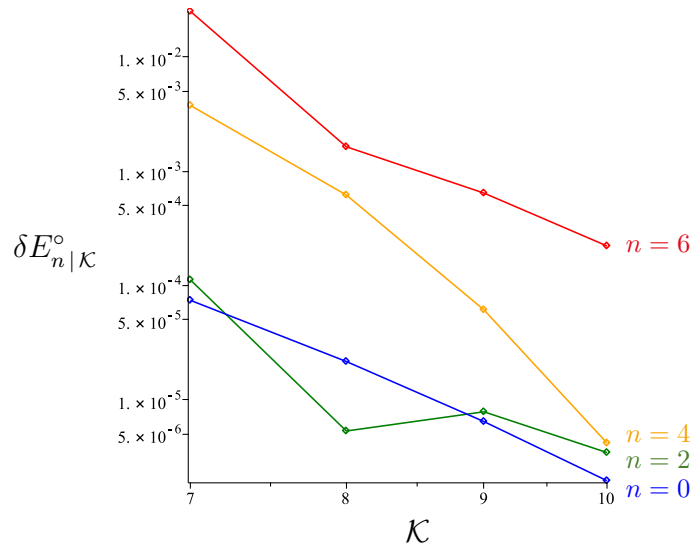The study of the convergence behaviour of the other multipole moments is carried out analogously.

Figure 6.8: Convergence estimate of the normalized multipole moments E_0°, E_2°, E_4° and E_6° at order $k = \mathcal{K}$, plotted for $g = 0.65$ and $\epsilon = 0$ (after [11]).

According to fig. 6.8, the relative change by adding the last order is for all E_n°

$(n = 0, .., 6)$ less than or equal to 2.2×10^{-4} for $g = 0.65$. (In this case $\epsilon = 0$ shows the worst convergence behaviour.) Moreover, as can already be guessed from the calculation scheme, the higher the multipole moments, the less good the convergence. For the mass, angular momentum and magnetic moments we get an even better, but otherwise analogous convergence behaviour.[7]

Table 6.1: Normalized multipole moments M_6°, J_7°: charged disc in the limit $\epsilon = 0$ (post-Newtonian expansion up to tenth order) versus uncharged disc (exact solution) (after [11]).

		charged disc$|_{\epsilon=0}$	uncharged disc
$g = 0.55$	$|M_6^\circ|$	$1.628\,655\,0 \times 10^{-3}$	$1.628\,655\,1 \times 10^{-3}$
	$|J_7^\circ|$	$8.066\,392\,4 \times 10^{-4}$	$8.066\,395\,2 \times 10^{-4}$
$g = 0.6$	$|M_6^\circ|$	$1.487\,599\,7 \times 10^{-3}$	$1.487\,600\,0 \times 10^{-3}$
	$|J_7^\circ|$	$7.363\,625\,1 \times 10^{-4}$	$7.363\,645\,0 \times 10^{-4}$
$g = 0.65$	$|M_6^\circ|$	$1.314\,102\,5 \times 10^{-3}$	$1.314\,103\,3 \times 10^{-3}$
	$|J_7^\circ|$	$6.359\,058\,8 \times 10^{-4}$	$6.359\,180\,7 \times 10^{-4}$

A direct comparison of the derived multipole moments (in terms of the post-Newtonian expansion) in the limit $\epsilon = 0$ with the exact solutions of the uncharged rotating disc of dust [63] shows an excellent agreement. In table 6.1 we compare the sixth and seventh gravitational multipole moments for different values of the relativity parameter. In particular, the relative error of the multipole moments of the charged rotating disc of dust in the limit $\epsilon = 0$ with respect to the exact solutions at $g = 0.65$ is 6.1×10^{-7} for M_6° and 1.9×10^{-5} for J_7°.

6.2.2 Multipole conjecture

Filter and Kleinwächter [64] formulated an interesting conjecture about the multipole moments of (uncharged) rigidly rotating perfect fluid bodies: The absolute values of all higher multipole moments P_n $(n \geq 2)$ of an axistationary, rigidly rotating, perfect fluid body, surrounded by vacuum, are always greater than those of the corresponding moments of the Kerr spacetime with the same mass and angular momentum.

An obvious question now is whether this conjecture can be extended to more general, particularly charged, bodies.

The multipole moments of the Kerr-Newman spacetime, with mass M^{KN}, angular

---

[7]For $\epsilon = 0$ and $g = 0.65$ one gets: $\delta M_{6\,|\,10}^\circ = 7.5 \times 10^{-5}$, $\delta J_{7\,|\,10}^\circ = 1.9 \times 10^{-4}$, $\delta B_{7\,|\,10}^\circ = 9.7 \times 10^{-5}$.

momentum J^{KN} and charge Q^{KN}, are given by [60]:

$$P_n^{\text{KN}} = m_n^{\text{KN}} = M^{\text{KN}} \left(\mathrm{i} \frac{J^{\text{KN}}}{M^{\text{KN}}} \right)^n , \tag{6.46}$$

$$Q_n^{\text{KN}} = q_n^{\text{KN}} = Q^{\text{KN}} \left(\mathrm{i} \frac{J^{\text{KN}}}{M^{\text{KN}}} \right)^n . \tag{6.47}$$

With these we state:

Generalized multipole conjecture. *For the gravitational and electromagnetic multipole moments, P_n and Q_n, of an isolated, axisymmetric, stationary, physically well-defined body of ordinary matter, with mass M, angular momentum J and charge Q, holds for all $n \geq 2$:*

$$|P_n| \geq \left| \frac{J^n}{M^{n-1}} \right| , \quad |Q_n| \geq \left| \frac{QJ^n}{M^n} \right| . \tag{6.48}$$

Furthermore, in case of $J \neq 0$, equalities apply if and only if the body reaches a black hole limit.

The goal of this section is to test the generalized multipole conjecture using the charged rotating disc of dust as a concrete and physically meaningful candidate that satisfies the requirements of the conjecture.[8] To this end we plot the quantities X_n and Y_n that have to be less than or equal to 1 if the conjecture is valid:

$$X_n := \left| \frac{J^n}{M^{n-1} P_n} \right| \leq 1 , \quad Y_n := \left| \frac{QJ^n}{M^n Q_n} \right| \leq 1 . \tag{6.49}$$

Notice that due to the global prefactors of P_n and Q_n the quantities X_n and Y_n stay regular in the limits $\epsilon \to 1$ and $\epsilon \to 0$. In fact, X_n and Y_n vanish for $\epsilon \to 1$ and take finite values in the limit $\epsilon \to 0$ (see also fig. 6.10).

In the limit $\epsilon \to 1$ the angular momentum J vanishes and therefore also all Kerr-Newman multipole moments, P_n^{KN} and Q_n^{KN}, with $n \geq 1$. Since the multipole moments of the disc, P_n and Q_n, become zero only for odd, but not for even n, the disc spacetime clearly does not attain the Reissner-Nordström solution in this limit.

As can be seen in figs. 6.9 and 6.10, indeed all X_n and Y_n are smaller than 1 in the region $g \in [0, 0.65]$. Furthermore, there is a similar ordering as for the individual moments:

$$X_n \geq X_{n+1} , \quad Y_n \geq Y_{n+1} . \tag{6.50}$$

Therefore, most critical are X_2 and Y_2 and for increasing n the conjecture is even better fulfilled.

---

[8]Note that the Kerr-Newman spacetime furnished with the mass M, angular momentum J and charge Q of the charged rotating disc of dust does not describe a black hole but a hyperextreme solution ($Q^2 + \frac{J^2}{M^2} > M^2$).
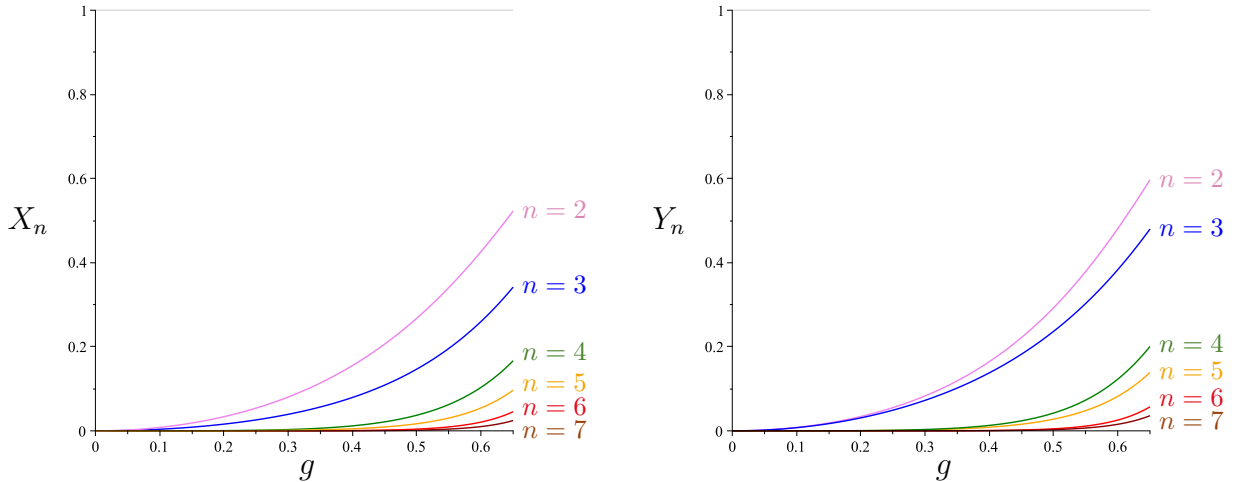
Figure 6.9: X_n (left) and Y_n (right) for $n \in \{2, 3, ..., 7\}$ as functions of the relativity parameter g, plotted for $\epsilon = 0$ (after [11]).
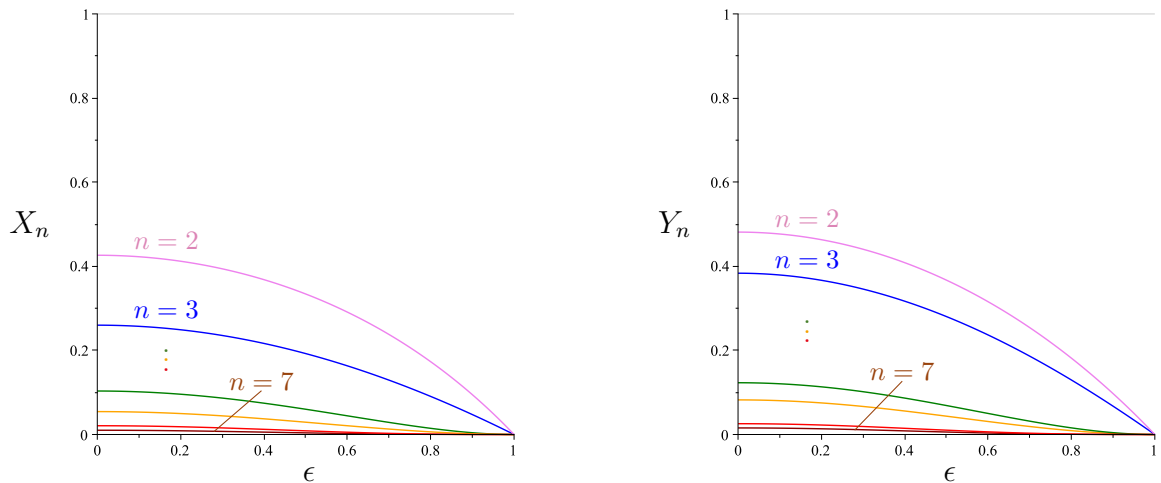

Figure 6.10: X_n (left) and Y_n (right) for $n \in \{2, 3, ..., 7\}$ as functions of the specific charge ϵ, plotted for $g = 0.6$ (after [11]).

On the other hand, the first X_n and Y_n are also the quantities with the best convergence behaviour. As n becomes larger, the convergence of X_n and Y_n (as it contains P_n and Q_n, respectively) becomes less and less good. The relative change (as defined in eq. (6.45)) by adding the last order is $\delta X_{7|10} = 1.9 \times 10^{-2}$ and $\delta Y_{7|10} = 9.7 \times 10^{-3}$, where $g = 0.65$ and $\epsilon = 0$.[9]

The good convergence of X_2 and Y_2 allows verification of the conjecture for slightly higher values of the relativity parameter until $g \approx 0.8$ and $g \approx 0.75$, respectively.[10] The conjecture remains true there. For the limit $g \to 1$, Breithaupt et al. [9] provided strong evidence that the multipole moments of the charged rotating disc of dust converge to

---

[9]Specifically for X_7 and Y_7, the convergence gets slightly worse for higher ϵ: $\delta X_{7|10} = 4.1 \times 10^{-2}$ and $\delta Y_{7|10} = 3.4 \times 10^{-2}$, for $\epsilon = 1$ and $g = 0.65$. However, as X_n and Y_n for high n are not decisive for the verification of the conjecture, this is not problematic.

[10]For $\epsilon = 0$: $\delta X_{2|10} = 1.9 \times 10^{-2}$ at $g = 0.8$ and $\delta Y_{2|10} = 2.8 \times 10^{-2}$ at $g = 0.75$.

those of the (extreme) Kerr-Newman spacetime.

Additionally, one can observe from fig. 6.10 that all values of X_n and Y_n decrease equally with increasing ϵ. This fact is very convenient for our purposes, since for the most critical case, $\epsilon = 0$, the exact multipole moments [63] of the uncharged disc of dust are available. The relative error of $X_2|_{\epsilon=0}$ with respect to the corresponding exact value of the uncharged disc of dust is 1.3×10^{-2} for $g = 0.8$. For the gravitational multipole moments of the uncharged disc of dust Filter and Kleinwächter showed that the conjecture is fulfilled [64].

In summary, the conjecture holds at least up to $g \approx 0.8$ for the gravitational and up to $g \approx 0.75$ for the electromagnetic multipole moments. In the limit $g \to 1$ the quantities X_n and Y_n converge to 1 according to Breithaupt et al. and for the most critical case, $\epsilon = 0$, by means of the exact solution of the uncharged disc of dust it was proven that $X_n \leq 1$. All this taken together, we conclude that (within the scope of accuracy of the post-Newtonian expansion) the generalized multipole conjecture stated above is fulfilled for the multipole moments of the charged rotating disc of dust.

6.2.3 Newtonian and ECD-body

Besides the charged rotating disc of dust that serves as the main candidate to test the generalized multipole conjecture, there are two other physical bodies that can be readily examined.

First, we consider an isolated, axisymmetric, stationary, physically reasonable, constantly charged, rigidly rotating body within Newtonian theory. The only metric function that plays a role for this Newtonian body is U, where $f = 1 + 2U$, see also subsection 5.2.2. The electric potential $U^{\mathrm{E}} := \alpha = -A_t$ can also be expressed in terms of the Newtonian potential: $U^{\mathrm{E}} = -\epsilon U$. The resulting potentials from which the multipole moments are derived read:

$$\Xi^{\mathrm{N}} = -U\,, \quad \Lambda^{\mathrm{N}} = -\epsilon U\,. \tag{6.51}$$

As U is a real function, we can immediately conclude that all angular and magnetic moments, J_n^{N} and B_n^{N}, and in particular the angular momentum J^{N}, vanish.[11] This implies that all multipole moments P_n^{KN} and Q_n^{KN} on the right side of the conjecture are zero. (In fact, P_n^{KN} and Q_n^{KN} thus describe a Reissner-Nordström spacetime.) The generalized multipole conjecture is therefore trivially fulfilled.

Second, we discuss an isolated, axisymmetric body of electrically counterpoised dust,

---

[11]In general, the angular momentum and the magnetic field does not always vanish in the Newtonian limit. There is no strict definition of the Newtonian limit and for each situation one has to decide carefully what is actually relevant. For the charged rotating disc of dust, for instance, the magnetic field does not play a role for the Newtonian balance of forces in the disc, eq. (5.19), and the angular momentum does not contribute to the Newtonian gravitational field, eq. (5.25).

see subsection 5.2.3. As described, such ECD-configurations have a specific charge $\epsilon = \pm 1$ and are static, i.e. they are non-rotating. Similar to the Newtonian case, the only appearing potentials are U and α and they are connected via the relation $f^{1/2} = e^U = 1 - \epsilon\alpha$. As it turns out, the resulting potentials Ξ^{ECD} and Λ^{ECD} are perfectly analogous to the Newtonian ones:

$$\Xi^{\text{ECD}} = -V\,, \quad \Lambda^{\text{ECD}} = -\epsilon V\,, \tag{6.52}$$

where $V = 1 - e^{-U}$. With the same reasoning as above, since V is real, we conclude that the generalized multipole conjecture also holds for the described ECD-body.

6.3 Ergosphere

When a rotating source becomes sufficiently relativistic, a region with an extreme version of frame dragging, called an ergosphere, is expected to form. Within this region the normally timelike Killing vector $\boldsymbol{\xi}$, which is associated with stationarity, becomes spacelike

$$\xi^i \xi_i > 0\,. \tag{6.53}$$

The boundary surface where $\xi^i \xi_i = 0$ is referred to as ergosurface and represents a "static limit". Static observers (relative to spatial infinity) with $(\rho, \zeta, \varphi) = \text{const.}$ and thus a four-velocity vector proportional to $\boldsymbol{\xi}$ can no longer exist here. For $\xi^i \xi_i > 0$, the only term in the Lewis-Papapetrou line element (2.1) that can provide a negative contribution to a timelike world line ($\mathrm{d}s^2 < 0$) is $2g_{\varphi t}\mathrm{d}\varphi\mathrm{d}t$. Generally, $g_{\varphi t} < 0$ for a source rotating uniformly with $\Omega > 0$.[12] The ergosphere therefore forces any observer to rotate with an angular velocity

$$\frac{\mathrm{d}\varphi}{\mathrm{d}t} > 0 \tag{6.54}$$

in the same direction as the source [12].

Note that even though the Killing vector $\boldsymbol{\xi}$ is no longer timelike inside the ergosphere, the spacetime is still stationary in a local sense if there exists locally a linear combination of $\boldsymbol{\xi}$ and $\boldsymbol{\eta}$ which is timelike, see, e.g., [71]. In general, one can assume that this is the case for rotating fluid bodies in equilibrium [12].[13]

Examining the metric function $f = -g_{tt} = -\xi^i \xi_i$ corresponding to the charged rotating disc of dust shows that for sufficiently high values of the relativity parameter g (and $\epsilon \neq 1$) indeed an ergosphere emerges.[14]

---

[12]Conversely, for a source rotating uniformly with $\Omega < 0$ holds $g_{\varphi t} > 0$.

[13]However, at the horizon and in the interior of a black hole there is no such timelike linear combination of $\boldsymbol{\xi}$ and $\boldsymbol{\eta}$.

[14]A brief discussion of ergospheres in context of the charged rotating disc of dust can also be found in [22] by Breithaupt.
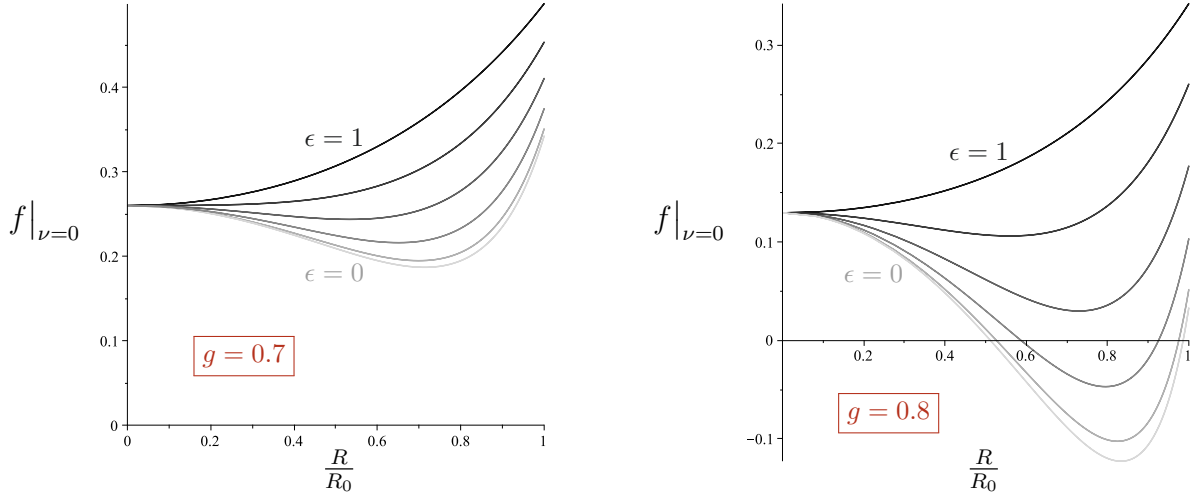
Figure 6.11: Metric function $f\big|_{\nu=0}$ depending on the normalized proper radius $\frac{R}{R_0}$, shown for $\epsilon \in \{0, 0.2, 0.4, 0.6, 0.8, 1\}$ and $g = 0.7$ (left) or $g = 0.8$ (right).
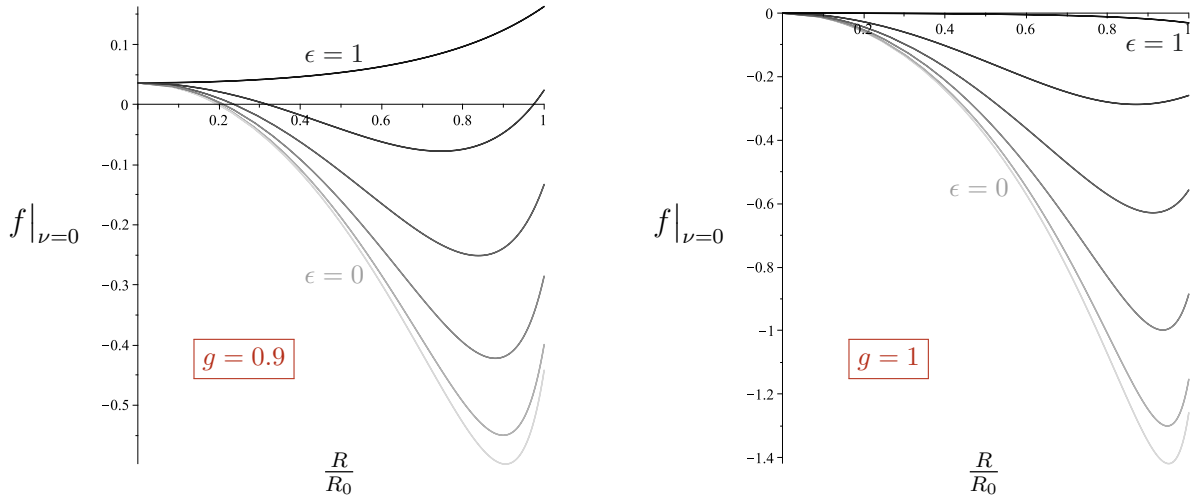

Figure 6.12: Metric function $f\big|_{\nu=0}$ depending on the normalized proper radius $\frac{R}{R_0}$, shown for $\epsilon \in \{0, 0.2, 0.4, 0.6, 0.8, 1\}$ and $g = 0.9$ (left) or $g = 1$ (right).

According to figs. 6.11 and 6.12, the ergosphere forms within the disc and grows with increasing g. In particular, for a uncharged disc configuration the ergosphere appears for $g = 0.764\,870\,6$ at $\frac{R}{R_0} = 0.798\,368\,1$ and reaches the rim of the disc ($\frac{R}{R_0} = 1$) for $g = 0.808\,655\,5$, see table 6.2. For even higher g the ergosphere extends radially beyond the disc and approaches the centre in the limit $g \to 1$. With increasing specific charge ϵ, the necessary values for g at which an ergosphere occurs and at which it reaches the rim rise as well. This is an expected behaviour, since ergospheres are generated by rotating sources and the rotation speed of the disc decreases with growing ϵ. The location within the disc where the ergosphere emerges shifts slightly towards the centre for increasing ϵ, which might be related to the changing surface mass density (see section 6.1).

In the case of $\epsilon = 1$, the disc is static and therefore the formation of an ergosphere is impossible. As shown in [9], in the limit $g \to 1$ the charged rotating disc of dust (most

Table 6.2: Evolution of the ergosphere within the charged rotating disc of dust for different values of the specific charge ϵ.

		emergence of the ergosphere	ergosphere reaches rim
$\epsilon = 0$	g	0.764 870 6	0.808 655 5
	$\frac{R}{R_0}$	0.798 368 1	1
$\epsilon = 0.2$	g	0.769 578 1	0.813 950 4
	$\frac{R}{R_0}$	0.793 490 6	1
$\epsilon = 0.4$	g	0.784 420 8	0.830 535 7
	$\frac{R}{R_0}$	0.777 508 1	1
$\epsilon = 0.6$	g	0.812 038 7	0.860 738 7
	$\frac{R}{R_0}$	0.745 335 6	1
$\epsilon = 0.8$	g	0.859 750 0	0.909 259 1
	$\frac{R}{R_0}$	0.682 831 7	1

certainly) approaches the extreme Kerr-Newman black hole solution and therefore in the case of $\epsilon = 1$ the extreme Reissner-Nordström black hole solution. On the black hole horizon holds the condition $f \overset{\epsilon=1}{=} f' = 0$, which explains the curve with $\epsilon = 1$ in the right panel of fig. 6.12. The remaining curves in fig. 6.12 (right) represent (most likely) the ergosphere of the extreme Kerr-Newman solution for different values of $\epsilon < 1$. Fig. 6.12 (right), however, takes the perspective of the "inner world".[15]

The ergosphere is of course not restricted to the layer of the disc, as can be seen in fig. 6.13. Taking the rotation symmetry into account, the ergosphere has in fact a torus-like shape. With increasing g the ergosphere inflates and spreads out (in all directions) across the disc. The characteristic shapes of the ergosphere (for some ϵ) coincide with those of the exact solution of the uncharged rotating disc of dust in [74] (see also [12]).

The convergence is examined, as before, via eq. (5.52). Even for $g = 1$ the estimated error is, according to fig. 6.14, only $\delta \left(f\big|_{\nu=0} \right)_{|10} = 0.01$. Beyond the disc, based on the ζ-values used in fig. 6.13, the estimated error is still within 0.01 to 0.02.[16]

---

[15]For some fluid bodies (in particular the uncharged rotating disc of dust) a quasi-stationary transition to a black hole leads to a separation of spacetimes into an asymptotically flat "outer world" with the extreme Kerr metric outside the event horizon and a non-asymptotically flat "inner world", containing the fluid body, with the extreme near-horizon geometry at spatial infinity [12, 16, 72] (see also [73]). A corresponding separation of spacetimes also occurs for ECD-configurations [51] and most probably for the charged rotating disc of dust.

[16]A direct comparison with the exact solution of the uncharged disc of dust also shows an excellent agreement. The two values for g in the first line of table 6.2 in terms of the relativity parameter μ (see subsection 5.2.4) read 1.68843657... and 1.99999999..., whereas the exact values are 1.68849467... and 2 (see [12]).
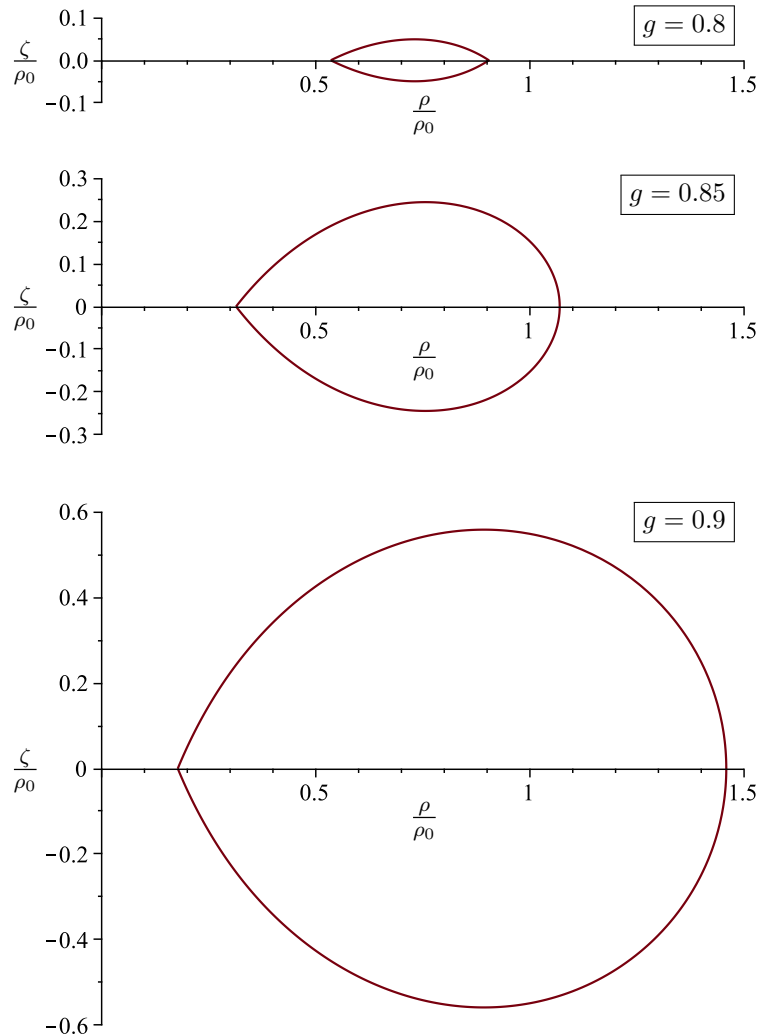
Figure 6.13: Illustration of the ergosurface in the ρ,ζ-plane (in units of ρ_0), plotted for configurations with $\epsilon = 0.4$ and $g = 0.8$ (top), $g = 0.85$ (middle) or $g = 0.9$ (bottom).

6.4 Motion of test particles

Investigating the motion of test particles is a very direct and instructive method for analysing the geometric structure of a given spacetime within the framework of general relativity. It is well known that freely falling neutral test particles travel along geodesics and (electrically) charged ones generally move under the influence of the gravitational and the electromagnetic field (if present).

The motion of test particles also plays a role in astrophysics, for instance in the accretion of matter by a central object and in the (indirect) formation of black hole shadows by circular photon orbits.

Various aspects of geodesic motion around Kerr and Kerr-Newman black holes have been studied, see, e.g., the publications by Bardeen et al. [75] and Dadhich and Kale [76]. Also charged particle orbits in the Kerr-Newman spacetime have been explored
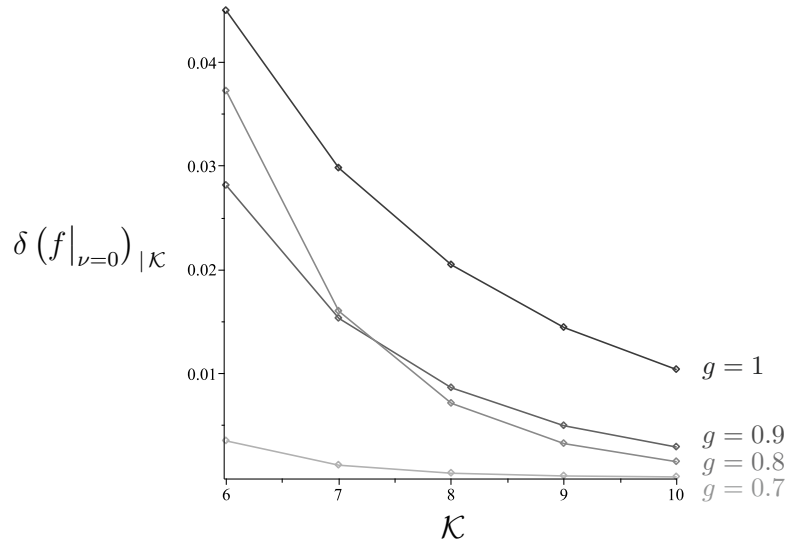
Figure 6.14: Convergence estimate of the metric function $f\big|_{\nu=0}$ depending on $\mathcal{K}$, plotted for $g \in \{0.7, 0.8, 0.9, 1\}$, $\epsilon = 0$ and $\eta = 0.5$.

(see, e.g., [77, 78]).

Meinel and Kleinwächter [74] (see also [12]) and Ansorg [79] analysed (timelike) geodesic motion in the gravitational field of the uncharged rotating disc of dust.

In this section we investigate circular orbits of neutral and charged test particles in the equatorial plane of an isolated, axisymmetric, stationary, reflection symmetric, charged, rotating body. Remarkably, even without knowing the explicit solution of the rotating body, energy, angular momentum and angular velocity of the test particles can be specified in closed form solely as functions of the metric, the electromagnetic four-potential and their radial derivatives.

The general examination of equatorial circular orbits of neutral and charged test particles is followed in the former case by a specialisation on the spacetime of the charged rotating disc of dust. A detailed discussion of these results is provided.

This section is based on [80] by Rumler.

6.4.1 Circular geodesic orbits of uncharged test particles

We first consider the exterior spacetime of an isolated, axisymmetric, stationary, reflection symmetric, charged, rotating body. These qualifications, besides a non-zero charge, are expected to be fulfilled for most astrophysical bodies. (Note that the special cases of zero charge and vanishing rotation are included.)

A freely falling uncharged test particle moves through spacetime along a (timelike) curve determined by the geodesic equation,

$$\frac{\mathrm{d}^2 x^i}{\mathrm{d}\tau^2} + \Gamma^i_{mn} \frac{\mathrm{d}x^m}{\mathrm{d}\tau} \frac{\mathrm{d}x^n}{\mathrm{d}\tau} = 0 \,, \tag{6.55}$$

where τ is the proper time of the test particle and Γ^i_{mn} are the Christoffel symbols.

The body is arranged so that the axis of rotation coincides with the ζ-axis and its equatorial plane is defined by $\zeta = 0$. We restrict the motion of the test particles to this plane, i.e. $\zeta = 0$, $\frac{d\zeta}{d\tau} = 0$ and $\frac{d^2\zeta}{d\tau^2} = 0$. (In order to keep the notation simple, the dependency on the coordinates is suppressed and, e.g., g_{ab} is written instead of $g_{ab}(\rho, \zeta = 0)$ in the following.) Let the geodesics, furthermore, be circular orbits.

Due to stationarity and axisymmetry the metric of the exterior spacetime of the body can be expressed in terms of Weyl-Lewis-Papapetrou coordinates, see eq. (2.45).

The circular motion of a test particle with constant angular velocity $\Omega_{\text{tp}} = \frac{d\varphi}{dt}$ (as seen from infinity) is also stationary and the four-velocity is therefore, according to eqs. (2.24) and (2.25), given by

$$(u_{\text{tp}})^i = \frac{dx^i}{d\tau} = \left(0, 0, \Omega_{\text{tp}} e^{-U'}, e^{-U'}\right), \quad \left(u'_{\text{tp}}\right)^i = \left(0, 0, 0, e^{-U'}\right), \tag{6.56}$$

where the primes denote the frame of reference co-rotating to the test particle, with $\varphi' = \varphi - \Omega_{\text{tp}} t$, from now on.[17]

Using eq. (6.56), the only non-vanishing component of the geodesic equation (6.55) is obtained for $i = \rho$:

$$g'_{tt,\rho} = 0. \tag{6.57}$$

The ζ-component vanishes due to the restriction of the motion to the equatorial plane of the body and reflection symmetry of the metric. In other words, setting $\zeta = 0$, $\frac{d\zeta}{d\tau} = 0$ and $\frac{d^2\zeta}{d\tau^2} = 0$ is actually solving the ζ-component of the geodesic equation.

Note that the transformation law for a transition to the co-rotating frame of the test particle reads in case of g_{tt}:

$$g'_{tt} = g_{tt} + 2\Omega_{\text{tp}} g_{\varphi t} + \Omega_{\text{tp}}^2 g_{\varphi\varphi}. \tag{6.58}$$

Eq. (6.57) is therefore equivalent to

$$g_{\varphi\varphi,\rho}\Omega_{\text{tp}}^2 + 2g_{\varphi t,\rho}\Omega_{\text{tp}} + g_{tt,\rho} = 0. \tag{6.59}$$

This immediately gives the solution for the angular velocity of the test particle:

$$\Omega_{1/2} = \frac{-g_{\varphi t,\rho} \pm \sqrt{g_{\varphi t,\rho}^2 - g_{\varphi\varphi,\rho} g_{tt,\rho}}}{g_{\varphi\varphi,\rho}}, \tag{6.60}$$

where (in general) one of the solutions corresponds to a prograde and the other one to a retrograde orbit.

---

[17]Notation-wise this does not cause a problem, as no reference to the co-rotating frame of the disc is made in this section.

The two symmetries, axisymmetry and stationarity, give rise to two conserved quantities associated with the motion of the test particle. Axisymmetry represented by the spacelike Killing vector $\boldsymbol{\eta} = \frac{\partial}{\partial \varphi}$ implies a conserved specific angular momentum $L = \eta_i \left(u_{\mathrm{tp}} \right)^i$ and stationarity with a timelike Killing vector $\boldsymbol{\xi} = \frac{\partial}{\partial t}$ ensures the conservation of the specific energy $E = -\xi_i \left(u_{\mathrm{tp}} \right)^i$. With the four-velocity from eq. (6.56) one obtains the specific angular momentum

$$L_{1/2} = \frac{g_{\varphi\varphi}\Omega_{1/2} + g_{\varphi t}}{\sqrt{-g_{\varphi\varphi}\Omega_{1/2}^2 - 2g_{\varphi t}\Omega_{1/2} - g_{tt}}} \tag{6.61}$$

and the specific energy

$$E_{1/2} = -\frac{g_{\varphi t}\Omega_{1/2} + g_{tt}}{\sqrt{-g_{\varphi\varphi}\Omega_{1/2}^2 - 2g_{\varphi t}\Omega_{1/2} - g_{tt}}} \tag{6.62}$$

of the test particle. Prograde orbits are defined by the positive specific angular momentum solution and retrograde orbits by the negative one.

It should be stressed that eqs. (6.60) to (6.62) hold for any (exterior) asymptotically flat, axisymmetric, stationary and reflection symmetric (electro-)vacuum spacetime and the solutions could be derived in a closed form without knowledge of the concrete spacetime metric.

Circular orbits only exist for

$$g_{\varphi\varphi}\Omega_{1/2}^2 + 2g_{\varphi t}\Omega_{1/2} + g_{tt} \leq 0 \,, \tag{6.63}$$

according to eqs. (6.61) and (6.62). In the limiting case of equality, specific angular momentum and specific energy diverge. This characterizes a photon orbit for prograde and retrograde motion respectively. Prograde or retrograde circular motion of uncharged test particles is therefore only possible for radii larger than that of the associated photon orbit.[18]

Due to frame dragging, there are so-called zero angular momentum observers, who are non-rotating with respect to the local geometry, but still have a non-zero angular velocity as seen from infinity:

$$\Omega_{\mathrm{nr}} = -\frac{g_{\varphi t}}{g_{\varphi\varphi}} \,. \tag{6.64}$$

Note that the motion of zero angular momentum observers is not necessarily geodesic.

There is an equivalent way of deriving eqs. (6.60) to (6.62) via the Lagrange formalism. Generally, the Lagrangian describing the (timelike) motion of a test particle in

---

[18]For charged test particles this innermost boundary of circular orbits generally no longer coincides with the photon orbit (as a result of the electromagnetic interaction between the rotating body and the test particle), see e.g. [78].

a spacetime furnished with the metric g_{ab} is

$$\mathcal{L} = \frac{1}{2} g_{ab} \dot{x}^a \dot{x}^b \, , \tag{6.65}$$

where $\dot{x}^a = \frac{\mathrm{d}x^a}{\mathrm{d}\tau}$. The resulting Euler-Lagrange equation is equivalent to the geodesic equation, i.e. the extremal path between two points is also straightest possible path.

As the Lagrangian corresponding to the above defined rotating body does not depend on φ and t (g_{ab} is axisymmetric and stationary), there are two conserved quantities:

$$L := \frac{\partial \mathcal{L}}{\partial \dot{\varphi}} = g_{\varphi\varphi} \dot{\varphi} + g_{\varphi t} \dot{t} \, , \tag{6.66}$$

$$E := -\frac{\partial \mathcal{L}}{\partial \dot{t}} = -g_{\varphi t} \dot{\varphi} - g_{tt} \dot{t} \, . \tag{6.67}$$

L and E coincide with the specific angular momentum and the specific energy, defined previously via the Killing vectors ($L = \eta_i (u_{\mathrm{tp}})^i$ and $E = -\xi_i (u_{\mathrm{tp}})^i$).

From eqs. (6.66) and (6.67), the angular velocity of the test particle $\Omega_{\mathrm{tp}} = \frac{\mathrm{d}\varphi}{\mathrm{d}t}$ (as seen from infinity) can be deduced:

$$\Omega_{\mathrm{tp}} = -\frac{g_{tt} L + g_{\varphi t} E}{g_{\varphi t} L + g_{\varphi\varphi} E} \, . \tag{6.68}$$

As above, we restrict the motion of the test particle to the equatorial plane of the body. Inserting $\dot{\varphi}$ and $\dot{t}$, using eqs. (6.66) and (6.67), into the normalization condition of the four-velocity for timelike curves, $g_{ab} \dot{x}^a \dot{x}^b = -1$, leads to

$$\frac{1}{2} g_{\rho\rho} \left(\frac{\mathrm{d}\rho}{\mathrm{d}\tau} \right)^2 + \mathcal{U} = 0 \, , \tag{6.69}$$

where

$$\mathcal{U} := -\frac{1}{2\rho^2} \left(g_{tt} L^2 + 2 g_{\varphi t} LE + g_{\varphi\varphi} E^2 \right) + \frac{1}{2} \tag{6.70}$$

is an effective potential. The motion of the test particle in the equatorial plane can therefore also be described by a motion in an effective potential.

A useful relation that was applied to $\mathcal{U}$ and that is also employed in subsequent calculations is

$$g_{\varphi t}^2 - g_{\varphi\varphi} g_{tt} = \rho^2 \, . \tag{6.71}$$

Differentiation of eq. (6.69) with respect to the particles proper time τ leads to the equation of motion:

$$g_{\rho\rho} \frac{\mathrm{d}^2 \rho}{\mathrm{d}\tau^2} + \frac{1}{2} g_{\rho\rho,\rho} \left(\frac{\mathrm{d}\rho}{\mathrm{d}\tau} \right)^2 + \mathcal{U}_{,\rho} = 0 \, . \tag{6.72}$$

One can verify that eq. (6.72) corresponds to the ρ-component of the geodesic equa-

tion.[19]

Circular orbits must fulfil the requirements $\frac{\mathrm{d}\rho}{\mathrm{d}\tau} = 0$ and $\frac{\mathrm{d}^2\rho}{\mathrm{d}\tau^2} = 0$. According to eqs. (6.69) and (6.72), the conditions for circular orbits (in the equatorial plane) are therefore $\mathcal{U} = 0$ and $\mathcal{U}_{,\rho} = 0$. These conditions imply:

$$g_{tt}L^2 + 2g_{\varphi t}LE + g_{\varphi\varphi}E^2 - \rho^2 = 0 \,, \tag{6.73}$$

$$g_{tt,\rho}L^2 + 2g_{\varphi t,\rho}LE + g_{\varphi\varphi,\rho}E^2 - 2\rho = 0 \,. \tag{6.74}$$

Notice that the above equations agree with those derived in [79].

Solving eqs. (6.73) and (6.74) reveals the specific angular momentum and the specific energy of the test particle:

$$\left|L_{1/2}\right| = \left|l_{1/2}\right| \frac{\rho}{\sqrt{g_{tt}l_{1/2}^2 + 2g_{\varphi t}l_{1/2} + g_{\varphi\varphi}}} \,, \tag{6.75}$$

$$\left|E_{1/2}\right| = \frac{\rho}{\sqrt{g_{tt}l_{1/2}^2 + 2g_{\varphi t}l_{1/2} + g_{\varphi\varphi}}} \,, \tag{6.76}$$

where

$$l_{1/2} := \frac{L_{1/2}}{E_{1/2}} = -\frac{2g_{\varphi t} - \rho g_{\varphi t,\rho} \pm \rho \sqrt{g_{\varphi t,\rho}^2 - g_{\varphi\varphi,\rho}g_{tt,\rho}}}{2g_{tt} - \rho g_{tt,\rho}} \,. \tag{6.77}$$

The sign of $E_{1/2}$ follows from eq. (6.67) (where $\dot{t} > 0$) and the sign of $L_{1/2}$ is then automatically given by $L_{1/2} = l_{1/2}E_{1/2}$. Clearly, the angular velocity (see eq. (6.68)) can also be expressed in terms of $l_{1/2}$:

$$\Omega_{1/2} = -\frac{g_{tt}l_{1/2} + g_{\varphi t}}{g_{\varphi t}l_{1/2} + g_{\varphi\varphi}} \,. \tag{6.78}$$

It can be shown explicitly that the two sets of equations for specific angular momentum, specific energy and angular velocity, i.e. eqs. (6.60) to (6.62) and eqs. (6.75) to (6.78), are indeed equivalent. In particular, the following relation holds:

$$g_{tt}l_{1/2}^2 + 2g_{\varphi t}l_{1/2} + g_{\varphi\varphi} = \frac{-\rho^2}{\left(-g_{\varphi t}\Omega_{1/2} - g_{tt}\right)^2} \left(g_{\varphi\varphi}\Omega_{1/2}^2 + 2g_{\varphi t}\Omega_{1/2} + g_{tt}\right) \,. \tag{6.79}$$

Eq. (6.78) can furthermore be easily converted to

$$l_{1/2} = -\frac{g_{\varphi\varphi}\Omega_{1/2} + g_{\varphi t}}{g_{\varphi t}\Omega_{1/2} + g_{tt}} \,. \tag{6.80}$$

The advantage of the second approach (using the Lagrange formalism in conjunction

---

[19]For not necessarily circular motion, the ρ-component of the geodesic equation is given by:
$g_{\rho\rho}\frac{\mathrm{d}^2\rho}{\mathrm{d}\tau^2} + \frac{1}{2}g_{\rho\rho,\rho}\left(\frac{\mathrm{d}\rho}{\mathrm{d}\tau}\right)^2 - \frac{1}{2}\left(g_{\varphi\varphi,\rho}\Omega_{\mathrm{tp}}^2 + 2g_{\varphi t,\rho}\Omega_{\mathrm{tp}} + g_{tt,\rho}\right)\left(\frac{\mathrm{d}t}{\mathrm{d}\tau}\right)^2 = 0.$

with the effective potential) is that the stability of the circular orbits can be analysed directly on the basis of the effective potential. According to eq. (6.69), non-circular motion is only possible for $\mathcal{U} < 0$. For given L and E, circular orbits are therefore stable (with respect to radial and angular perturbations) if and only if the extremum of $\mathcal{U}$ is a minimum, i.e. $\mathcal{U}_{,\rho\rho} > 0$. Using $\mathcal{U} = 0$ and $\mathcal{U}_{,\rho} = 0$, $\mathcal{U}_{,\rho\rho} > 0$ is equivalent to

$$g_{tt,\rho\rho}L^2 + 2g_{\varphi t,\rho\rho}LE + g_{\varphi\varphi,\rho\rho}E^2 - 2 < 0 \,. \tag{6.81}$$

For $\mathcal{U}_{,\rho\rho} < 0$ circular orbits are thus unstable.[20] Moreover, if $E^2 < 1$ circular orbits are bound, i.e. the test particle cannot reach infinity.[21]

Inserting the metric functions of the uncharged rotating disc of dust at the rim into the above formulae (of the first or second approach) reveals the same expressions for $\Omega_{1/2}$, $L_{1/2}$ and $E_{1/2}$ (with $1/2 = +/-$) as in [74]. Also the corresponding results for equatorial circular geodesic orbits in the (exterior) Kerr [75] and Kerr-Newman spacetime [76] can be obtained from the above formulae (using either approach).[22]
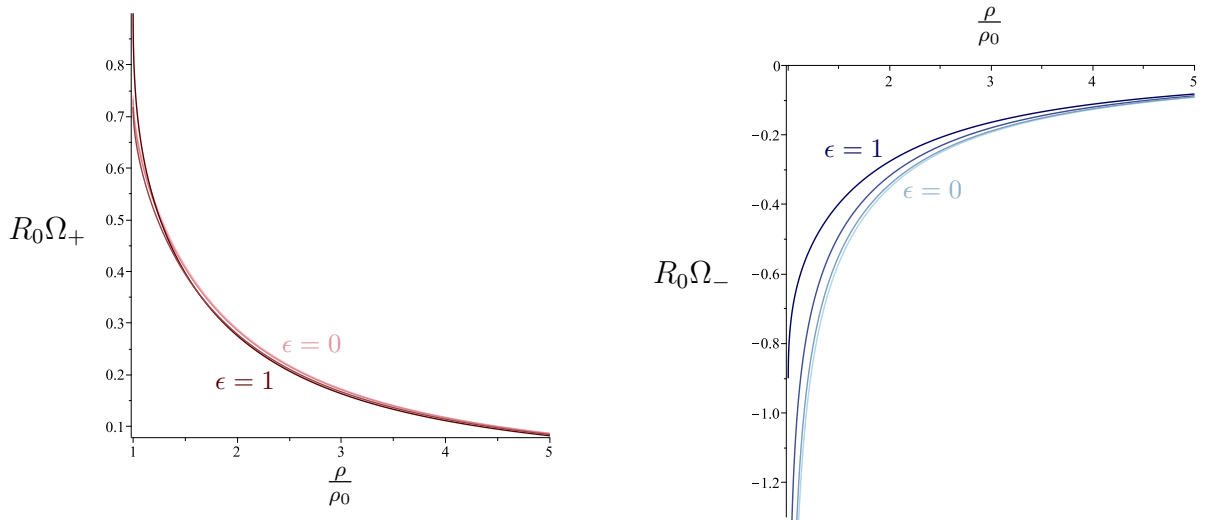

Figure 6.15: Normalized angular velocities $R_0\Omega_+$ (left) and $R_0\Omega_-$ (right) of test particles moving along (prograde/retrograde) circular geodesic orbits, shown for $g = 0.7$ and $\epsilon \in \{0, 1/3, 2/3, 1\}$ (after [80]).

Now circular geodesic orbits in the equatorial plane ($\eta = 0$) of the charged rotating disc of dust are to be discussed. By evaluating eqs. (6.60) to (6.62) or eqs. (6.75) to (6.78) with the metric of the disc, using eqs. (3.16) and (3.17), the angular velocity $\Omega_{1/2} = \Omega_{+/-}$, the specific angular momentum $L_{1/2} = L_{+/-}$ and the specific energy $E_{1/2} = E_{+/-}$ can be expressed in terms of a post-Newtonian expansion, see appendix A.2. Here "+" denotes direct and "−" retrograde orbits. The angular velocity

---

[20] A discussion of the stability of circular orbits in stationary, axisymmetric spacetimes can also be found in [81] and [82].

[21] For $E^2 > 1$ there can also be additional bound orbits, see, e.g., [79].
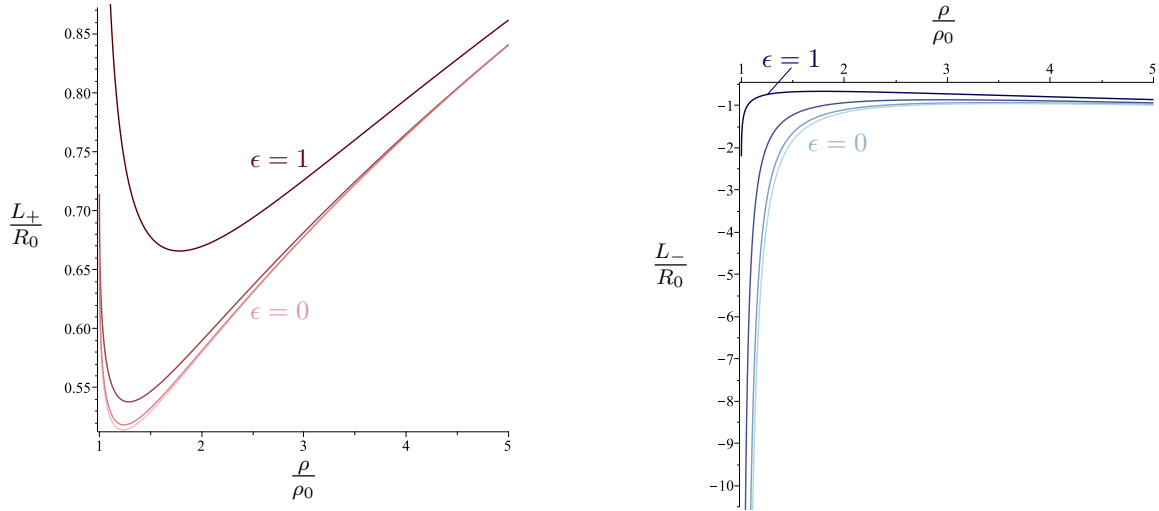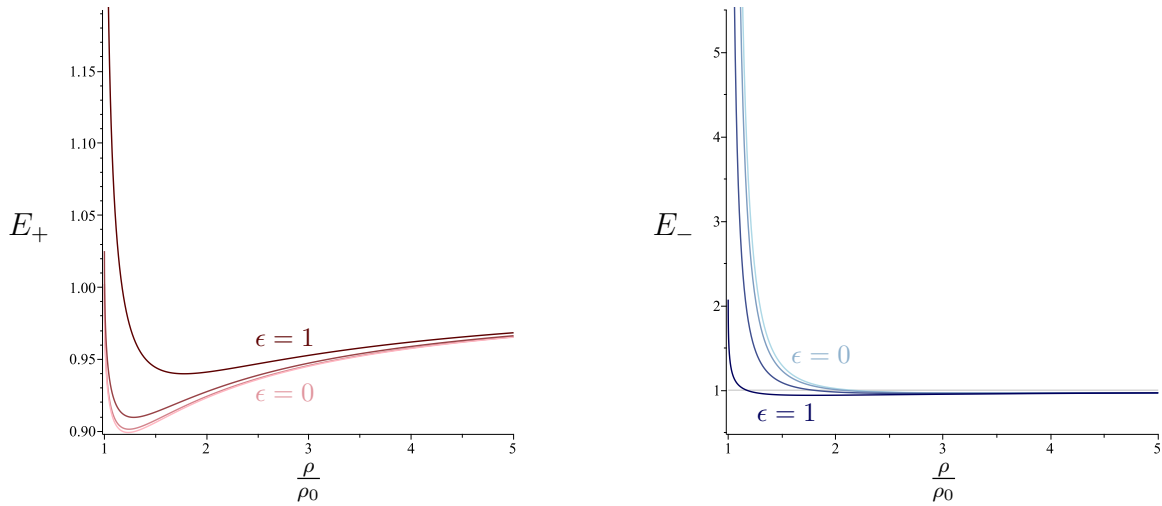
[22] Note that $\rho \geq 0$.

Figure 6.16: Normalized specific angular momenta $\frac{L_+}{R_0}$ (left) and $\frac{L_-}{R_0}$ (right) of test particles moving along (prograde/retrograde) circular geodesic orbits, shown for $g = 0.7$ and $\epsilon \in \{0, 1/3, 2/3, 1\}$ (after [80]).

Figure 6.17: Specific energies E_+ (left) and E_- (right) of test particles moving along (prograde/retrograde) circular geodesic orbits, shown for $g = 0.7$ and $\epsilon \in \{0, 1/3, 2/3, 1\}$ (after [80]).

of the disc, Ω, is non-negative.

It should be noted that the angular velocity $\Omega_{+/-}$ and the specific angular momentum $L_{+/-}$ are odd functions and the specific energy $E_{+/-}$ is an even function in g. This ensures that $\Omega_{+/-}$ and $L_{+/-}$ change their sign and $E_{+/-}$ remains unchanged under a change of sense of rotation of the disc (for $g \to -g$).

In the Newtonian limit (i.e. up to and including $\mathcal{O}(g^2)$) prograde and retrograde orbits coincide, as the angular momentum of disc, J, does not contribute to the Newtonian gravitational field.[23] In particular, it holds $\Omega_+ = -\Omega_-$, $L_+ = -L_-$ and $E_+ = E_-$.

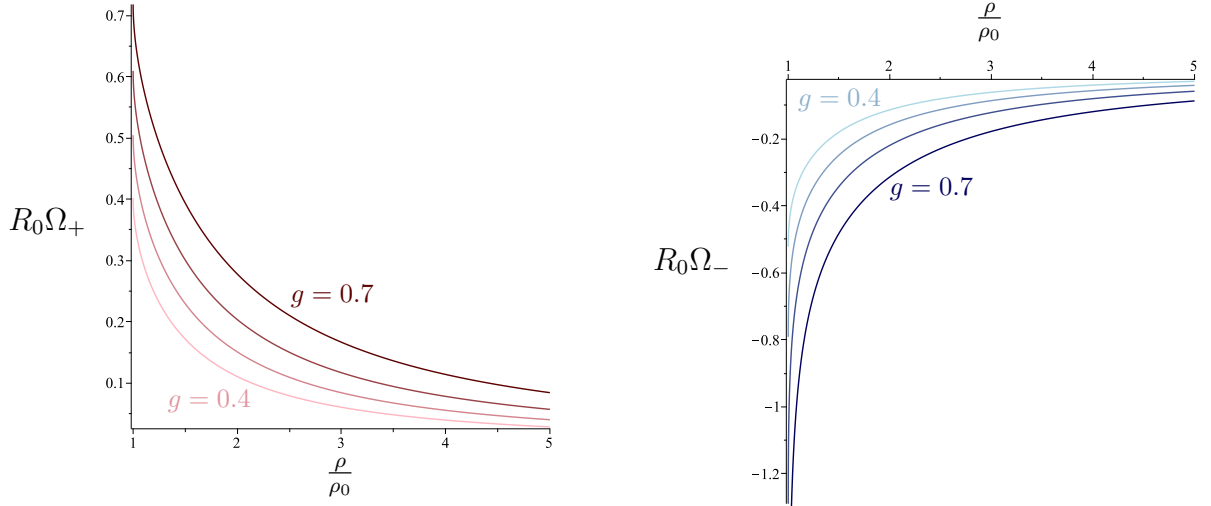[23]Indeed, the angular momentum of the disc starts at order g^3, see subsection 6.2.1.

Figure 6.18: Normalized angular velocities $R_0\Omega_+$ (left) and $R_0\Omega_-$ (right) of test particles moving along (prograde/retrograde) circular geodesic orbits, shown for $\epsilon = 0.7$ and $g \in \{0.4, 0.5, 0.6, 0.7\}$ (after [80]).
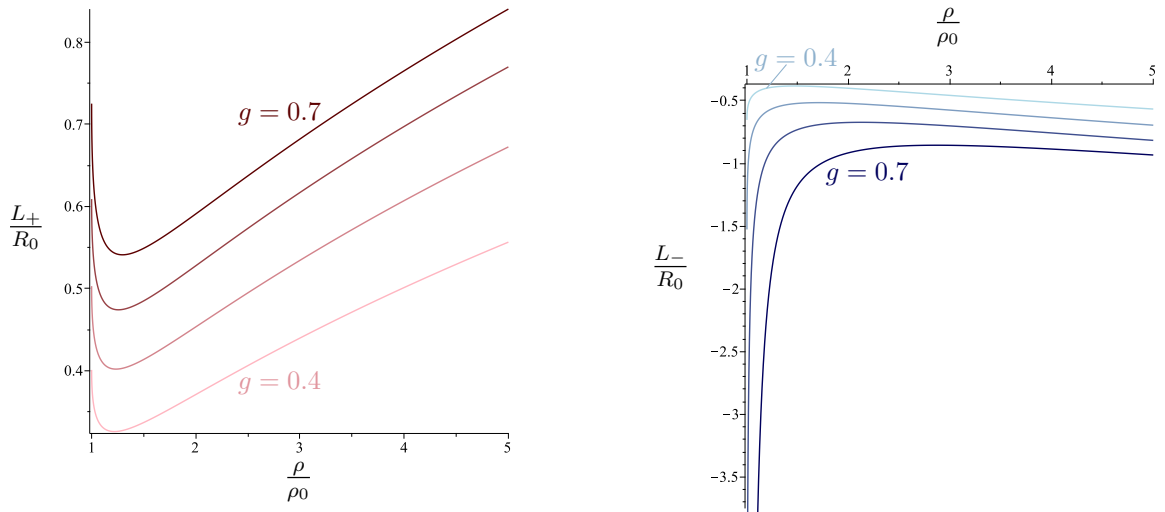

Figure 6.19: Normalized specific angular momenta $\frac{L_+}{R_0}$ (left) and $\frac{L_-}{R_0}$ (right) of test particles moving along (prograde/retrograde) circular geodesic orbits, shown for $\epsilon = 0.7$ and $g \in \{0.4, 0.5, 0.6, 0.7\}$ (after [80]).

Since the angular momentum of the disc vanishes in the limiting case of $\epsilon = 1$ (see subsection 6.2.1), prograde and retrograde orbits also coincide for $\epsilon = 1$.

It was further confirmed that the simultaneous limit $\epsilon \to 0$, $\rho \to \rho_0$ leads to the same results for $\Omega_\pm$ and $L_\pm$, $E_\pm$, in terms of a series expansion in g, as in [74]. Especially noteworthy is the fact that $\Omega_+ = \Omega$ in this limiting case. The reason is that the ρ-component of the geodesic equation of a test particle, eq. (6.57), also represents a boundary condition of the uncharged rotating disc of dust (see [12] and also eq. (2.71)).

Figs. 6.15 to 6.20 show, for fixed R_0, the radial dependence of the angular velocity $\Omega_\pm$, the specific angular momentum $L_\pm$ and the specific energy $E_\pm$ for different values
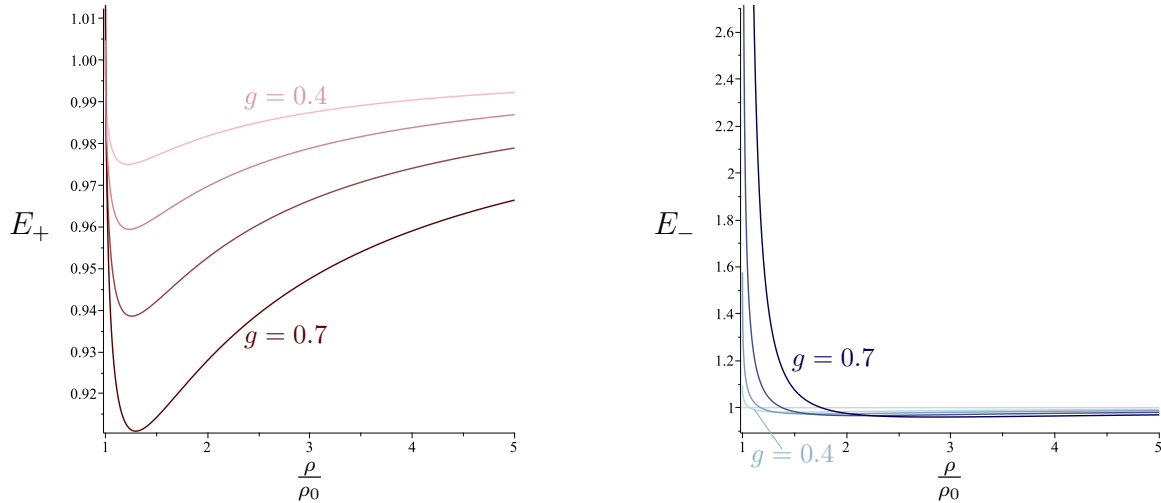
Figure 6.20: Specific energies E_+ (left) and E_- (right) of test particles moving along (prograde/retrograde) circular geodesic orbits, shown for $\epsilon = 0.7$ and $g \in \{0.4, 0.5, 0.6, 0.7\}$ (after [80]).

of the specific charge ϵ and the relativity parameter g. Apart from the region directly adjacent to the rim of the disc, the qualitative behaviour of the curves is very similar to the ones corresponding to the (exterior) spacetime of a Kerr-Newman black hole.

As can be seen in figs. 6.15 to 6.17, reducing the specific charge ϵ from 1 to 0 results (for fixed R_0) in a decrease in the absolute values of L_+ and E_+ and an increase in the absolute values of Ω_-, L_- and E_-. Ω_+ shows a mixed behaviour (for sufficiently large radii, however, it increases). Furthermore, raising the angular momentum of a Kerr-Newman black hole leads to the same qualitative change of the absolute values as for the charged rotating disc of dust by decreasing ϵ (with the exception of Ω_+). This is plausible, since the angular momentum of the disc comes with the global prefactor $\sqrt{1 - \epsilon^2}$, see subsection 6.2.1.[24]

On the other hand, the absolute values of $R_0\Omega_\pm$ and $\frac{L_\pm}{R_0}$ increase and E_+ decreases with the relativity parameter g, see figs. 6.18 to 6.20. E_- increases close to the rim and decreases for sufficiently large radii.

Interesting in the context of (equatorial) circular motion of neutral test particles are also the radii of photon orbits ($g'_{tt} = 0$), marginally bound orbits ($E^2 = 1$) and marginally stable orbits ($\mathcal{U}_{,\rho\rho} = 0$). They are shown as functions of ϵ and g in fig. 6.21.[25] The corresponding radii of the retrograde orbits decrease and those of the prograde orbits increase with $\epsilon \in [0, 1]$. In the case of $\epsilon = 1$ they coincide. For growing g both the radii of retrograde and prograde orbits increase and they merge in the Newtonian

---

[24]Increasing the charge parameter of the Kerr-Newman black hole qualitatively coincides with an increase of the specific charge of the disc in case of Ω_-, L_- and E_- (as well as Ω_+ for sufficiently large radii).

[25]Note that circular orbits with radii smaller than that of the photon orbit / marginally bound orbit / marginally stable orbit are forbidden / unbound / unstable and those with larger radii are permitted / bound / stable.
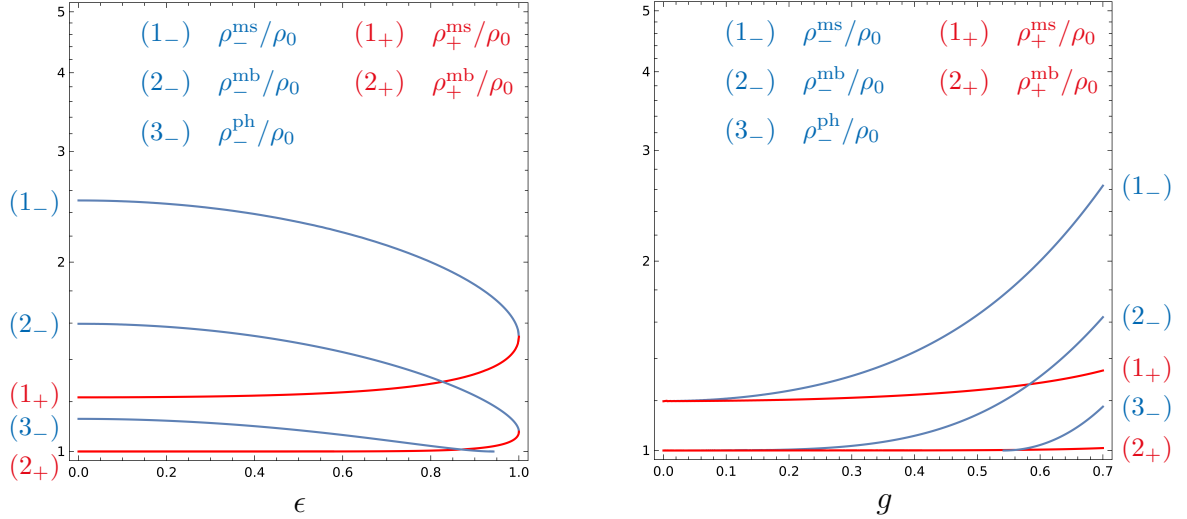
Figure 6.21: Radii of photon, marginally bound and marginally stable orbits, $\frac{\rho^{\mathrm{ph}}_-}{\rho_0}$, $\frac{\rho^{\mathrm{mb}}_\pm}{\rho_0}$ and $\frac{\rho^{\mathrm{ms}}_\pm}{\rho_0}$, as functions of ϵ (left), for $g = 0.6$, and g (right), for $\epsilon = 0.8$ (after [80]).

limit ($g \ll 1$). For sufficiently large values of ϵ and g there are both retrograde and prograde photon, marginally bound and marginally stable orbits. However, in contrast to the (exterior) spacetime of a Kerr-Newman black hole, for sufficiently small g there are no prograde photon orbits (as shown in fig. 6.21) and for even smaller g there are also no retrograde photon orbits (each depending on ϵ).[26] In other words, there are disc configurations for which both prograde and retrograde circular motion is possible arbitrarily close to the rim of the disc, i.e. no orbits are forbidden. For $g \to 0$ all orbits are bound. Moreover, in comparison to the uncharged rotating disc of dust, for $\epsilon > 0$ not all prograde orbits are bound (and for sufficiently large ϵ and g there are prograde photon orbits). Note that for $g = 0.7$ there is no ergosphere yet, see table 6.2.

As shown in fig. 6.22, the angular velocity of zero angular momentum observers vanishes for $\epsilon = 1$ and is maximal for $\epsilon = 0$. The reason for this is the growing angular momentum of the disc ($J \sim \sqrt{1 - \epsilon^2}$) and the resulting enhanced dragging of frames. Frame dragging occurs in the same direction as the disc rotates, both Ω_{nr} and Ω are non-negative. In addition, the more relativistic the disc is, the greater Ω_{nr} is. As is to be expected, Ω_{nr} is zero in the Newtonian limit (i.e. the first contribution in the post-Newtonian expansion is of $\mathcal{O}(g^3)$).

Finally, the convergence behaviour of the normalized angular velocity $R_0 \Omega_\pm$, the normalized specific angular momentum $\frac{L_\pm}{R_0}$, the specific energy $E_\pm$ and the normalized angular velocity of zero angular momentum observers $R_0 \Omega_{\mathrm{nr}}$ (based on eq. (5.52)) is illustrated in fig. 6.23. Generally, the quantities corresponding to prograde circular motion exhibit a significantly better convergence behaviour than those of retrograde

---

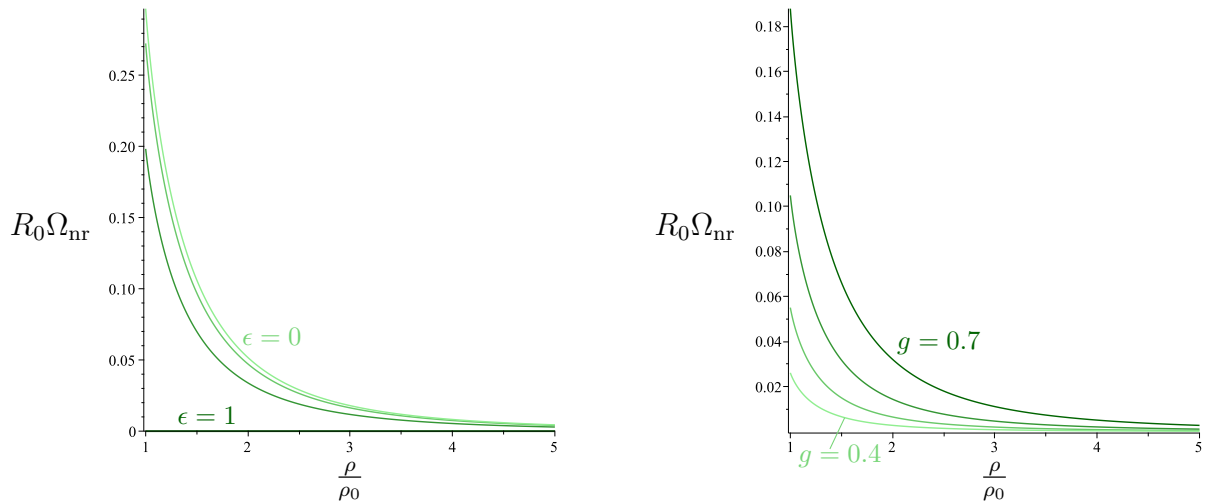[26]In the Newtonian theory of gravity there are in general no photon orbits.

Figure 6.22: Normalized angular velocity $R_0\Omega_{\mathrm{nr}}$ of zero angular momentum observers, displayed for $g = 0.7$, $\epsilon \in \{0, 1/3, 2/3, 1\}$ (left) and $\epsilon = 0.7$, $g \in \{0.4, 0.5, 0.6, 0.7\}$ (right) (after [80]).

circular motion. It should be noted that $\Omega_\pm$ and $L_\pm$ are only exact up to ninth order.

6.4.2 Circular orbits of charged test particles

Instead of electrically neutral particles, we now use charged test particles to analyse the exterior spacetime of the isolated, axisymmetric, stationary, reflection symmetric, charged, rotating body of the previous subsection.

We also only consider circular orbits that are confined to the equatorial plane of the body. However, since there is additionally an electromagnetic interaction between the body and a charged test particle, the corresponding curve is no longer geodesic. The (timelike) motion of the charged test particle is determined by the gravitational field and the Lorentz force. Therefore, the underlying equation of motion is given by

$$\frac{\mathrm{D}\,(u_{\mathrm{tp}})^a}{\mathrm{d}\tau} = \epsilon_{\mathrm{tp}} F^{ab}\,(u_{\mathrm{tp}})_b \,, \tag{6.82}$$

where $\frac{\mathrm{D}(u_{\mathrm{tp}})^a}{\mathrm{d}\tau} = (u_{\mathrm{tp}})^a{}_{;c}\,(u_{\mathrm{tp}})^c$ and ϵ_{tp} is the specific charge of the test particle. $F_{ab} = A_{b,a} - A_{a,b}$ is the field strength tensor of the present electromagnetic field. Compare eq. (6.82) with eq. (2.36).

Analogous to the uncharged test particles, the only non-vanishing component of the equation of motion (6.82) is the ρ-component:

$$\left[(-g'_{tt})^{1/2} - \epsilon_{\mathrm{tp}} A'_t\right]_{,\rho} = 0\,. \tag{6.83}$$

Notice that for $\epsilon_{\mathrm{tp}} = \epsilon$ and $\Omega_{\mathrm{tp}} = \Omega$, eq. (6.83) becomes the boundary condition (2.68) of the charged rotating disc of dust. The ζ-component vanishes due to the motion
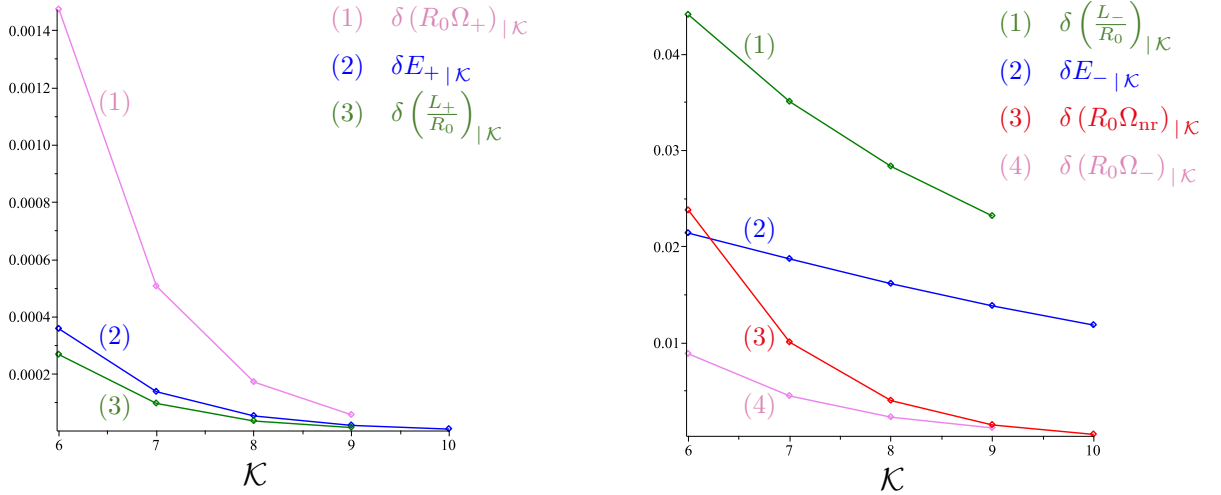
Figure 6.23: Convergence estimate of the functions $R_0\Omega_+$, $\frac{L_+}{R_0}$, E_+ (left) and $R_0\Omega_-$, $\frac{L_-}{R_0}$, E_-, $R_0\Omega_{\mathrm{nr}}$ (right), displayed for $g = 0.7$, $\epsilon = 0$ and $\frac{\rho}{\rho_0} = \sqrt{3}$ (after [80]).

being restricted to the equatorial plane of the body as well as reflection symmetry of the metric and the electromagnetic four-potential.

Using eq. (6.58), the equation of motion (6.83) leads to a quartic equation in Ω_{tp}:

$$\mathscr{A}\Omega_{\mathrm{tp}}^4 + \mathscr{B}\Omega_{\mathrm{tp}}^3 + \mathscr{C}\Omega_{\mathrm{tp}}^2 + \mathscr{D}\Omega_{\mathrm{tp}} + \mathscr{E} = 0 \,, \tag{6.84}$$

where

$$\mathscr{A} := 4\epsilon_{\mathrm{tp}}^2 g_{\varphi\varphi} A_{\varphi,\rho}^2 + g_{\varphi\varphi,\rho}^2 \,, \tag{6.85}$$

$$\mathscr{B} := 8\epsilon_{\mathrm{tp}}^2 \left(g_{\varphi\varphi} A_{\varphi,\rho} A_{t,\rho} + g_{\varphi t} A_{\varphi,\rho}^2 \right) + 4 g_{\varphi\varphi,\rho} g_{\varphi t,\rho} \,, \tag{6.86}$$

$$\mathscr{C} := 4\epsilon_{\mathrm{tp}}^2 \left(g_{\varphi\varphi} A_{t,\rho}^2 + 4 g_{\varphi t} A_{\varphi,\rho} A_{t,\rho} + g_{tt} A_{\varphi,\rho}^2 \right) + 2 g_{\varphi\varphi,\rho} g_{tt,\rho} + 4 g_{\varphi t,\rho}^2 \,, \tag{6.87}$$

$$\mathscr{D} := 8\epsilon_{\mathrm{tp}}^2 \left(g_{\varphi t} A_{t,\rho}^2 + g_{tt} A_{\varphi,\rho} A_{t,\rho} \right) + 4 g_{\varphi t,\rho} g_{tt,\rho} \,, \tag{6.88}$$

$$\mathscr{E} := 4\epsilon_{\mathrm{tp}}^2 g_{tt} A_{t,\rho}^2 + g_{tt,\rho}^2 \,. \tag{6.89}$$

A polynomial of degree four has four zeros, however, not all of them are necessarily real or permitted under physical terms. In general, the existence of the physical solutions depends strongly on the relation between ϵ_{tp} and ϵ (with ϵ being the specific charge of the rotating body) and these solutions may also be constrained to certain ranges of the radial coordinate ρ. It is to be assumed that generally direct and retrograde orbits are possible.

The specific angular momentum and the specific energy of the test particle are given by

$$\tilde{L} = \tilde{p}^i \eta_i \quad \text{and} \quad \tilde{E} = -\tilde{p}^i \xi_i \,, \tag{6.90}$$

where

$$\tilde{p}^i := (u_{\text{tp}})^i + \epsilon_{\text{tp}} A^i \, . \tag{6.91}$$

It can be easily verified that $\tilde{L}$ and $\tilde{E}$ are indeed conserved.

From eq. (6.90) follows

$$\tilde{L} = \frac{g_{\varphi\varphi}\Omega_{\text{tp}} + g_{\varphi t}}{\sqrt{-g_{\varphi\varphi}\Omega_{\text{tp}}^2 - 2g_{\varphi t}\Omega_{\text{tp}} - g_{tt}}} + \epsilon_{\text{tp}} A_\varphi \tag{6.92}$$

and

$$\tilde{E} = -\frac{g_{\varphi t}\Omega_{\text{tp}} + g_{tt}}{\sqrt{-g_{\varphi\varphi}\Omega_{\text{tp}}^2 - 2g_{\varphi t}\Omega_{\text{tp}} - g_{tt}}} - \epsilon_{\text{tp}} A_t \, . \tag{6.93}$$

Notice that $\tilde{L}$ and $\tilde{E}$ can be written as:

$$\tilde{L} = L + \epsilon_{\text{tp}} A_\varphi \, , \tag{6.94}$$

$$\tilde{E} = E - \epsilon_{\text{tp}} A_t \, , \tag{6.95}$$

where L and E, apart from a different Ω_{tp}, formally correspond to the specific angular momentum and the specific energy of an uncharged test particle, see eqs. (6.61) and (6.62).

Similar to the treatment of the uncharged test particles, the Lagrange formalism together with the introduction of an effective potential offers a physically equivalent[27] way to derive Ω_{tp}, $\tilde{L}$ and $\tilde{E}$.

The (timelike) motion of a charged test particle in the exterior spacetime of the (isolated, axisymmetric, stationary, reflection symmetric) charged, rotating body is determined by the Lagrangian

$$\tilde{\mathcal{L}} = \frac{1}{2}g_{ab}\dot{x}^a\dot{x}^b + \epsilon_{\text{tp}} A_a \dot{x}^a \, , \tag{6.96}$$

where the corresponding Euler-Lagrange equation is equivalent to the equation of motion (6.82).

Due to axisymmetry and stationarity, the variables φ and t are cyclic and imply (as in the previous section) the conservation of the specific angular momentum

$$\tilde{L} := \frac{\partial \tilde{\mathcal{L}}}{\partial \dot{\varphi}} = g_{\varphi\varphi}\dot{\varphi} + g_{\varphi t}\dot{t} + \epsilon_{\text{tp}} A_\varphi \, , \tag{6.97}$$

---

[27]In general, the two methods (in case of the charged test particles) can yield different mathematical solutions that, however, can be ruled out on the basis of physical arguments.

and the specific energy

$$\tilde{E} := -\frac{\partial\tilde{\mathcal{L}}}{\partial\dot{t}} = -g_{\varphi t}\dot{\varphi} - g_{tt}\dot{t} - \epsilon_{\text{tp}}A_t \,. \tag{6.98}$$

Eqs. (6.97) and (6.98) clearly coincide with $\tilde{L} = \tilde{p}^i\eta_i$ and $\tilde{E} = -\tilde{p}^i\xi_i$, see eq. (6.90). At this point, the role of $\tilde{p}_i$ now also becomes apparent. In fact, $\tilde{p}_i = \frac{\partial\tilde{\mathcal{L}}}{\partial\dot{x}^i} = \dot{x}_i + \epsilon_{\text{tp}}A_i$ is the canonical momentum of the charged test particle.[28]

By using eqs. (6.97) and (6.98), the angular velocity of the charged test particle $\Omega_{\text{tp}} = \frac{\text{d}\varphi}{\text{d}t}$ (as seen from infinity) is obtained:

$$\Omega_{\text{tp}} = -\frac{g_{tt}\left(\tilde{L} - \epsilon_{\text{tp}}A_\varphi\right) + g_{\varphi t}\left(\tilde{E} + \epsilon_{\text{tp}}A_t\right)}{g_{\varphi t}\left(\tilde{L} - \epsilon_{\text{tp}}A_\varphi\right) + g_{\varphi\varphi}\left(\tilde{E} + \epsilon_{\text{tp}}A_t\right)} \,. \tag{6.99}$$

Also the motion of the charged test particle in the equatorial plane of the body can be understood as a motion in an effective potential $\mathcal{U}$:

$$\frac{1}{2}g_{\rho\rho}\left(\frac{\text{d}\rho}{\text{d}\tau}\right)^2 + \mathcal{U} = 0 \,, \tag{6.100}$$

where

$$\mathcal{U} := -\frac{1}{2\rho^2}\left[g_{tt}\left(\tilde{L} - \epsilon_{\text{tp}}A_\varphi\right)^2 + 2g_{\varphi t}\left(\tilde{L} - \epsilon_{\text{tp}}A_\varphi\right)\left(\tilde{E} + \epsilon_{\text{tp}}A_t\right) + g_{\varphi\varphi}\left(\tilde{E} + \epsilon_{\text{tp}}A_t\right)^2\right]$$
$$+ \frac{1}{2} \,. \tag{6.101}$$

Notice that by writing $L = \tilde{L} - \epsilon_{\text{tp}}A_\varphi$ and $E = \tilde{E} + \epsilon_{\text{tp}}A_t$, eqs. (6.99) and (6.101) formally coincide with the corresponding equations of an uncharged test particle, eqs. (6.68) and (6.70).

Based on eq. (6.101), the conditions for circular orbits, $\mathcal{U} = 0$ and $\mathcal{U}_{,\rho} = 0$, imply the following equations:

$$g_{tt}L^2 + 2g_{\varphi t}LE + g_{\varphi\varphi}E^2 - \rho^2 = 0 \,, \tag{6.102}$$

$$g_{tt,\rho}L^2 + 2g_{\varphi t,\rho}LE + g_{\varphi\varphi,\rho}E^2 - 2\rho$$
$$= 2\epsilon_{\text{tp}}\left[(g_{tt}A_{\varphi,\rho} - g_{\varphi t}A_{t,\rho})L + (g_{\varphi t}A_{\varphi,\rho} - g_{\varphi\varphi}A_{t,\rho})E\right] \,, \tag{6.103}$$

where $L = \tilde{L} - \epsilon_{\text{tp}}A_\varphi$ and $E = \tilde{E} + \epsilon_{\text{tp}}A_t$ are to be understood.

The above system of equations leads to:

$$L = -\frac{g_{\varphi t}E \pm \rho\sqrt{E^2 + g_{tt}}}{g_{tt}} \tag{6.104}$$

---

[28]The Hamiltonian corresponding to $\tilde{\mathcal{L}}$ reads: $\tilde{\mathcal{H}} = \dot{x}^i\tilde{p}_i - \tilde{\mathcal{L}} = \frac{1}{2}\left(\tilde{p}^i - \epsilon_{\text{tp}}A^i\right)\left(\tilde{p}_i - \epsilon_{\text{tp}}A_i\right)$.

and

$$\mathfrak{A}E^4 + \mathfrak{B}E^3 + \mathfrak{C}E^2 + \mathfrak{D}E + \mathfrak{E} = 0\,, \tag{6.105}$$

where

$$\mathfrak{A} := (g_{\varphi t}g_{tt,\rho} - g_{tt}g_{\varphi t,\rho})^2 - (g_{tt} - \rho g_{tt,\rho})^2\,, \tag{6.106}$$

$$\mathfrak{B} := 2\epsilon_{\mathrm{tp}}g_{tt}\left[(g_{\varphi t}g_{tt,\rho} - g_{tt}g_{\varphi t,\rho})(g_{tt}A_{\varphi,\rho} - g_{\varphi t}A_{t,\rho}) - \rho(g_{tt} - \rho g_{tt,\rho})A_{t,\rho}\right]\,, \tag{6.107}$$

$$\mathfrak{C} := g_{tt}\left[(g_{\varphi t}g_{tt,\rho} - g_{tt}g_{\varphi t,\rho})^2 - (g_{tt} - \rho g_{tt,\rho})(2g_{tt} - \rho g_{tt,\rho})\right]$$
$$+ \epsilon_{\mathrm{tp}}^2 g_{tt}^2\left[(g_{tt}A_{\varphi,\rho} - g_{\varphi t}A_{t,\rho})^2 - \rho^2 A_{t,\rho}^2\right]\,, \tag{6.108}$$

$$\mathfrak{D} := \epsilon_{\mathrm{tp}}g_{tt}^2\left[2(g_{\varphi t}g_{tt,\rho} - g_{tt}g_{\varphi t,\rho})(g_{tt}A_{\varphi,\rho} - g_{\varphi t}A_{t,\rho}) - \rho(2g_{tt} - \rho g_{tt,\rho})A_{t,\rho}\right]\,, \tag{6.109}$$

$$\mathfrak{E} := -\frac{1}{4}g_{tt}^2(2g_{tt} - \rho g_{tt,\rho})^2 + \epsilon_{\mathrm{tp}}^2 g_{tt}^3(g_{tt}A_{\varphi,\rho} - g_{\varphi t}A_{t,\rho})^2\,. \tag{6.110}$$

After determining the analytical solutions for E from eq. (6.105), L can be calculated via eq. (6.104). The specific angular momentum $\tilde{L}$ and the specific energy $\tilde{E}$ of the charged test particle can then be easily obtained using $\tilde{L} = L + \epsilon_{\mathrm{tp}}A_\varphi$ and $\tilde{E} = E - \epsilon_{\mathrm{tp}}A_t$. Eq. (6.99), combined with $\tilde{L}$ and $\tilde{E}$, furthermore provides the particle's angular velocity Ω_{tp}. Note that the physically relevant solutions for $\tilde{L}$, $\tilde{E}$ and Ω_{tp} have to be determined by physical considerations (depending on ϵ_{tp}, ϵ and ρ).

Finally, the stability condition $\mathcal{U}_{,\rho\rho} > 0$ in case of equatorial circular motion of charged test particles (using $\mathcal{U} = 0$ and $\mathcal{U}_{,\rho} = 0$) reads

$$\begin{aligned}
g_{tt,\rho\rho}L^2 &+ 2g_{\varphi t,\rho\rho}LE + g_{\varphi\varphi,\rho\rho}E^2 - 2\\
&< -4\epsilon_{\mathrm{tp}}\left[(g_{\varphi t,\rho}A_{t,\rho} - g_{tt,\rho}A_{\varphi,\rho})L + (g_{\varphi\varphi,\rho}A_{t,\rho} - g_{\varphi t,\rho}A_{\varphi,\rho})E\right]\\
&\quad - 2\epsilon_{\mathrm{tp}}\left[(g_{\varphi t}A_{t,\rho\rho} - g_{tt}A_{\varphi,\rho\rho})L + (g_{\varphi\varphi}A_{t,\rho\rho} - g_{\varphi t}A_{\varphi,\rho\rho})E\right]\\
&\quad - 2\epsilon_{\mathrm{tp}}^2\left[g_{tt}A_{\varphi,\rho}^2 - 2g_{\varphi t}A_{\varphi,\rho}A_{t,\rho} + g_{\varphi\varphi}A_{t,\rho}^2\right]
\end{aligned} \tag{6.111}$$

and orbits are bound if $\tilde{E}^2 < 1$.

Applying either method to charged test particles moving in the (exterior) Reissner-Nordström spacetime reproduces the results for the specific angular momentum and the specific energy obtained in [83].[29]

---

[29]The angular velocity is not given in [83]. However, it can easily be calculated from eq. (6.99) and indeed it also coincides.

7 Conclusions

7.1 Summary

The objective of this thesis is a comprehensive investigation of geometrical and physical properties of the charged rotating disc of dust.[1]

Based on the derivation of the proper spatial line element, the proper radius R' and the proper circumference C' of the charged rotating disc of dust, which are measured[2] by co-rotating observers, could be introduced. Circumference C and radius R, seen by non-rotating observers, could be defined analogously. This made it possible to address questions related to the Ehrenfest paradox. In particular, the spatial geometry of an accelerated disc which is initially at rest evolves as follows: for both co-rotating and non-rotating observers, the geometric ratios $\frac{C'}{R'}$ and $\frac{C}{R}$, respectively, increase. However, while non-rotating observers always perceive smaller values than 2π for the ratio $\frac{C}{R}$, for co-rotating observers $\frac{C'}{R'}$ can be less than, equal to or greater than 2π depending on the specific charge ϵ.[3] As it turns out, the charged rotating disc of dust furthermore possesses material-like properties.

Subsequently, the Gaussian curvature of the charged rotating disc of dust was determined and discussed in detail. It was shown that the geometric transition found in $\frac{C'}{R'}$ is also reflected in the Gaussian curvature. Indeed, by decreasing the specific charge there occurs a transition from positive to negative curvature. In addition, the Gaussian curvature of the analytic limiting cases (charged rotating) Maclaurin disc, electrically counterpoised dust-disc and uncharged rotating disc of dust was calculated. These coincide with the charged rotating disc of dust in the respective limits.

By analysing the proper surface mass density of the charged rotating disc of dust, it can be observed that for sufficiently relativistic configurations ($g \gtrsim 0.7$) a global maximum forms near the rim of the disc by reducing the specific charge ϵ. On one hand, this resembles the behaviour of viscous fluids or elastic materials. On the other hand, the transition of the Gaussian curvature by altering ϵ manifests itself in this particular way in the proper surface mass density of the disc.

---

[1] This chapter is partly orientated on [10], [11] and [80].

[2] Measuring or seeing means using the radar method, see subsection 5.1.1.

[3] Note that the specific charge ϵ serves as a regulator of the rotation speed of the disc. Disc configurations with $\epsilon = 1$ are non-rotating and those with $\epsilon = 0$ rotate with maximal speed.

The exterior spacetime of the disc (or generally a physical body) can be characterized by its gravitational and electromagnetic multipole moments. Those were calculated and thoroughly discussed. It was found that the individual mass, angular momentum, electric and magnetic moments are ordered in the sense that higher moments have a lower absolute value. Also a generalized multipole conjecture was formulated. In particular, the conjecture holds for the charged rotating disc of dust (within the given accuracy of the post-Newtonian expansion).

For sufficiently high values of the relativity parameter g (e.g. $g = 0.78$ for $\epsilon = 0.4$) an ergosphere of torus-like shape forms within the disc. The ergosphere expands beyond the disc for growing g. With increasing ϵ, the disc's rotation speed decreases and the necessary value for g at which the ergosphere emerges rises.

Finally, circular motion of neutral test particles in the equatorial plane of the disc was studied. Angular velocity, specific angular momentum and specific energy of the test particles were discussed in dependence of the specific charge and the relativity parameter. Also the radii of photon, marginally bound and marginally stable orbits were determined. In addition, for both neutral and charged test particles, formulae for angular velocity, specific angular momentum and specific energy were derived that can be applied to the (exterior) spacetime of any isolated, axisymmetric, stationary, reflection symmetric, charged, rotating body.

7.2 Conclusions and outlook

A central assumption in cosmology is that the universe is spatially homogeneous and isotropic on large length scales. This is the cosmological principle and indeed observations confirm that it is fulfilled on scales of about 100 Mpc. Using the cosmological principle one can straightforwardly derive the Friedmann-Robertson-Walker metric that reduces the Einstein equations to the famous Friedmann equations. Due to homogeneity and isotropy the solutions exhibit a globally constant geometry with only three possible spatial curvatures: flat (k = 0), positive (k = +1) or negative (k = −1).[4] Remarkably, observations of the CMB suggest that our universe might indeed be flat. The first Friedmann equation reveals that there is a critical energy density that leads to a flat universe. If the density is higher than the critical density the universe is positively curved and if it is lower it is negatively curved.[5]

In some sense the proper spatial geometry of the charged rotating disc of dust behaves analogous to the spatial curvature of the Friedmann universe. High values of the specific charge ϵ (defined as the ratio of electric charge density to baryonic mass density)

---

[4] The curvature parameter k should not be confused with the summation index k of the post-Newtonian expansion or the metric function $k = k(\rho, \zeta)$.

[5] For more details see, e.g., [84].

cause positive and low values negative curvature. Furthermore, for given g and η there is a critical value of ϵ that gives rise to Euclidean geometry. However, unlike in Friedmann cosmology the geometry of the charged disc of dust is not globally constant. The geometry remains unchanged only in angular direction, but not in radial one. A beautiful exception of this represents the Newtonian limit with a radially independent curvature. In fact, for the critical value $\epsilon = \frac{1}{\sqrt{3}}$ the disc is globally flat.

The individual mass, angular momentum, electric and magnetic moments of the charged rotating disc of dust, in agreement with the uncharged disc, follow an ordering in which the higher they are, the less they contribute to the gravitational and electromagnetic field. This effect is in addition to the suppression of higher orders in the asymptotic expansions. Therefore, primarily the first multipole moments are relevant for the far-field behaviour of the gravitational and electromagnetic field of the charged rotating disc of dust.

Regarding the stated generalized multipole conjecture, it would of course be highly desirable if it could also be rigorously proven. This, however, would first require a precise notion of physical well-definedness.[6] In case of non-vanishing angular momentum the conjecture could serve as a powerful tool to distinguish ordinary physical bodies from black holes by measuring their multipole moments in the far-field. Indeed, if the necessary condition $Q^2 + \frac{J^2}{M^2} \leq M^2$ for a black hole is satisfied, the measurement of the multipole moment P_2 or Q_2 (apart from M, J and Q) would already be sufficient to determine if a given object is a black hole.

Various aspects of circular motion of uncharged test particles in the equatorial plane of the charged rotating disc of dust were analysed. It can be concluded that for sufficiently large radii (at least $\rho > \rho_+^{\mathrm{ms}}$), the qualitative behaviour of equatorial circular motion around the disc is very similar to that in the exterior spacetime of a Kerr-Newman black hole. In the close vicinity of the disc, however, circular motion shows a very distinct behaviour from the one near the event horizon of a black hole.[7]

A logical next step is to apply the derived general formulae for charged test particles also to the charged rotating disc of dust. Similar to the transition from neutral to charged test particles in the case of the Kerr-Newman spacetime, this should reveal all kinds of new facets.

Furthermore, both methods can also be adapted to null geodesics. In this way also circular photon orbits in the equatorial plane of the disc can be studied. In particular, for the effective potential $\mathcal{U}$, see eq. (6.70), only the term $\frac{1}{2}$ needs to be removed. Another possibility is to investigate circular motion (of either neutral/charged test

---

[6]It might also be necessary to choose a more restrictive formulation of the conjecture with the additional condition of a uniformly rotating, charged perfect fluid body with only convective electric currents, see [85].

[7]This is consistent with the conclusion drawn in [79] about equatorial circular motion around the uncharged rotating disc of dust.

particles or photons) in the interior of the disc. Without further ado, the formulae for neutral and charged test particles can also be used for the interior spacetime of the disc, since the metric of the disc is globally written in terms of Weyl-Lewis-Papapetrou coordinates. Clearly, circular motion in the interior of the disc is quite different from that in the exterior.

After all, finding an exact solution for the charged rotating disc of dust remains an open and extremely challenging problem! However, as this thesis has shown, the discussed geometrical and physical properties of the disc can be investigated just as well (if not better) with the semi-analytical solution in terms of the post-Newtonian expansion.

A Post-Newtonian expansions

A.1 Expansion of the ratio of proper radius to proper circumference and the normalized Gaussian curvature

The post-Newtonian expansion of the ratio of proper radius to proper circumference $\frac{C'}{R'}$ and the normalized Gaussian curvature $R_0^2 K$, each evaluated at the rim, reads (up to the fifth order) [10]:

$$\frac{1}{2\pi}\frac{C'}{R'}(\eta = 0)$$

$$= 1 - \frac{1}{2}\left(\epsilon^2 - \frac{1}{3}\right)g^2 + \frac{5}{24\pi^2}\left[\left(\epsilon^4 - \frac{52}{75}\epsilon^2 - \frac{53}{75}\right)\pi^2 - \frac{224\epsilon^2}{25} + \frac{224}{25}\right]g^4$$

$$- \frac{223}{1920\pi^2}\left[\left(\epsilon^6 - \frac{3457}{892}\epsilon^4 + \frac{113453}{112392}\epsilon^2 + \frac{31336}{14049}\right)\pi^2\right.$$

$$\left. - \frac{2560}{669}\left(\epsilon^2 - 1\right)\left(\epsilon^4 - \frac{313}{70}\epsilon^2 - \frac{257}{42}\right)\right]g^6$$

$$+ \frac{3145}{48384\pi^4}\left[\left(\epsilon^8 - \frac{313007839}{40256000}\epsilon^6 + \frac{3055678201}{193228800}\epsilon^4 - \frac{6005877459}{644096000}\epsilon^2 - \frac{29078}{235875}\right)\pi^4\right.$$

$$- \frac{111104}{15725}\left(\epsilon^2 - 1\right)\left(\epsilon^6 - \frac{69012347}{9374400}\epsilon^4 + \frac{113190529}{24998400}\epsilon^2 + \frac{78691}{13020}\right)\pi^2$$

$$\left. + \frac{802816}{15725}\left(\epsilon^2 - 1\right)^2\left(\epsilon^2 - \frac{15227}{1960}\right)\right]g^8$$

$$- \frac{2815391}{66355200\pi^4}\left[\left(\epsilon^{10} - \frac{379034234759}{41622740544}\epsilon^8 + \frac{95728571097211}{3874698756096}\epsilon^6\right.\right.$$

$$- \frac{103871864922476873}{2727787924291584}\epsilon^4 + \frac{14955289324645259}{495961440780288}\epsilon^2 - \frac{5355807104}{650355321}\Bigg)\pi^4$$

$$- \frac{238424064}{19707737}\left(\epsilon^2 - 1\right)\left(\epsilon^8 - \frac{10000383870041}{1084307938560}\epsilon^6 + \frac{104207736848353}{5046960586752}\epsilon^4\right.$$

$$\left. - \frac{49539410937953809}{5921767088455680}\epsilon^2 - \frac{91863454}{13446279}\right)\pi^2$$

$$\left. + \frac{78643200}{2815391}\left(\epsilon^2 - 1\right)^2\left(\epsilon^6 - \frac{4169}{350}\epsilon^4 + \frac{6055401553}{271656000}\epsilon^2 + \frac{2656693}{46200}\right)\right]g^{10} + \mathcal{O}\left(g^{12}\right),$$

A Post-Newtonian expansions

$R_0^2 K \, (\eta = 0)$

$$
\begin{aligned}
= \;& \left(3\epsilon^2 - 1\right) g^2 - 5 \left(\epsilon^2 - \frac{7}{30}\right) \left(\epsilon^2 - 1\right) g^4 \\
& + \frac{1703}{320\pi^2} \left[\left(\epsilon^6 - \frac{52261}{20436}\epsilon^4 + \frac{219665}{122616}\epsilon^2 - \frac{3968}{15327}\right)\pi^2 - \frac{2560\epsilon^6}{5109} + \frac{34816\epsilon^4}{15327} \right. \\
& \left. - \frac{11776\epsilon^2}{5109} + \frac{8192}{15327}\right] g^6 \\
& - \frac{9769}{2016\pi^2} \left[\left(\epsilon^8 - \frac{274414949}{60020736}\epsilon^6 + \frac{119546257}{18756480}\epsilon^4 - \frac{249550409}{80027648}\epsilon^2 + \frac{16824}{48845}\right)\pi^2 \right. \\
& \left. - \frac{94976}{48845}\left(\epsilon^6 - \frac{964087}{142464}\epsilon^4 + \frac{1525885}{284928}\epsilon^2 - \frac{856}{1113}\right)\left(\epsilon^2 - 1\right)\right] g^8 \\
& + \frac{316977977}{77414400\pi^4} \left[\left(-\frac{158969856}{316977977} + \epsilon^{10} - \frac{425179610969}{60859771584}\epsilon^8 + \frac{1000003956304379}{62320406102016}\epsilon^6 \right.\right. \\
& \left. - \frac{61149890345347447}{3988505990529024}\epsilon^4 + \frac{15274226506312301}{2659003993686016}\epsilon^2\right)\pi^4 - \frac{1296420864}{316977977}\left(\epsilon^2 - 1\right)\left(\epsilon^8 \right. \\
& - \frac{32218659817}{3646183680}\epsilon^6 + \frac{47760895613989}{2800269066240}\epsilon^4 - \frac{566746281193567}{59739073413120}\epsilon^2 + \frac{1129856}{949527}\right)\pi^2 \\
& \left. + \frac{550502400}{316977977}\left(\epsilon^4 - \frac{56}{5}\epsilon^2 + \frac{5296}{175}\right)\left(\epsilon^2 - 1\right)^2 \left(\epsilon^2 - \frac{1}{3}\right)\right] g^{10} + \mathcal{O}\left(g^{12}\right) .
\end{aligned}
$$

A.2 Expansion of the normalized angular velocity, the normalized specific angular momentum and the specific energy of neutral test particles

The post-Newtonian expansion of the normalized angular velocity $R_0\Omega_\pm$ (up to first order), the normalized specific angular momentum $\frac{L_\pm}{R_0}$ (up to first order) and the specific energy $E_\pm$ (up to second order) of uncharged test particles moving along equatorial

circular geodesics is as follows [80]:

$$
R_0\Omega_+
$$
$$
= \frac{\sqrt{(\pi - 2\arctan(\nu))\,(1 + \nu^2) - 2\nu}\, g}{\sqrt{\pi}\,\sqrt{1 + \nu^2}}
$$
$$
+ \frac{1}{\pi^2 \sqrt{(\pi - 2\arctan(\nu))\,(1 + \nu^2) - 2\nu}\,\sqrt{1 + \nu^2}}
$$
$$
\cdot \left[\left(\frac{13}{4}\,(1 + \nu^2) \left(\left(\epsilon^2 - \frac{36}{13} \right) \nu^2 + \frac{23\epsilon^2}{39} + \frac{2}{13} \right) \arctan(\nu) - 9\nu^3 - \frac{11\nu}{2} \right. \right.
$$
$$
\left. + \frac{13\epsilon^2\nu^3}{4} + \frac{15\nu\,\epsilon^2}{4} \right) \pi^{\frac{3}{2}} - \frac{15}{8}\,(1 + \nu^2) \left(\left(\epsilon^2 - \frac{8}{5} \right) \nu^2 + \frac{17\epsilon^2}{45} - \frac{2}{15} \right) \pi^{\frac{5}{2}}
$$
$$
+ \left(\arctan(\nu)\,(1 + \nu^2) + \nu \right) \sqrt{\pi} \left((\nu^2\,(\epsilon^2 + 6) - \epsilon^2 - 2)\arctan(\nu) + (\epsilon^2 + 6)\,\nu \right)
$$
$$
- 3\sqrt{1 - \epsilon^2}\,\sqrt{(\pi - 2\arctan(\nu))\,(1 + \nu^2) - 2\nu}\,\sqrt{1 + \nu^2} \left(\pi\,\nu^2 - 2\arctan(\nu)\,\nu^2 \right.
$$
$$
\left. + \frac{\pi}{3} - 2\nu - \frac{2\arctan(\nu)}{3} \right) \pi + \frac{5\pi^{3/2}}{6} \left((\pi - 2\arctan(\nu))\,(1 + \nu^2) - 2\nu \right) \Bigg] g^3
$$
$$
+ \mathcal{O}\left(g^5 \right),
$$

$$
R_0\Omega_-
$$
$$
= -\frac{\sqrt{(\pi - 2\arctan(\nu))\,(1 + \nu^2) - 2\nu}\, g}{\sqrt{\pi}\,\sqrt{1 + \nu^2}}
$$
$$
+ \frac{1}{\pi^2 \sqrt{(\pi - 2\arctan(\nu))\,(1 + \nu^2) - 2\nu}\,\sqrt{1 + \nu^2}}
$$
$$
\cdot \left[-\left(\left(\frac{13}{4}\,(1 + \nu^2) \left(\left(\epsilon^2 - \frac{36}{13} \right) \nu^2 + \frac{23\epsilon^2}{39} + \frac{2}{13} \right) \arctan(\nu) - 9\nu^3 - \frac{11\nu}{2} \right. \right. \right.
$$
$$
\left. + \frac{13\epsilon^2\nu^3}{4} + \frac{15\nu\,\epsilon^2}{4} \right) \pi^{\frac{3}{2}} - \frac{15}{8}\,(1 + \nu^2) \left(\left(\epsilon^2 - \frac{8}{5} \right) \nu^2 + \frac{17\epsilon^2}{45} - \frac{2}{15} \right) \pi^{\frac{5}{2}}
$$
$$
\left. + \left(\arctan(\nu)\,(1 + \nu^2) + \nu \right) \sqrt{\pi} \left((\nu^2\,(\epsilon^2 + 6) - \epsilon^2 - 2)\arctan(\nu) + (\epsilon^2 + 6)\,\nu \right) \right)
$$
$$
- 3\sqrt{1 - \epsilon^2}\,\sqrt{(\pi - 2\arctan(\nu))\,(1 + \nu^2) - 2\nu}\,\sqrt{1 + \nu^2} \left(\pi\,\nu^2 - 2\arctan(\nu)\,\nu^2 \right.
$$
$$
\left. + \frac{\pi}{3} - 2\nu - \frac{2\arctan(\nu)}{3} \right) \pi - \frac{5\pi^{3/2}}{6} \left((\pi - 2\arctan(\nu))\,(1 + \nu^2) - 2\nu \right) \Bigg] g^3
$$
$$
+ \mathcal{O}\left(g^5 \right),
$$

A Post-Newtonian expansions

$$\frac{L_+}{R_0}$$

$$= \frac{\sqrt{(\pi - 2\arctan(\nu))(1+\nu^2) - 2\nu}\,\sqrt{1+\nu^2}\,g}{\sqrt{\pi}}$$

$$- \frac{3}{2\pi^{\frac{27}{2}}\left((\pi - 2\arctan(\nu))(1+\nu^2) - 2\nu\right)}$$

$$\cdot \left[\frac{5\pi^{12}}{4} \left(-\frac{8}{15}\left(\nu^2\left(\epsilon^2 + 2\right) - \epsilon^2 + 6\right)\left(1+\nu^2\right)\arctan^2(\nu) + \left(\pi\left(-\frac{26\epsilon^2}{15} + \frac{8}{3}\right)\nu^4 \right. \right.$$

$$+ \left(-\frac{32}{15} - \frac{16\epsilon^2}{15}\right)\nu^3 + \pi\left(\frac{20}{3} - \frac{124\epsilon^2}{45}\right)\nu^2 - \frac{64\nu}{15} + \pi\left(4 - \frac{46\epsilon^2}{45}\right)\right) \arctan(\nu)$$

$$+ \pi^2\left(\epsilon^2 - \frac{16}{15}\right)\nu^4 + \pi\left(-\frac{26\epsilon^2}{15} + \frac{8}{3}\right)\nu^3 + \left(\left(-\frac{34}{15} + \frac{62\epsilon^2}{45}\right)\pi^2 - \frac{16}{15} - \frac{8\epsilon^2}{15}\right)\nu^2$$

$$\left. + \left(-2\epsilon^2 + 4\right)\pi\nu + \pi^2\left(\frac{17\epsilon^2}{45} - \frac{6}{5}\right)\right)\sqrt{1+\nu^2}\,\sqrt{(\pi - 2\arctan(\nu))(1+\nu^2) - 2\nu}$$

$$+ \left(4\left(\left(1+\nu^2\right)^2\arctan(\nu) + \nu^3 + \frac{5\nu}{3}\right)\left(\left(1+\nu^2\right)\arctan(\nu) + \nu\right)\pi^{\frac{25}{2}}\right)$$

$$+ \left(-4\left(1+\nu^2\right)^2\arctan(\nu) + \pi\nu^4 + 2\pi\nu^2 - 4\nu^3 + \pi - \frac{16\nu}{3}\right)\pi^{\frac{27}{2}}\left(1+\nu^2\right)\right)\sqrt{1-\epsilon^2}$$

$$\left. + \frac{5\pi^{13}}{9}\left((\pi - 2\arctan(\nu))(1+\nu^2) - 2\nu\right)^{3/2}\sqrt{1+\nu^2}\right] g^3 + \mathcal{O}\left(g^5\right)\,,$$

$$\frac{L_-}{R_0}$$

$$= -\frac{\sqrt{(\pi - 2\arctan(\nu))(1+\nu^2) - 2\nu}\,\sqrt{1+\nu^2}\,g}{\sqrt{\pi}}$$

$$- \frac{3}{2\pi^{\frac{27}{2}}\left((\pi - 2\arctan(\nu))(1+\nu^2) - 2\nu\right)}$$

$$\cdot \left[-\frac{5\pi^{12}}{4} \left(-\frac{8}{15}\left(\nu^2\left(\epsilon^2 + 2\right) - \epsilon^2 + 6\right)\left(1+\nu^2\right)\arctan^2(\nu) + \left(\pi\left(-\frac{26\epsilon^2}{15} + \frac{8}{3}\right)\nu^4 \right. \right.$$

$$+ \left(-\frac{32}{15} - \frac{16\epsilon^2}{15}\right)\nu^3 + \pi\left(\frac{20}{3} - \frac{124\epsilon^2}{45}\right)\nu^2 - \frac{64\nu}{15} + \pi\left(4 - \frac{46\epsilon^2}{45}\right)\right) \arctan(\nu)$$

$$+ \pi^2\left(\epsilon^2 - \frac{16}{15}\right)\nu^4 + \pi\left(-\frac{26\epsilon^2}{15} + \frac{8}{3}\right)\nu^3 + \left(\left(-\frac{34}{15} + \frac{62\epsilon^2}{45}\right)\pi^2 - \frac{16}{15} - \frac{8\epsilon^2}{15}\right)\nu^2$$

$$\left. + \left(-2\epsilon^2 + 4\right)\pi\nu + \pi^2\left(\frac{17\epsilon^2}{45} - \frac{6}{5}\right)\right)\sqrt{1+\nu^2}\,\sqrt{(\pi - 2\arctan(\nu))(1+\nu^2) - 2\nu}$$

$$+ \left(4\left(\left(1+\nu^2\right)^2\arctan(\nu) + \nu^3 + \frac{5\nu}{3}\right)\left(\left(1+\nu^2\right)\arctan(\nu) + \nu\right)\pi^{\frac{25}{2}}\right)$$

$$+ \left(-4\left(1+\nu^2\right)^2\arctan(\nu) + \pi\nu^4 + 2\pi\nu^2 - 4\nu^3 + \pi - \frac{16\nu}{3}\right)\pi^{\frac{27}{2}}\left(1+\nu^2\right)\right)\sqrt{1-\epsilon^2}$$

$$\left. - \frac{5\pi^{13}}{9}\left((\pi - 2\arctan(\nu))(1+\nu^2) - 2\nu\right)^{3/2}\sqrt{1+\nu^2}\right] g^3 + \mathcal{O}\left(g^5\right)\,,$$

E_+

$$= 1 + \frac{\nu\left(\pi\nu - 2\arctan(\nu)\,\nu - 2\right)g^2}{\pi}$$

$$- \frac{3}{\sqrt{1+\nu^2}\,\pi^{\frac{11}{2}}}\left[\frac{\pi^4}{3}\sqrt{(\pi - 2\arctan(\nu))\,(1+\nu^2) - 2\nu}\,\left(1+\nu^2\right)\right.$$

$$\cdot\left(\left(-6\nu^2 - 2\right)\arctan(\nu) + 3\pi\,\nu^2 + \pi - 6\nu\right)\sqrt{1-\epsilon^2} + \frac{15}{16}\left(\left(\left(-\frac{16}{9} - \frac{8\epsilon^2}{15}\right)\nu^4\right.\right.$$

$$+ \left(-\frac{32}{15} + \frac{16\epsilon^2}{45}\right)\nu^2 - \frac{16}{15} + \frac{8\epsilon^2}{45}\right)\arctan^2(\nu) + \left(\left(\left(\frac{152}{45} - \frac{26\epsilon^2}{15}\right)\nu^4\right.\right.$$

$$+ \left(\frac{64}{15} - \frac{68\epsilon^2}{27}\right)\nu^2 - \frac{58\epsilon^2}{135} + \frac{56}{45}\right)\pi - \frac{16\nu}{15}\left(\left(\frac{10}{3} + \epsilon^2\right)\nu^2 - \frac{\epsilon^2}{3} + 2\right)\right)\arctan(\nu)$$

$$+ \left(1+\nu^2\right)\left(\left(-\frac{56}{45} + \epsilon^2\right)\nu^2 + \frac{23\epsilon^2}{135} - \frac{16}{45}\right)\pi^2 + \left(-\frac{26}{15}\epsilon^2\nu^3 - \frac{214}{135}\nu\,\epsilon^2 + \frac{152}{45}\nu^3 + \frac{8}{3}\nu\right)\pi$$

$$\left.\left.- \frac{8}{15}\left(\frac{10}{3} + \epsilon^2\right)\nu^2\right)\pi^{\frac{7}{2}}\sqrt{1+\nu^2}\right]g^4 + \mathcal{O}\left(g^6\right)\,,$$

E_-

$$= 1 + \frac{\nu\left(\pi\nu - 2\arctan(\nu)\,\nu - 2\right)g^2}{\pi}$$

$$- \frac{45}{16\sqrt{1+\nu^2}\,\pi^{\frac{11}{2}}}\left[-\frac{16}{15}\sqrt{1-\epsilon^2}\,\left(1+\nu^2\right)\left(\pi\,\nu^2 - 2\arctan(\nu)\,\nu^2 + \frac{\pi}{3} - 2\nu\right.\right.$$

$$\left.- \frac{2\arctan(\nu)}{3}\right)\pi^4\sqrt{(\pi - 2\arctan(\nu))\,(1+\nu^2) - 2\nu}$$

$$+ \left(\left(\left(-\frac{16}{9} - \frac{8\epsilon^2}{15}\right)\nu^4 + \left(-\frac{32}{15} + \frac{16\epsilon^2}{45}\right)\nu^2 - \frac{16}{15} + \frac{8\epsilon^2}{45}\right)\arctan^2(\nu)\right.$$

$$+ \left(\left(\left(\frac{152}{45} - \frac{26\epsilon^2}{15}\right)\nu^4 + \left(\frac{64}{15} - \frac{68\epsilon^2}{27}\right)\nu^2 - \frac{58\epsilon^2}{135} + \frac{56}{45}\right)\pi\right.$$

$$- \frac{16\nu}{15}\left(\left(\frac{10}{3} + \epsilon^2\right)\nu^2 - \frac{\epsilon^2}{3} + 2\right)\right)\arctan(\nu) + \left(1+\nu^2\right)\left(\left(-\frac{56}{45} + \epsilon^2\right)\nu^2 + \frac{23\epsilon^2}{135} - \frac{16}{45}\right)\pi^2$$

$$\left.\left.+ \left(-\frac{26}{15}\epsilon^2\nu^3 - \frac{214}{135}\nu\,\epsilon^2 + \frac{152}{45}\nu^3 + \frac{8}{3}\nu\right)\pi - \frac{8}{15}\left(\frac{10}{3} + \epsilon^2\right)\nu^2\right)\pi^{\frac{7}{2}}\sqrt{1+\nu^2}\right]g^4 + \mathcal{O}\left(g^6\right)\,.$$

Acknowledgements

First and foremost, I would like to thank Prof. Dr. Reinhard Meinel for his excellent and caring supervision and for introducing me to the interesting as well as challenging research topic of this thesis. I am very grateful for his constant support and for all the valuable discussions from which I benefited greatly.

Secondly, I would like to express my sincere thanks to Dr. Andreas Kleinwächter for interesting discussions, especially about the uncharged rotating disc of dust and for calculating the corresponding numerical values.

I also thank Dr. Martin Breithaupt for providing me with the results of the post-Newtonian expansion of the charged rotating disc of dust.

Special thanks goes to Prof. Dr. Holger Gies, who initiated and managed the Research Training Group and thus created a stimulating research environment. I would like to acknowledge the assistance of Katrin Kanter and Lisann Schmidt as part of the administrative staff.

I am very grateful for valuable scientific discussions with Florian Atteneder and Lars Maiwald and their support in IT matters.

Beyond that, I would like to thank several of the great people I had the pleasure of meeting during my doctorate, some of whom were not only colleagues but also became friends: Dr. Dimitrios Gkiatas, Kirian Winter, Dr. Abdol Sabor Salek, Dr. Michael Mandl, Mustafa Kemal Döner, Dr. Leonhard Klar, Dr. Seán Sohrab Gray, Dr. Jobst Ziebell, Richard Schmieden, José Diogo Simão, Ivan Soler Calero, Marta Picciau, Katharina Wölfl, Daniela Cors, Alexander Jercher, Markus Schröfl, Tim Stötzel, Julian Schirrmeister, Claire Moran and Linda van Manen.

Finally, I want to thank my girlfriend Lisa Busch and my family for their continuous support.

Bibliography

[1] C. M. Will, 'The confrontation between general relativity and experiment', Living Reviews in Relativity **17**, 4 (2014).

[2] B. P. Abbott et al. (LIGO Scientific Collaboration and Virgo Collaboration), 'Tests of general relativity with gw170817', Phys. Rev. Lett. **123**, 011102 (2019).

[3] R. Abbott et al. (LIGO Scientific Collaboration and Virgo Collaboration), 'Tests of general relativity with binary black holes from the second ligo-virgo gravitational-wave transient catalog', Phys. Rev. D **103**, 122002 (2021).

[4] R. P. Kerr, 'Gravitational field of a spinning mass as an example of algebraically special metrics', Phys. Rev. Lett. **11**, 237–238 (1963).

[5] E. T. Newman et al., 'Metric of a rotating, charged mass', Journal of Mathematical Physics **6**, 918–919 (1965).

[6] G. Neugebauer and R. Meinel, 'The Einsteinian gravitational field of the rigidly rotating disk of dust', Astrophys. J. Lett. **414**, L97–L99 (1993).

[7] G. Neugebauer and R. Meinel, 'General relativistic gravitational field of a rigidly rotating disk of dust: solution in terms of ultraelliptic functions', Phys. Rev. Lett. **75**, 3046–3047 (1995).

[8] S. Palenta and R. Meinel, 'Post-Newtonian expansion of a rigidly rotating disc of dust with a constant specific charge', Classical and Quantum Gravity **30**, 085010 (2013).

[9] M. Breithaupt et al., 'On the black hole limit of rotating discs of charged dust', Classical and Quantum Gravity **32**, 135022 (2015).

[10] D. Rumler, A. Kleinwächter and R. Meinel, 'Geometry of charged rotating discs of dust in Einstein-Maxwell theory', General Relativity and Gravitation **55**, 35 (2023).

[11] D. Rumler and R. Meinel, 'Multipole moments of a charged rotating disc of dust in general relativity', Phys. Rev. D **108**, 064047 (2023).

[12] R. Meinel et al., *Relativistic Figures of Equilibrium* (Cambridge University Press, 2008).

Bibliography

[13] G. Neugebauer, A. Kleinwächter and R. Meinel, 'Relativistically rotating dust', Helvetica Physica Acta **69**, 472–489 (1996).

[14] R. Meinel, M. Breithaupt and Y.-C. Liu, 'Black holes and quasiblack holes in Einstein-Maxwell theory', in 13th Marcel Grossmann Meeting on Recent Developments in Theoretical and Experimental General Relativity, Astrophysics, and Relativistic Field Theories (2015), pages 1186–1188.

[15] R. Meinel, *Spezielle und allgemeine Relativitätstheorie für Bachelorstudenten* (Springer Spektrum Berlin, Heidelberg, 2019).

[16] M. Ansorg and R. Meinel, 'Differentially rotating disks of dust', General Relativity and Gravitation **32**, 1365–1380 (2000).

[17] L. Lindblom and W. A. Hiscock, 'On the stability of rotating stellar models in general relativity theory', Astrophysical Journal **267**, 384 (1983).

[18] H. Stephani et al., *Exact Solutions of Einstein's Field Equations*, 2nd edition, Cambridge Monographs on Mathematical Physics (Cambridge University Press, 2003).

[19] T. Lewis and G. A. Schott, 'Some special solutions of the equations of axially symmetric gravitational fields', Proceedings of the Royal Society of London. Series A, Containing Papers of a Mathematical and Physical Character **136**, 176–192 (1932).

[20] A. Papapetrou, 'Champs gravitationnels stationnaires à symétrie axiale', Annales de l'institut Henri Poincaré. Section A, Physique Théorique **4**, 83–105 (1966).

[21] H. Stephani, *Relativity: An Introduction to Special and General Relativity*, 3rd edition (Cambridge University Press, 2004).

[22] M. Breithaupt, 'Untersuchungen von rotierenden und geladenen Staubscheiben mit hochgenauen Näherungslösungen und der Grenzübergang zu Schwarzen Löchern', Friedrich-Schiller-Universität Jena, PhD thesis (Germany, Jena, 2016).

[23] F. J. Ernst, 'New formulation of the axially symmetric gravitational field problem. II', Phys. Rev. **168**, 1415–1417 (1968).

[24] S. Novikov et al., *Theory of solitons: The inverse scattering method* (Springer New York, 1984).

[25] M. J. Ablowitz et al., 'The inverse scattering transform: Fourier analysis for nonlinear problems', Studies in Applied Mathematics **53**, 249–315 (1974).

[26] G. Neugebauer and R. Meinel, 'Progress in relativistic gravitational theory using the inverse scattering method', Journal of Mathematical Physics **44**, 3407–3429 (2003).

[27] R. Meinel, 'The rigidly rotating disk of dust and its black hole limit', in Proceedings of the Second Mexican School on Gravitation and Mathematical Physics, eds. A. Garcia et al. (1998).

[28] G. Neugebauer and D. Kramer, 'Einstein-Maxwell solitons', Journal of Physics A: Mathematical and General **16**, 1927 (1983).

[29] G. Neugebauer, 'Rotating bodies as boundary value problems', Annalen der Physik **512**, 342–354 (2000).

[30] J. M. Bardeen and R. V. Wagoner, 'Relativistic disks. I. Uniform rotation', Astrophysical Journal **167**, 359–423 (1971).

[31] D. Petroff and R. Meinel, 'Post-Newtonian approximation of the rigidly rotating disc of dust to arbitrary order', Phys. Rev. D **63**, 064012 (2001).

[32] P. Ehrenfest, 'Gleichförmige Rotation starrer Körper und Relativitätstheorie', Physikalische Zeitschrift **10**, 918 (1909).

[33] M. Born, 'Die Theorie des starren Elektrons in der Kinematik des Relativitätsprinzips', Annalen der Physik **335**, 1–56 (1909).

[34] Ø. Grøn, 'Space geometry in rotating reference frames: a historical appraisal', in *Relativity in Rotating Frames: Relativistic Physics in Rotating Reference Frames*, edited by G. Rizzi and M. L. Ruggiero (Springer Netherlands, 2004), pages 285–333.

[35] Ø. Grøn, 'Relativistic description of a rotating disk', American Journal of Physics **43**, 869–876 (1975).

[36] G. Herglotz, 'Über den vom Standpunkt des Relativitätsprinzips aus als "starr" zu bezeichnenden Körper', Annalen der Physik **336**, 393–415 (1910).

[37] F. Noether, 'Zur Kinematik des starren Körpers in der Relativtheorie', Annalen der Physik **336**, 919–944 (1910).

[38] G. Salzman and A. H. Taub, 'Born-type rigid motion in relativity', Phys. Rev. **95**, 1659–1669 (1954).

[39] M. Planck, 'Gleichförmige Rotation und Lorentz-Kontraktion', Physikalische Zeitschrift **11**, 294 (1910).

[40] A. Einstein, 'Die Grundlage der allgemeinen Relativitätstheorie', Annalen der Physik **354**, 769–822 (1916).

[41] H. A. Lorentz, 'The Michelson-Morley experiment and the dimensions of moving bodies', Nature **106**, 793–795 (1921).

[42] A. S. Eddington, *The Mathematical Theory of Relativity* (Cambridge University Press, 1923).

Bibliography

[43] N. Rosen, 'Notes on rotation and rigid bodies in relativity theory', Phys. Rev. **71**, 54–58 (1947).

[44] Ø. Grøn, 'Rotating frames in special relativity analyzed in light of a recent article by M. Strauss', International Journal of Theoretical Physics **16**, 603–614 (1977).

[45] G. Cavalleri and G. Spinelli, 'Does a rod, pushed by a force, accelerate less than the same rod pulled by the same force?', Il Nuovo Cimento B (1965-1970) **66**, 11–20 (1970).

[46] L. D. Landau and E. M. Lifshitz, *The Classical Theory of Fields* (Pergamon Press, 1971).

[47] P. Langevin, 'Remarques au sujet de la note de M. Prunier', Comptes Rendus des Séances de l'Académie des Sciences **200** (1935).

[48] Ø. Grøn, 'Relativistic description of a rotating disk with angular acceleration', Foundations of Physics **9**, 353–369 (1979).

[49] E. J. Post, 'Sagnac effect', Rev. Mod. Phys. **39**, 475–493 (1967).

[50] G. Lugo, *Differential Geometry in Physics* (University of North Carolina Wilmington William Madison Randall Library, 2021).

[51] R. Meinel and M. Hütten, 'On the black hole limit of electrically counterpoised dust configurations', Classical and Quantum Gravity **28**, 225010 (2011).

[52] A. Papapetrou, 'A static solution of the equations of the gravitational field for an arbitary charge-distribution', Proceedings of the Royal Irish Academy. Section A: Mathematical and Physical Sciences **51**, 191–204 (1945).

[53] S. D. Majumdar, 'A class of exact solutions of Einstein's field equations', Phys. Rev. **72**, 390–398 (1947).

[54] R. Meinel, 'Black holes: a physical route to the Kerr metric', Annalen der Physik **514**, 509–521 (2002).

[55] R. Geroch, 'Multipole moments. II. Curved space', Journal of Mathematical Physics **11**, 2580–2588 (1970).

[56] R. O. Hansen, 'Multipole moments of stationary space-times', Journal of Mathematical Physics **15**, 46–52 (1974).

[57] G. Fodor, C. Hoenselaers and Z. Perjés, 'Multipole moments of axisymmetric systems in relativity', Journal of Mathematical Physics **30**, 2252–2257 (1989).

[58] W. Simon, 'The multipole expansion of stationary Einstein-Maxwell fields', Journal of Mathematical Physics **25**, 1035–1038 (1984).

[59] C. Hoenselaers and Z. Perjes, 'Multipole moments of axisymmetric electrovacuum spacetimes', Classical and Quantum Gravity **7**, 1819 (1990).

[60] T. P. Sotiriou and T. A. Apostolatos, 'Corrections and comments on the multipole moments of axisymmetric electrovacuum spacetimes', Classical and Quantum Gravity **21**, 5727 (2004).

[61] G. Fodor, E. d. S. Costa Filho and B. Hartmann, 'Calculation of multipole moments of axistationary electrovacuum spacetimes', Phys. Rev. D **104**, 064012 (2021).

[62] Y.-C. Liu Pynn et al., 'Gyromagnetic factor of rotating disks of electrically charged dust in general relativity', Phys. Rev. D **94**, 104035 (2016).

[63] A. Kleinwächter, R. Meinel and G. Neugebauer, 'The multipole moments of the rigidly rotating disk of dust in general relativity', Physics Letters A **200**, 82–86 (1995).

[64] R. Filter and A. Kleinwächter, 'On the multipole moments of a rigidly rotating fluid body', Annalen der Physik **521**, 102–106 (2009).

[65] P. Kordas, 'Reflection-symmetric, asymptotically flat solutions of the vacuum axistationary Einstein equations', Classical and Quantum Gravity **12**, 2037 (1995).

[66] R. Meinel and G. Neugebauer, 'Asymptotically flat solutions to the Ernst equation with reflection symmetry', Classical and Quantum Gravity **12**, 2045 (1995).

[67] L. A. Pachón and J. D. Sanabria-Gómez, 'Note on reflection symmetry in stationary axisymmetric electrovacuum spacetimes', Classical and Quantum Gravity **23**, 3251 (2006).

[68] F. J. Ernst, V. S. Manko and E. Ruiz, 'Equatorial symmetry/antisymmetry of stationary axisymmetric electrovac spacetimes', Classical and Quantum Gravity **23**, 4945 (2006).

[69] R. Meinel, 'Constructive proof of the Kerr-Newman black hole uniqueness including the extreme case', Classical and Quantum Gravity **29**, 035004 (2012).

[70] R. M. Wald, *General Relativity* (University of Chicago Press, 1984).

[71] C. W. Misner, K. S. Thorne and J. A. Wheeler, *Gravitation* (W. H. Freeman, 1973).

[72] H. Labranche, D. Petroff and M. Ansorg, 'The parametric transition of strange matter rings to a black hole', General Relativity and Gravitation **39**, 129–143 (2007).

[73] R. Meinel and A. Kleinwächter, 'Bäcklund transforms of the extreme Kerr near-horizon geometry', Physics Letters A **384**, 126572 (2020).

Bibliography

[74] R. Meinel and A. Kleinwächter, 'Dragging effects near a rigidly rotating disk of dust', in Mach's Principle: From Newton's Bucket to Quantum Gravity, edited by J. B. Barbour and H. Pfister (1995), pages 339–346.

[75] J. M. Bardeen, W. H. Press and S. A. Teukolsky, 'Rotating black holes: Locally nonrotating frames, energy extraction, and scalar synchrotron radiation', Astrophysical Journal **178**, 347–370 (1972).

[76] N. Dadhich and P. P. Kale, 'Equatorial circular geodesics in the Kerr–Newman geometry', Journal of Mathematical Physics **18**, 1727–1728 (2008).

[77] J. Bicak, Z. Stuchlik and V. Balek, 'The motion of charged particles in the field of rotating charged black holes and naked singularities. I. The general features of the radial motion and the motion along the axis of symmetry', Bulletin of the Astronomical Institutes of Czechoslovakia **40**, 65 (1989).

[78] V. Balek, J. Bicak and Z. Stuchlik, 'The motion of the charged particles in the field of rotating charged black holes and naked singularities. II. The motion in the equatorial plane', Bulletin of the Astronomical Institutes of Czechoslovakia **40**, 133 (1989).

[79] M. Ansorg, 'Timelike geodesic motions within the general relativistic gravitational field of the rigidly rotating disk of dust', Journal of Mathematical Physics **39**, 5984–6000 (1998).

[80] D. Rumler, 'Circular geodesic orbits in the equatorial plane of a charged rotating disc of dust', arXiv:2405.01998 [gr-qc] (2024).

[81] J. M. Bardeen, 'Stability of circular orbits in stationary, axisymmetric spacetimes', Astrophysical Journal **161**, 103 (1970).

[82] S. Beheshti and E. Gasperín, 'Marginally stable circular orbits in stationary axisymmetric spacetimes', Phys. Rev. D **94**, 024015 (2016).

[83] D. Pugliese, H. Quevedo and R. Ruffini, 'Motion of charged test particles in Reissner-Nordström spacetime', Phys. Rev. D **83**, 104052 (2011).

[84] V. Mukhanov, *Physical Foundations of Cosmology* (Cambridge University Press, 2005).

[85] J. Novak and E. Marcq, 'The gyromagnetic ratio of rapidly rotating compact stars in general relativity', Classical and Quantum Gravity **20**, 3051 (2003).

Ehrenwörtliche Erklärung

Hiermit erkläre ich ehrenwörtlich,

1. dass mir die geltende Promotionsordnung bekannt ist;

2. dass ich die Dissertation selbst angefertigt habe, keine Textabschnitte eines Dritten oder eigener Prüfungsarbeiten ohne Kennzeichnung übernommen und alle von mir benutzten Hilfsmittel, persönlichen Mitteilungen und Quellen in meiner Arbeit angegeben habe;

3. dass bei der Auswahl und Auswertung folgenden Materials mich die nachstehend aufgeführten Personen in der jeweils beschriebenen Weise unterstützt haben:
   - Dr. Martin Breithaupt - Bereitstellung der Lösung der geladenen Staubscheibe (f, α, b, β, a^*, A_φ^*, Ω^*) in Form der Post-Newtonschen Entwicklung
   - Dr. Andreas Kleinwächter - Bereitstellung ausgewählter Ergebnisse der ungeladenen Staubscheibe (Gleichungen (5.45) und (5.46), linke Seite von Abb. 5.7, linke Spalte von Tabelle 5.1, rechte Spalte von Tabelle 6.1, numerische Werte für X_n)
   - Prof. Dr. Reinhard Meinel - Betreuung über die gesamte Dauer der Promotion

4. dass die Hilfe einer kommerziellen Promotionsvermittlerin / eines kommerziellen Promotionsvermittlers nicht in Anspruch genommen wurde und dass Dritte weder unmittelbar noch mittelbar geldwerte Leistungen für Arbeiten erhalten haben, die im Zusammenhang mit dem Inhalt der vorgelegten Dissertation stehen;

5. dass die Dissertation noch nicht als Prüfungsarbeit für eine staatliche oder andere wissenschaftliche Prüfung eingereicht wurde;

6. dass eine gleiche, eine in wesentlichen Teilen ähnliche oder eine andere Abhandlung nicht bei einer anderen Hochschule als Dissertation eingereicht wurde.

....

Ort, Datum   David Rumler